

ALKALI-ACTIVATED CONCRETE:

Development of material properties (strength and stiffness) and flexural behaviour of reinforced beams over time.

- Silke Prinsse

MASTER THESIS

ALKALI-ACTIVATED CONCRETE:

development of material properties (strength and stiffness)
and flexural behaviour of reinforced beams over time.

by

Silke Prinsse

To obtain the degree of Master of Science after completing the master Building Engineering
– Structural Design at the Delft University of Technology, Faculty of Civil Engineering and
Geosciences, Stevinweg 1, Delft.

To be defended publicly on Wednesday the 25th of October, 2017.



Student number	4156676	
Project duration	February 2017 – October 2017	
Thesis committee	Prof.dr.ir. D.A. Hordijk (chair)	TU Delft - Structural and Building Engineering: Concrete Structures
	Dr. M. Luković (daily supervisor)	TU Delft - Structural and Building Engineering: Concrete Structures
	Dr. G. Ye	TU Delft – Materials and Environment
	Ir. P. Lagendijk	TU Delft - Structural and Building Engineering: Concrete Structures

Acknowledgements

This thesis is the product of several months of research in the final stage of the master degree Building Engineering at the faculty of Civil Engineering and Geosciences - Delft University of Technology. I am grateful to all those who supported me during this research.

First of all, the members of my thesis committee, who helped me a lot with their critical questions and valuable remarks. Many thanks to the head of my graduation committee, professor Dick Hordijk, his interest in the thesis topic has been stimulating throughout the project. Furthermore, his advice on when to dive deeper or when to stop, has been very helpful for me. I really appreciate the support I received from dr. Ye Guang, whose long-time experience with the material proved to be very valuable. I learned a lot from his explanations on the microstructural level, a topic that was completely new for me. I would like to thank ir. Paul Lagendijk for assisting me, especially with the part on structural behaviour of reinforced beams. Additionally, his practical view on the topic was very useful. And, of course, my daily supervisor is also greatly acknowledged, dr. Mladena Luković. She spent so much of her valuable time to personally assist me. Both her enthusiasm and knowledge were (and still are!) very inspiring. She kept me on the right track constantly by guiding me intensely throughout the process. I cannot imagine a better daily supervisor, thanks!

For casting the specimens and execution of the experiments, Albert Bosman, Ton Blom and Maiko van Leeuwen have been of great assistance in the Stevinlab. They are all indispensable, I really enjoyed working with them. I learned a lot and had a lot of fun at the same time. Furthermore I want to thank people from Microlab TU Delft for their support, especially Jiahua Liu, Zainab Aldin and Marija Nedeljković.

I am also very thankful to everyone from the Concrete Structures section, who adopted me as if I already worked there for ages. I enjoyed the good atmosphere and nice talks. And special thanks to Chengcheng, with whom I shared an office over the past seven months, I had a blast!

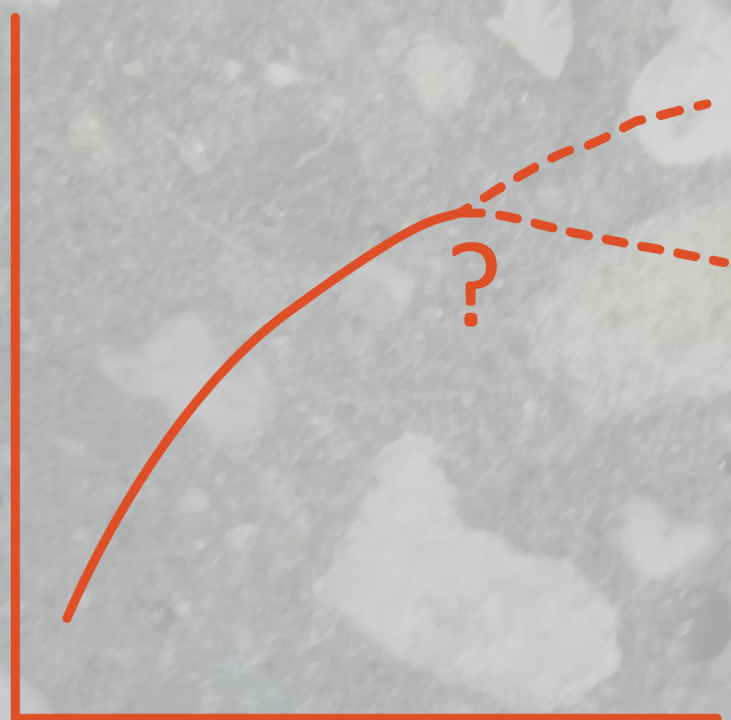
Furthermore, my friends. Especially Naomi, who had to listen to a lot of uninteresting stories about alkali-activated concrete or boring experimental results... And of course, U-BASE, for providing a lot of fun activities during my master studies. Being a member of the U-profiel magazine committee and joining the Study Tour to China, it all made studying way more enjoyable!

Also, I thank my family, my parents and Birte. I really appreciate all the help and assistance (also financial) that they gave me during my time at university in Delft. And, last but certainly not least, Milan. Thanks for the endless support and patience!

Silke Prinsse

Delft, October 2017

strength,
stiffness



time

Summary

Ordinary Portland Cement (OPC) consumption has grown nearly exponentially in the last twenty years. OPC has become the highest-volume manufactured product on the planet. Production of OPC is energy-intensive, consumes unrenewable natural resources and is one of the primary contributors to global warming (accounting for at least 5-8% of worldwide anthropogenic CO₂ emissions). Therefore, the concrete industry is actively trying to reduce energy consumption, natural resource exploitation and greenhouse gas emissions. One of the solutions that is applied already, is to reduce the Portland cement clinker consumption by using industrial byproducts like Blast Furnace Slag (BFS) or Fly Ash (FA) as Supplementary Cementitious Materials (SCMs) in conventional concrete. Another alternative is Alkali-Activated Concrete (AAC), for which Portland cement is completely substituted by an alternative binder. Instead of using OPC and water, precursors (raw materials) like BFS or FA are activated with an alkaline activator solution.

Although AAC seems to have promising qualities for structural application in terms of sustainability, worldwide use is not yet established. One of the reasons for this is the fact that there are no available regulations or codes to apply it, the material is relatively new and limited research has been conducted. Furthermore, the codes that are used for conventional concrete are probably not applicable for AAC. For OPC concrete, the design codes are based on compressive strength at 28 days (strength at later ages stays either constant or is higher) and most other mechanical properties used in calculations are estimated based on this compressive strength. For AAC it is not yet sure if the same relations and assumptions as for OPC are also valid. First, because mechanical properties that have been reported for AAC in literature vary a lot, depending on mixture composition and curing conditions. Second, the long-term strength development of AAC is scarcely investigated and it is not clear if the compressive strength at 28 days can be used as a safe reference for design. Namely, a few researchers reported a decrease of strength or stiffness over time, for AAC mixtures that contain blast furnace slag. The observed decrease might not be a very desirable phenomenon and should be well-understood prior to wider structural application of AAC. Therefore, the main research question of this thesis is: *Can a decrease of stiffness and strength over time, as sometimes reported in literature for AAC, also be found for AAC used at TU Delft¹ and if so, what could be an explanation for this behaviour? Does the amount of BFS in the binder play a role, as a decrease over time has only been reported for AAC containing BFS? And if not, what other cause could lead to a decrease of properties over time?* The intention is to make some first steps towards a better understanding of this phenomenon.

The research question is investigated in an experimental manner. Compressive strength, elastic modulus, splitting tensile strength and flexural strength are tested at different ages (28, 56 and 91 days) after being wet-cured (20°C and 95% RH) for 28 days. Two different AAC mixtures are investigated, S100 and S50, characterized by a BFS/FA binder ratio of 100:0 and 50:50 respectively. Furthermore, the flexural behaviour of reinforced beams is investigated by conducting four-point bending tests on both S100 and S50 concrete of two different ages (33/34 days and 69/70 days) and compared to an OPC concrete control beam.

¹ There where in this thesis "TU Delft alkali-activated concrete mixtures" is mentioned, it is meant to be referred to Arbi et al. (2015), Arbi et al. (2016) and Nedeljković (2014).

Most of the obtained results show a decrease of mechanical properties (elastic modulus, splitting tensile and flexural strength) over time, for both S50 and S100. Elastic modulus shows the highest decrease (of approximately 30% for S50), whereas compressive strength is approximately constant over time, for both mixtures. This is consistent with the few results that have been reported in literature. Furthermore, it is observed that S50 shows a higher degree of decrease over time than S100 for all tested properties. Based on these results, it is obvious that the decrease is not directly related to the amount of BFS. If the amount of slag would be the only reason for the decrease over time, it would be logical to assume that S100 shows a higher degree of decrease than S50 concrete, which has not been observed.

The four-point bending tests on reinforced AAC beams exhibited flexural failure for all four beams; for three beams, reinforcement failure was observed, but for the S50 beam tested at 69 days, crushing of the concrete in the compression zone occurred. The failure load for the S50 beam tested at 69 days is lower when compared to the AAC beams (S50 at 33 days and S100 at 34 and 70 days) that show flexural reinforcement failure. For the same load, AAC beams show higher deflections than an OPC concrete control beam (that has a lower compressive strength than the AAC beams, but similar E-modulus as the S100 mixture), as has also been reported in literature (Shah & Shah, 2017). The overall stiffness of the AAC reinforced beams is lower than for the OPC concrete beam, both in the pre-cracking but also in the crack formation stage, following the same trend of E-modulus tests on the material that also showed a relatively lower E-modulus for AAC when compared to OPC concrete. The results of the four-point bending tests confirm that the overall stiffness of reinforced AAC is decreasing over time, as the beams tested at an age of 69/70 days show a lower stiffness than the beams tested at an age of 33/34 days. This is also consistent with the observed decrease of E-modulus for S50 and S100 concrete over time.

Structural behavior and cracking patterns (spacing and width), were found to be similar for reinforced AAC and conventional concrete, both in literature (Kumaravel & Thirugnanasambandam, 2013) as well as in the conducted four-point bending tests. But, possibly due to the relatively lower stiffness, reinforced AAC beams show larger deflections and exhibits more ductile behavior (higher rotational capacity) compared to reinforced OPC concrete. This should be taken into account with considering possible structural applications for AAC.

With the acquired results from the conducted experiments, the main research question has been answered partially. The development of strength and stiffness for AAC over time is known, for the chosen mixture compositions and curing conditions. For most mechanical properties, a decrease over time is observed. Steps towards understanding the cause for this phenomenon are made, by conducting additional research.

All the samples were wet-cured for 28 days and then exposed to laboratory conditions, while tests were performed at different ages (28, 56 and 91 days). It might be that exposing the samples to dry after the wet-curing period has influence on the strength development. A few extra samples that were wet-cured for 92 days were also tested. Samples that are exposed after 28 days of wet-curing show a decrease in properties, while extra samples that are tested after 92 days of wet-curing show an increase when compared to the 28 day properties. Therefore, the acquired results indicate that the decrease of strength and stiffness that has been observed might be related to drying. Drying might therefore be the reason for the fact that the S50 reinforced beam tested after approximately two months showed compressive failure (while a similar beam tested after one month showed reinforcement failure). Drying in the outer layer of the beam can result in a lower capacity and thus a different failure mode.

For one sample (wet-cured for 92 days), weight loss was measured after exposing the sample to laboratory conditions. An approximately linear relationship between moisture loss and decrease of elastic modulus was observed, giving another indication that drying (moisture loss) might be causing the decrease in properties. For OPC concrete, this is also the case: specimens that are tested in wet conditions show an E-modulus that is approximately fifteen percent higher than corresponding specimens tested in a dry condition, disregarding any difference in mix proportions or curing age (Monteiro & Kuhmar Mehta, 2006). Depending on the microstructure, alkali-activated concrete might lose more moisture because, compared to OPC concrete, less water is required in the alkali-activation process and more water can evaporate during drying. However, while generally for regular OPC concrete the compressive strength is higher when specimens are tested in a dry condition, compared to testing under wet conditions (Monteiro & Kuhmar Mehta, 2006), the results on AAC show contradictory behaviour. Therefore, it is not yet clear if the decrease in elastic modulus can be explained by only moisture loss.

To investigate if any difference in microstructure was visible, an ESEM (Environmental Scanning Electron Microscope) analysis was performed on samples that were wet-cured for 28 days and then exposed to drying at laboratory conditions and samples that were wet-cured for 92 days. The ESEM analysis did not show explicit differences in microstructure between the samples that were cured for 28 days or 92 days.

In order to use the material for practical applications, it is important that the observed phenomenon of a decrease of properties over time is understood. Subsequently, it can be judged what this phenomenon means for structural application of the material, or how it can be dealt with. So, further research should focus on a deeper understanding of the strength and stiffness reduction over time. A suggestion is to analyze the microstructure of the material for different curing conditions and concrete mixtures and to study the influence of drying (moisture loss). However, apart from zooming in, it is also recommended to upscale. It could be that the observed decrease only plays a role for small-sizes samples, or at least, that the effect is (almost) negligible in large reinforced elements. In addition to this, it is advised to investigate the behaviour of AAC over a longer period of time. As long as it does not cause cracking, it might be that the observed decrease is only temporary (due to eigenstresses caused by shrinkage gradient), so examining the material behaviour over a longer period of time could lead to other conclusions.

It should be emphasized that the physical and chemical properties of alkali-activated concrete vary a lot. For traditional OPC concrete, a lot of properties can be adjusted by modifying the water-cement ratio, this is not exactly the same in AAC. Instead of using Portland cement and water, a lot of different raw materials and alkali activator solutions can be combined to form a binder. The properties of alkali-activated concrete depend largely on the used raw materials, chosen activator and the curing conditions. Therefore, this does not mean that the observed phenomenon of a drop of properties over time would occur for every alkali-activated concrete mixture or for every curing regime. It is necessary to investigate how the composition of AAC mixtures and different types of curing can affect the properties of alkali-activated concrete.

To conclude, this research has confirmed that alkali-activated concrete containing BFS can show a decrease of strength and stiffness properties over time, at least for the investigated mixtures and chosen curing conditions. Especially for E-modulus, quite a significant decrease (of about 30%) has been observed. The acquired results indicate that the observed decrease of properties is related to drying (moisture loss). However, more research is needed to get a grip on the observed phenomenon, especially related to the aimed practical application of alkali-activated concrete.

e-modulus
beam
results tensile laboratory
bending zone
time higher drying beams
tested fly ash opc
specimens crack four-point aggregate
stiffness conditions flexural
alkali-activated concrete
reinforced degree tests ESEM days
modulus more cured
exposed regular mm compressive
between geopolymer different
ratio mixture OPC slag increase
decrease load RH failure
reinforcement cracks testing splitting
samples elastic binder
cubes mixtures strength
small development
paste properties
microstructure

Table of contents

List of terms and abbreviations.....	i
1 Introduction.....	1
1.1. Background.....	1
1.2. Problem statement	3
1.3. Research question.....	7
1.4. Outline of master thesis.....	7
2 Alkali-activated concrete	9
2.1. Introduction.....	9
2.2. Constituents of alkali-activated concrete	9
2.2.1. Blast furnace slag (BFS).....	11
2.2.2. Fly ash (FA)	11
2.3. Categorisation alkali-activated binders.....	12
2.3.1. High-calcium binder chemistry (BFS)	14
2.3.2. Low-calcium binder chemistry (FA).....	14
2.3.3. Combined systems	15
2.4. Benefits of using alkali-activated concrete	17
2.5. Factors that limit the use of alkali-activated concrete.....	18
2.6. Applications	19
2.6.1. Projects in the former USSR	19
2.6.2. Storehouse in Kraków	20
2.6.3. Global Change Institute in Brisbane.....	22
3 Material and structural properties of alkali-activated concrete.....	23
3.1. In general	23
3.2. Compressive strength	24
3.2.1. Influence of BFS/FA ratio	24
3.2.2. Influence of curing conditions	27
3.2.3. Development over time	28

3.3.	Modulus of elasticity	29
3.3.1.	Influence of BFS/FA ratio	30
3.3.2.	Influence of curing conditions	33
3.3.3.	Development over time	33
3.4.	Splitting tensile strength	35
3.4.1.	Influence of BFS/FA ratio	35
3.4.2.	Influence of curing conditions	37
3.4.3.	Development over time	38
3.5.	Flexural strength	39
3.5.1.	Influence of BFS/FA ratio	40
3.5.2.	Influence of curing conditions	41
3.5.3.	Development over time	41
3.6.	Flexural behaviour of reinforced beams	42
3.7.	Conclusion	44
4	Approach and methodology.....	49
4.1.	Plan.....	49
4.1.1.	Research objectives and goals.....	49
4.1.2.	Parameters	50
4.2.	Approach	52
4.3.	Method	52
4.3.1.	Materials and mixture designs	52
4.3.2.	Casting and curing procedures – prisms specimens	53
4.3.3.	Casting and curing procedures – reinforced beams	55
4.4.	Testing procedures.....	57
4.4.1.	Flexural test	57
4.4.2.	Compression test	58
4.4.3.	Splitting tension test	58
4.4.4.	Elastic modulus test	59
4.4.5.	4-point bending test – reinforced beams	60
5	Results.....	61
5.1.	In general	61

5.2.	Mechanical properties	61
5.2.1.	Compressive strength	62
5.2.2.	Tensile splitting strength	63
5.2.3.	Flexural strength	63
5.2.4.	Elastic modulus and poisson's ratio	64
5.3.	Bending capacity of reinforced beams.....	65
6	Discussion.....	71
6.1.	In general	71
6.2.	Influence of drying	73
6.3.	ESEM analysis of microstructure	76
6.4.	Size effects	78
6.5.	Bending capacity of reinforced beams.....	79
6.6.	Comparison with regular OPC concrete.....	80
6.6.1.	Effect of drying on the development of strength and stiffness for OPC concrete	80
6.6.2.	Measured properties for AAC versus Eurocode 2 for OPC concrete	82
7	Conclusions and recommendations	85
7.1.	Conclusions.....	85
7.2.	Recommendations for further research	88
	References	90
Appendix A.	– Generation and utilization of coal fly ash.....	94
Appendix B.	– Surfaces after curing.....	95
Appendix C.	– Reinforcement drawings	100
Appendix D.	– Calculation of reinforced beams.....	101
Appendix E.	– Development of cracks	110
Appendix F.	– Location of ESEM images.....	111

List of terms and abbreviations

AAC	Alkali-activated concrete
AAS	Alkali-activated slag
BFS	Blast furnace slag (from iron production)
Ca(OH)₂	Calcium di-hydroxide
CaCO₃	Calcium carbonate
C-(A)-S-H	Calcium-(Alumino)-Silicate-Hydrate (reaction product of alkali-activation for high-calcium materials, like BFS)
CO₂	Carbon dioxide
FA	Fly ash (industrial product from coal production)
ITZ	Interfacial transition zone
N-A-S-H	Sodium-Alumino-Silicate-Hydrate (reaction product of alkali-activation for low-calcium materials, like FA)
OPC	Ordinary Portland cement
OPCC	Ordinary Portland cement concrete
S50	Referring to a 50:50 BFS/FA binder ratio for the AAC mixture used in this thesis
S100	Referring to a 100:0 BFS/FA binder ratio for the AAC mixture used in this thesis
SF	Silica fume (from ferrosilicon production)
SP	Super plasticizer
w/c	Water to cement ratio
w/b	Water to binder ratio

Chemical notations cement industry

C	CaO
S	SiO ₂
A	Al ₂ O ₃
F	Fe ₂ O ₃
S	SO ₄
H	H ₂ O

1

Introduction

1.1. Background

During the last century, concrete has become the most popular construction material. Next to water, concrete is the most consumed substance on earth. In order to make concrete, a binder is needed. The combination of Ordinary Portland Cement (OPC) and water is widely used, because of the ease of use, freedom in form, and good performance. Furthermore, the widespread availability and relatively low costs of the needed materials and technologies contributed to the fact that OPC has become the highest-volume manufactured product on the planet (Zhang et al., 2014).

However, the production of cement is energy-intensive. The production of cement is one of the primary contributors to global warming, accounting for at least 5-8% of worldwide anthropogenic CO₂ emissions (Provis et al., 2014). Each produced tonne of OPC generates approximately one tonne of CO₂. This is not that much compared to other materials, like steel and aluminium (Fig. 1.1, left).

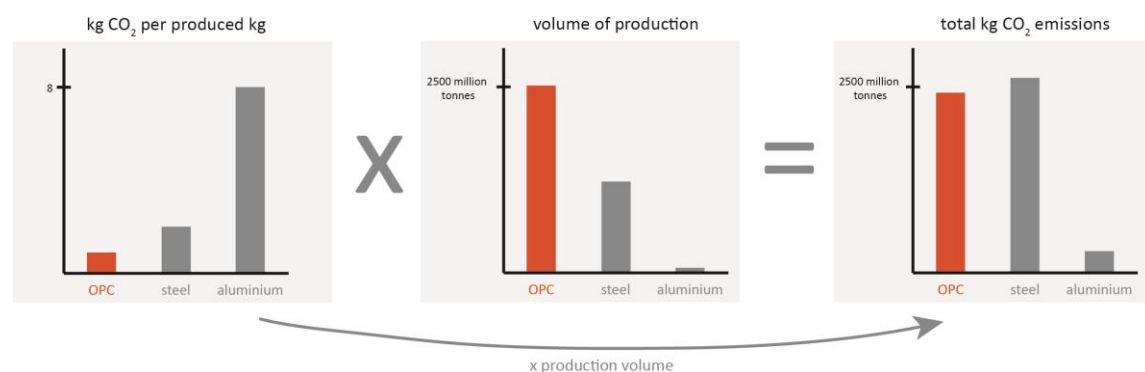


Fig. 1.1: Left: comparison of kg CO₂ emission per produced kg of material for Ordinary Portland Cement (OPC), steel and aluminium. Middle: volume of production in for these materials. Right: comparison of CO₂ emission per kg times volume of production per material. Based on data that were retrieved by de Rooij et al. (2010)

Still, the impact of cement production is enormous (Fig. 1.1, right), because of the enormous volume of production (Fig. 1.1, middle). Portland cement consumption has grown nearly exponentially in the last

twenty years and it is estimated that the overall demand will be about 3.6×10^9 tonnes by 2020 (Garcia-Lodeiro et al., 2015a). So, the demand for cement is continuously growing, particularly in the developing parts of the world due to urbanization and associated infrastructure development. Because of this, the cement production is still increasing substantially (Fig. 1.2). This does not only lead to an enormous flow of CO₂ emissions, the further growing cement production also implies overexploitation of natural resources like limestone quarries (Garcia-Lodeiro et al., 2015a).

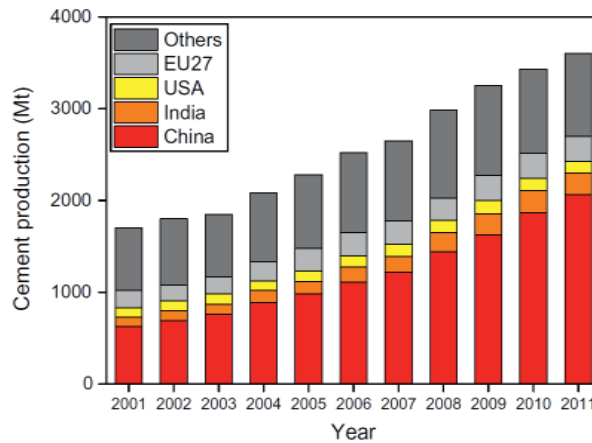


Fig. 1.2: Global cement production (Zhang et al., 2014, p. 115)

The cement and concrete industries are therefore actively trying to reduce greenhouse gas emissions and use of raw materials and energy. One of the solutions that is already applied, is to reduce the Portland cement clinker content in cement and concrete. This is done by using industrial byproducts as supplementary materials, as Supplementary Cementitious Materials (SCMs) in conventional concrete, as is shown in the overview in Table 1.1. Examples of these byproducts are Blast Furnace Slag (BFS), Fly Ash (FA), natural pozzolans and silica fume.

Table 1.1: Different types of cement (NEN, 2013)

CEM I	Portland cement	Portland cement + max. 5% of minor additional constituents
CEM II	Portland-composite cement	Portland cement + max. 35% of other constituents (BFS, FA)
CEM III	Blast furnace cement	Portland cement and higher perc. of BFS
		CEM III/A 36-65% BFS
		CEM III/B 66-80% BFS
		CEM III/C 81-95% BFS
CEM IV	Pozzolanic cement	Portland cement and up to 55% of pozzolanic constituents
CEM V	Composite cement	Portland cement, BFS or FA and pozzolans

In the Netherlands, about 50-60% of the cement used is CEM III, already for decades, that can contain as low as only 5% of Portland clinker (Cement&BetonCentrum, 2015). However, researchers are also focused on making concrete without any Portland cement. An example of this is alkali-activated or geopolymers concrete, where instead of ordinary Portland cement, an alternative binder is used. By using alternative

binders, with the aforementioned industrial byproducts (Fig. 1.3), lower energy and environmental costs can be realised.

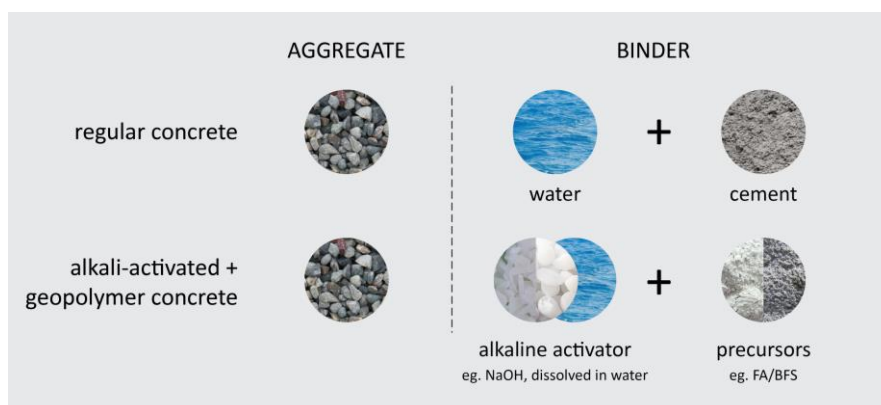


Fig. 1.3: Different binder for regular concrete and AAC/geopolymer concrete

In the past few years, geopolymer and alkali-activated binders have attracted considerable attention because they seem to have similar properties like regular concrete, but are claimed to have lower CO₂ emissions. Several studies praise the good performance of alkali-activated concrete, like high (early) strength, good fire performance and high resistance against acid and sulphate attack (Provis & van Deventer, 2014). Although alkali-activated concretes (AACs) seem to have good qualities, worldwide use is not yet established, due to several technical and non-technical reasons (Van Deventer et al., 2012). One of the reasons for this is the fact that there are no available regulations or codes to apply it, the material is relatively new and limited research has been conducted. Despite the amount of knowledge about the performance of alkali-activated paste and more material-related properties, less research has been conducted regarding the structural properties of the material. However, knowledge about the mechanical behaviour of alkali-activated concrete is essential for practical applications (Thomas & Peethamparan, 2015).

1.2. Problem statement

Most of the research that has been conducted regarding the engineering properties of alkali-activated concrete shows promising results, alkali-activated concrete can show even better performance than Portland cement concretes (Pacheco-Torgal, 2014). Although, this varies per mixture composition, as the specific characteristics of raw materials and activators used, have a lot of influence on the microstructural development and mechanical strength properties. The large amounts of different activators and raw materials (called precursors, see Fig. 1.3) result in a wide variety of alkali-activated binders.

The most common industrial byproducts used as binder precursors are Fly Ash (FA) and Blast Furnace Slag (BFS). Both have different chemical compositions, as shown in Fig. 1.4. Apart from the general differences between the two raw materials, the chemical and physical properties of BFS or FA are different for each specific furnace or factory. When fly ash is used as a precursor in a binder (or another low-calcium precursor), alumina and silica react with the alkaline activator solution. A three-dimensional polymeric structure with molecular bonds is formed. The final product is a sodium-aluminosilicate (N-A-S-H) gel

binder, called 'geopolymer'. This name was introduced by the French scientist Joseph Davidovits in 1979, because the raw materials used can be minerals of geological origin and a polymeric structure is formed. Geopolymer binders are a subcategory of all alkali-activated binders, as illustrated in Fig. 1.4. If blast furnace slag (calcium-rich) is used to make a binder, the main reaction product is a calcium-silicate-hydrate (C-A-S-H) gel, rather similar to the binder obtained when ordinary Portland cement (OPC) is used. So, the hardening process for low-calcium binders (eg. fly ash based) differs from high-calcium binders (eg. slag based). Therefore, strictly speaking, the term "geopolymer" is not suitable for high-calcium binders.

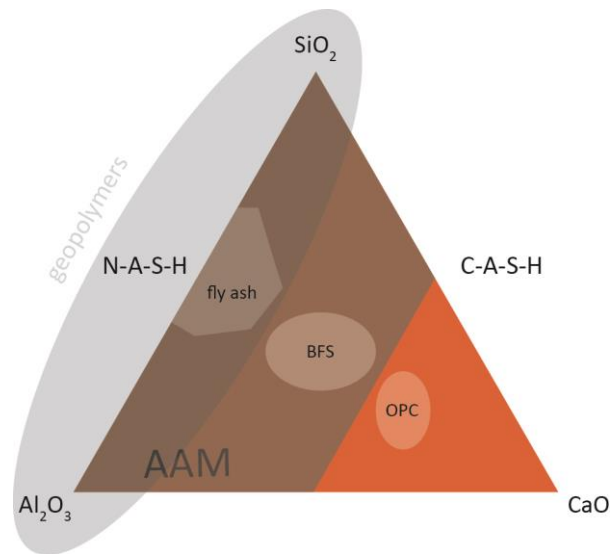


Fig. 1.4: Usual range of compositions of FA, BFS and OPC; categorization of alkali-activated materials (AAM) and 'geopolymers'.
Picture based upon Garcia-Lodeiro et al. (2015b, p. 50) and de Rooij et al. (2010, p. 79).

Because the chemical composition of alkali-activated concrete differs from OPC concrete, it is not yet sure if the codes that are used for conventional concrete are applicable for AAC. For OPC concrete, the design codes are based on compressive strength at 28 days (strength at later ages stays either constant or is higher) and most other mechanical properties used in calculations are estimated based on this compressive strength. For AAC it is not yet sure if the same relations and assumptions as for OPC are also valid. The mechanical properties that have been reported for AAC in literature vary a lot, ranging from low performance to very high performance in strength. Some of these results have been summarised in Table 1.2.

Table 1.2: An overview of the (mechanical) properties reported in literature, for different mixes, tested at 28 days after casting; CS = compressive strength; STS = splitting tensile strength; FS = flexural strength and MOE = modulus of elasticity.

	FA/BFS	Curing conditions				Density [kg/m ³]	CS		FS [MPa]	MOE [GPa]	Poisson's ratio
		temp [°C]	RH [%]	sealed?	duration		f _{c,28} [MPa]	f _{st,28} [MPa]			
Hardjito et al.	FA	60-80			24 h	2330-2430	30-80	3,74-6	5-12	23-31	0,12-0,16
Jimenez et al.	FA	85			20 h	-	29-43,5	-	6.86	10,7-18,4	-
Sofi et al.	S0-S20	23			till testing	2147-2408	47-56,5	2,8-4,1	4,9-6,2	23-39	0,23-0,26
Diaz-loya et al.	FA?	60			72 h	1890-2371	10-80	-	2,24-6,41	1,9-42	0,08-0,22
Pan et al.	FA?	60			24 h	1876-2555	65,1-77,9	2,8-5,1	-	11,2-41,2	0,15-0,19
Wardhono et al.	S0	80	dry oven	no	24 h	2302	22.4	2.1	4.7	8.02	-
Wardhono et al.	S100	23	water-cured	no	6 days	2453	39.5	3.3	6	26.77	-
Nath & Sarker	S0	18-23	70 ± 10	-	28 days	2378	25.6	-	4.89	-	-
Nath & Sarker	S10	18-23	70 ± 10	-	28 days	2382	38.3	-	5.79	-	-
Nath & Sarker	S15	18-23	70 ± 10	-	28 days	2398	46.6	-	5.26	-	-
Thomas & Peethamparan	S0	50	-	yes	48h	-	31,5-50,3	6,1-7,6	-	26,0-35,5	0,124-0,128
Thomas & Peethamparan	S0	22	95	yes	28 days	-	16,2-28,9	2,9-6,7	-	10,5-22,6	0,126-0,128
Thomas & Peethamparan	S100	50	-	yes	48h	-	29,5-50,8	6,1-7,7	-	22,9-33,5	0,124-0,129
Thomas & Peethamparan	S100	22	95	yes	28 days	-	33,7-52,6	6,3-8,4	-	22,4-34,2	0,125-0,134

For alkali-activated concrete, it is not yet clear if the compressive strength at 28 days can be used as a safe reference for design calculations, as is the case for OPC concrete. The long-term strength development of AAC is scarcely investigated. Most of the studies only considered the strength up to 28 days and there is no certainty about strength and stiffness development of alkali-activated concrete over the long term. Namely, a few researchers reported a decrease of strength or stiffness over time, for AAC mixtures that contain blast furnace slag.

Collins and Sanjayan (2001) were the first who reported strength reduction for alkali-activated slag concrete. In their research, cylinders exposed to 50% RH and 23°C directly after unmoulding, lose 17% of their compressive strength between 56 days and 1 year, as is shown in Fig. 1.5 (left). Furthermore, the graph indicates the importance of curing, as with sealed and bath curing, compressive strength is about 2-2.5 times higher than for samples that are directly exposed to laboratory conditions (50% RH and 23°C). Fig. 1.5 (right) shows the influence of curing on the development of compressive strength for regular OPC concrete, no decrease is visible.

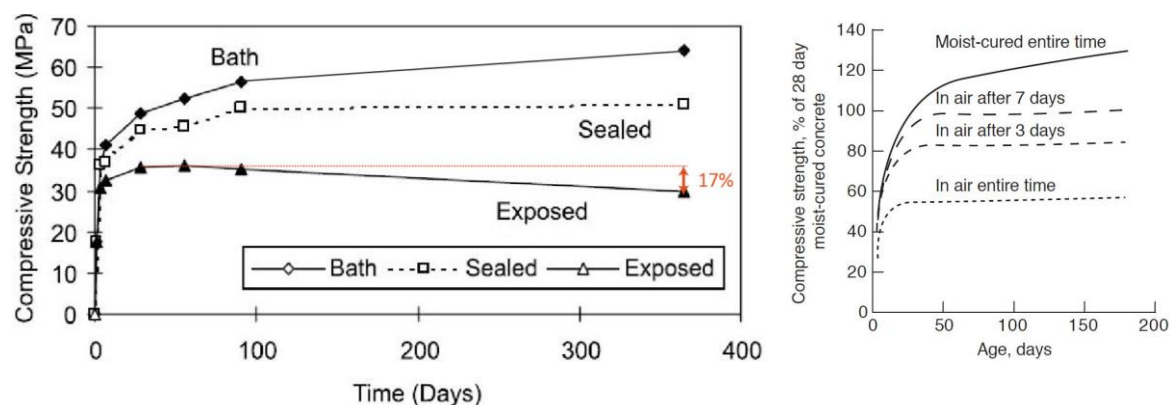


Fig. 1.5: Left: Effect of type of curing on compressive strength of alkali-activated slag (100%) concrete for w/b = 0.5. The exposed samples are kept in 50% RH and 23°C from day 1 onwards (Collins & Sanjayan, 2001, p. 348). Right: Effect of wet-curing duration on development of strength over time for regular OPC concrete, results from U.S. Bureau of Reclamation (1981). NB: curing age would not have any beneficial effect on concrete strength unless curing is carried out in presence of moisture (Monteiro & Kuhmar Mehta, 2006, p. 62)

Wardhono et al. (2017) reported a reduction of flexural strength over time for alkali-activated slag concrete, illustrated in Fig. 1.6, while compressive strength was approximately constant over time. Also, their research shows that the elastic modulus of alkali-activated slag concrete reduced with 43% between 28 and 540 days, as is shown in Fig. 1.7. Fly ash-based concrete does not show this behaviour.

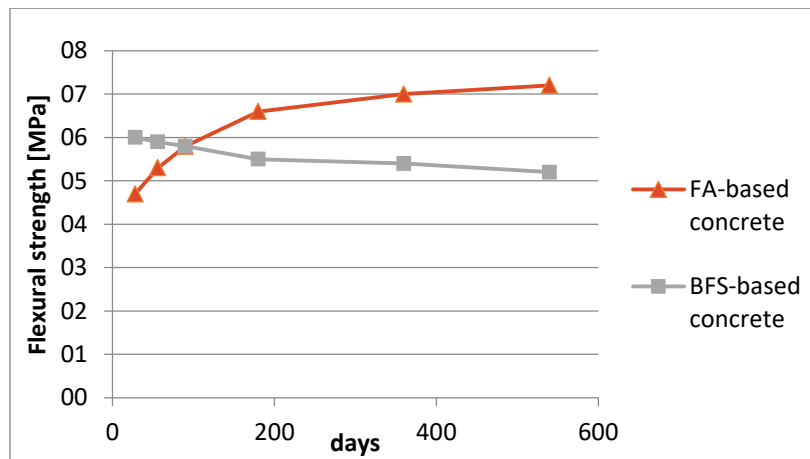


Fig. 1.6: Development of flexural strength over time for Alkali-Activated Concrete, data from Wardhono et al. (2017). BFS-samples are demoulded, water-cured (23°C) for 6 days and kept at room temp. until being tested. FA-samples were heat-cured (80°C) using dry oven for 24h, then demoulded and kept at room temp. until testing

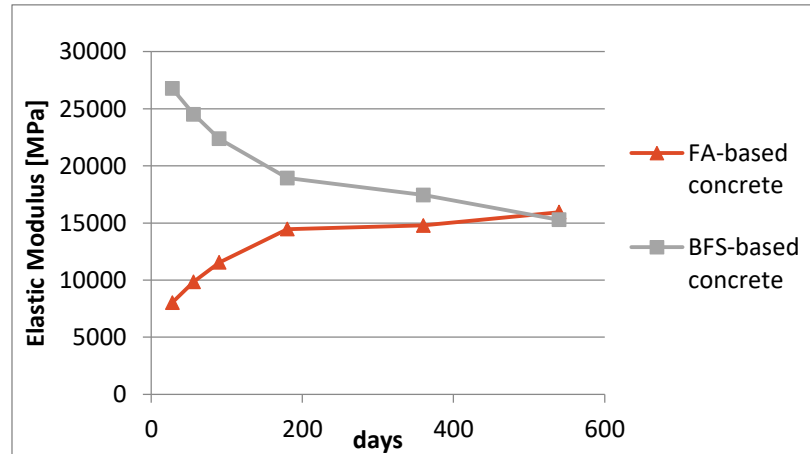


Fig. 1.7: Development of elastic modulus over time for Alkali-Activated Concrete, data from Wardhono et al. (2017). BFS-samples are demoulded, water-cured (23°C) for 6 days and kept at room temp. until being tested. FA-samples were heat-cured (80°C) using dry oven for 24h, then demoulded and kept at room temp. until testing

In order to use alkali-activated concrete as a construction material, it is evident that the material should maintain a certain performance during the design lifetime of a structure. Therefore, it is important to investigate the development of strength and stiffness properties for alkali-activated concrete and study possible strength and stiffness reductions as reported by a few researchers for alkali-activated slag concrete.

1.3. Research question

Some researchers reported a decrease of strength or stiffness over time for alkali-activated concrete containing blast furnace slag. The observed decrease might not be a very desirable phenomenon and should be well-understood prior to wider structural application of AAC. Therefore, the main research question of this thesis is: *Can a decrease of stiffness and strength over time, as sometimes reported in literature for alkali-activated concrete, also be found for alkali-activated concrete used at TU Delft and if so, what could be an explanation for this behaviour? Does the amount of blast furnace slag in the binder play a role, as a decrease over time has only been reported for alkali-activated concrete containing blast furnace slag? And if not, what other cause could lead to a decrease of properties over time?* The intention is to make some first steps into a better understanding of this phenomenon.

1.4. Outline of master thesis

In chapter 2, alkali-activated concrete is introduced. Apart from information on the binder chemistry, this chapter also addresses applications of alkali-activated concrete and the factors that limit the use of the material for practical applications. Chapter 3 gives an overview of the results that have been reported in literature, mainly about the mechanical properties of the material, like compressive strength, tensile strength and elastic modulus. Additionally, results that have been reported in literature on reinforced beams, more structural elements, are also presented. After this literature research, chapter 4 presents the approach and method that have been used for the experimental research conducted in order to answer the main research question of this master thesis. Chapter 5 deals with the results of the conducted experiments. In chapter 6, these results are analysed and discussed with respect to the main research question. Chapter 7 provides answers to the research question and summarizes the conclusions.

2

Alkali-activated concrete

2.1. Introduction

According to J. L. Provis (2014), the German chemist Kühl was the first who patented a solid material formed by the reaction of an alkali source with an alumina- and silica-containing material in 1908. The Belgian engineer Purdon further explored the creation of construction materials by alkaline-activation of blast furnace slags in the 1940s. In China and the former Soviet Union, alkali-activated binders were further developed, due to cement scarcity (J. L. Provis, Duxson, et al., 2014). Especially in the former Soviet Union a theoretical basis was established, by the Ukrainian scientist Glukhovsky. In the following decades there was not a lot of progress in the research field (Pacheco-Torgal, 2015). Important changes occurred in the 1970s, when the French scientist Joseph Davidovits researched the development of alkali-activated binders based on metakaolin. The resulting material, called 'geopolymer', was initially promoted for its good fire resistance. However, the high early strength got notable attention soon after. Davidovits introduced the term geopolymer to describe alkali-activated aluminosilicate binders. Nowadays, the term is also being used to describe a larger family of alkali-activated "calcium-aluminosilicate" binders, not only the aluminosilicate binders. In the 1980s and 1990s more important research has been conducted, but still it is only since the last decade that alkali-activated binders gained more interest. The focus on sustainable construction and the reduction of carbon dioxide emissions lead to a commercialization of more sustainable concrete binders like alkali-activated cements and geopolymers.

This chapter provides a general introduction on the constituents and chemistry of alkali-activated concrete. Furthermore, a brief overview of the (former) applications of alkali-activated concrete is presented.

2.2. Constituents of alkali-activated concrete

Concrete is a composite material that consists essentially of aggregate and a binder. Aggregate is a granular material, such as sand, gravel or stones. In regular OPC (Ordinary Portland Cement) concrete a binder consists of cement and water. Cement is not a binder by itself, but becomes a binder after hydration. However, in alkali-activated concrete the binder does not contain any cement, but is formed by an alkaline activator (dissolved in water) and a solid precursor (raw material) containing alumina and silica.

In theory, any material consisting of silica and aluminium can be alkali-activated (Li et al., 2010). When these so-called precursors are mixed with an alkaline activator, the substance will set and harden, resulting in a binder. Usually, the alkaline activator used is either an alkaline salt or a caustic (corrosive) solution in water. In *Handbook of alkali activated cements and mortars*, Garcia-Lodeiro et al. (2015b) distinguish six different categories of activators, identified by Glukhovskiy:

1. caustic solutions: MOH
2. slightly acid, non-siliceous salts: M_2CO_3 , M_2SO_3 , M_3PO_4 , MF;
3. silicates: $M_2O.nSiO_2$;
4. aluminates: $M_2O.nAl_2O_3$;
5. aluminosilicates: $M_2O.Al_2O_3.SiO_2$;
6. non-siliceous, highly acid salts: M_2SO_4 .

An interesting aspect of alkaline activation is the fact that both industrial by-products, recycled aluminosilicates and natural materials (such as clay) can be used as precursors (Garcia-Lodeiro et al., 2015b). Materials like glass waste, metakaolin, fly ash, pozzolans and blast furnace slag can all be used, as can be seen in Fig. 2.1. Furthermore, combining two or more of these materials is also possible.

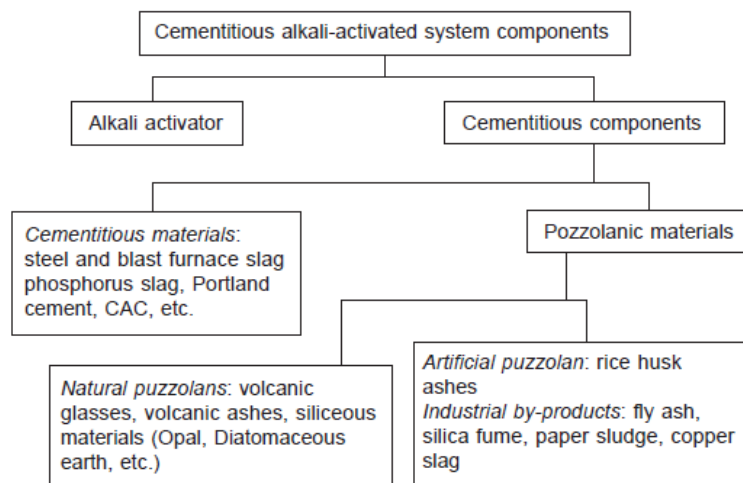


Fig. 2.1: Alkali-activated system components (Garcia-Lodeiro et al., 2015b, p. 49).

The most common industrial byproducts used as binder precursors are fly ash (FA) and blast furnace slag (BFS) (Fig. 2.2). Therefore, a brief description of those two materials is given in the following paragraphs.



Fig. 2.2: Fly ash (left) and blast furnace slag (right).

2.2.1. Blast furnace slag (BFS)

Blast furnace slag is a byproduct of pig iron production. It is formed when the slagging agents (e.g. limestone) are added to the iron ore for purification. A molten slag that floats on top of the molten iron is developed, separated from the liquid metal and cooled down. After subsequent quenching, the product is known as ground granulated blast furnace slag (GGBFS), a latent hydraulic material with pozzolanic and cementitious properties (Li et al., 2010). The chemical and physical properties of the slag are different for each specific furnace and ore, but properties of slag from a particular furnace are reasonably constant (Duxson, 2009). The common composition ranges are shown in Table 2.1. In general, blast furnace slag can be characterized as a calcium- and silicon-rich material.

Table 2.1: Mean chemical composition of blast furnace slag (Garcia-Lodeiro et al., 2015b, p. 50).

SiO ₂	CaO	Al ₂ O ₃	MgO	Fe ₂ O ₃	S	Cr ₂ O ₃	Na ₂ O+ K ₂ O	MnO ₂	P ₂ O ₅	TiO ₂
27–40%	30–50%	5–33%	1–2.1%	<1%	<3%	0.003– 0.007%	1–3%	< 2%	0.02– 0.09%	<3%

The reactivity of slag is, amongst other things, influenced by particle size. Big particles react very slow, the more 3– 20 μm particles are present, the higher the long-term strength is (Wan et al., 2004). So, the particle size is a key factor in the alkaline activation of blast furnace slag; influencing the reaction, setting, strength development and microstructure (Bernal et al., 2014).

2.2.2. Fly ash (FA)

Fly ash is a byproduct of coal-fired power plants. It is formed during coal combustion, used as fuel for the generation of electric power. The fly ash is removed as a fine particle residue, before the combustion gases are released into the atmosphere via the chimney. The composition of fly ash is very dependent on the impurities in the coal before combustion, as well as on the properties of the combustion process (Duxson, 2009). Therefore, the chemical properties of fly ash vary substantially. In general, silica and

alumina are its main constituents. However, fly ash is generally classified into two main categories, depending on the lime content present (Garcia-Lodeiro et al., 2015b). The common compositions of both types are shown in Table 2.2. Type F fly ash, characterized by lower calcium content, is mostly used for geopolymer binders. Research on the use of type C fly ash for geopolymerisation is limited, probably due to the rapid setting properties (Duxson, 2009).

Table 2.2: Average percentage (weight percentage) of the compounds in high- and low-calcium fly ash (Garcia-Lodeiro et al., 2015b, p. 54)

Component	Type C fly ash: with a high CaO content	Type F fly ash: with a low CaO content
SiO ₂	34.1	42.6–59.8
Al ₂ O ₃	14.2	21.8–34.5
Fe ₂ O ₃	7.2	6.3–18.1
CaO	38.0	2.8–7.0
SO ₃	4.2	0.19–1.9
MgO	1.5	1.2–2.6
K ₂ O	1.4	0.38–6.0
Na ₂ O	0.44	0.15–0.94
Reactive silica	30.9	0.94
Free lime	17.1	Very low 0.74

2.3. Categorisation alkali-activated binders

The large amount of different activators and precursors results in a wide variety of alkali-activated binders, Fig. 2.3 illustrates the most commonly used precursors, and their typical composition range. The hardening process for these alkali-activated cements is very dependent on the used precursor(s) or activator, and the ratio between both components.

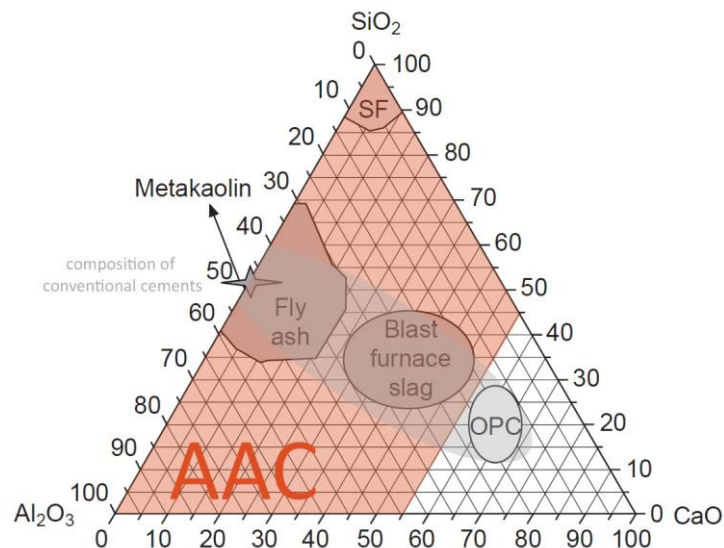


Fig. 2.3: Usual range of compositions of raw materials used to manufacture alkaline cements (Garcia-Lodeiro et al., 2015b, p. 50)

Both Palomo et al. (1999) and Garcia-Lodeiro et al. (2015a) divided the alkaline cements into two main categories. This division is shown in Table 2.3. The first type is the activation of a calcium-rich precursor

(eg. blast furnace slag) by a mild alkaline solution, with C(A)SH as a main reaction product. The second category of alkali activation is categorised by activating a low-calcium precursor (eg. metakaolin or class F fly ash) with medium or high alkaline solutions. This results in zeolite-like polymers, the French material scientist Davidovits named this second category ‘Geopolymer’ because of their polymeric structure.

Table 2.3: Products precipitating in different types of binders (Garcia-Lodeiro et al., 2015a, p. 23)

Binder type		OPC	Alkaline cement	
			$(Na,K)_2O-CaO-Al_2O_3-SiO_2-H_2O$	$(Na,K)_2O-Al_2O_3-SiO_2-H_2O$
Reaction product	Primary	C-S-H	C-A-S-H	N-A-S-H
	Secondary	Ca(OH) ₂ AF _m AF _t	Hydrotalcite [Mg ₆ Al ₂ CO ₃ (OH) ₁₆ ·4H ₂ O] C ₄ AH ₁₃ CASH ₈ C ₄ AcH ₁₁ C ₈ Ac ₂ H ₂₄	Zeolites: geopolymers hydroxysodalite, zeolite P, Na- chabazite, zeolite Y, faujasite

C = CaO, S = SiO₂, A = Al₂O₃, N = Na₂O, H = H₂O, c = CO₂

J. Provis and van Deventer (2014) made a simplified overview of alkali-activated materials, shown in Fig. 2.4, in which they classify geopolymers as a subset of alkali-activated materials. However, Davidovits does not agree with this, according to him, geopolymers are not a subset of AAM because they are not a calcium hydrate alternative and polymer chemistry is very different from hydrate chemistry (Geopolymer Institute, 2015).

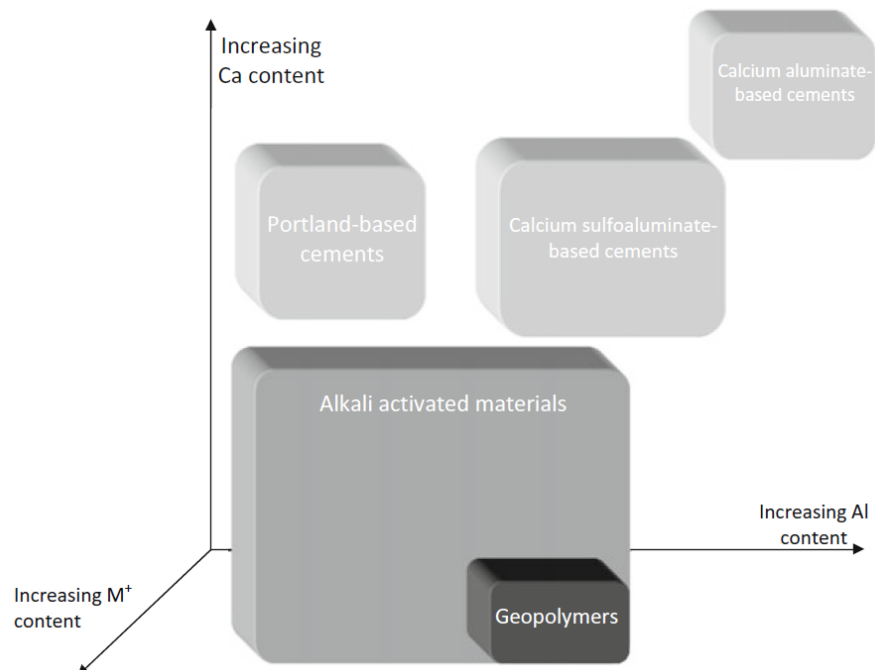


Fig. 2.4: Classification of alkali-activated materials, shading indicates alkali content, darker shading corresponds to higher Na and/or K concentrations. Diagram courtesy of I. Beleña (J. Provis & van Deventer, 2014, p. 8).

However, the term geopolymer is currently the generally accepted name for the whole range of alkali-activated binders. Still, in this thesis research, the term geopolymer will only be used for alkali-activated low-calcium binders. As pointed out before, the activation of the cementitious components is different for both categories. The following sections will provide a brief description of these different processes.

2.3.1. High-calcium binder chemistry (BFS)

When high-calcium precursors (like blast furnace slag) are used to make a binder, the main reaction product is a C-A-S-H (calcium-silicate-hydrate) gel, comparable to the product that is obtained during the hydration of ordinary Portland cement. According to Garcia-Lodeiro et al. (2015a) the gel has a lower calcium/silica (C/S) ratio than in Portland cement paste.

There is discussion in literature about the type of reaction products that are formed during the alkaline activation of high-calcium precursors. Nevertheless, it is clear that the structure of binders formed by alkali-activation of calcium-rich precursors like blast furnace slag is very dependent on the characteristics of the raw material and the type and amount of activator used. Sodium hydroxide and waterglass are the two types of activators that are most commonly used (Garcia-Lodeiro et al., 2015a). Fig. 2.5 shows a model that describes the reaction mechanism of slag alkaline-activation. First, the slag is attacked by the alkaline solution, then C-S-H reaction products are formed.

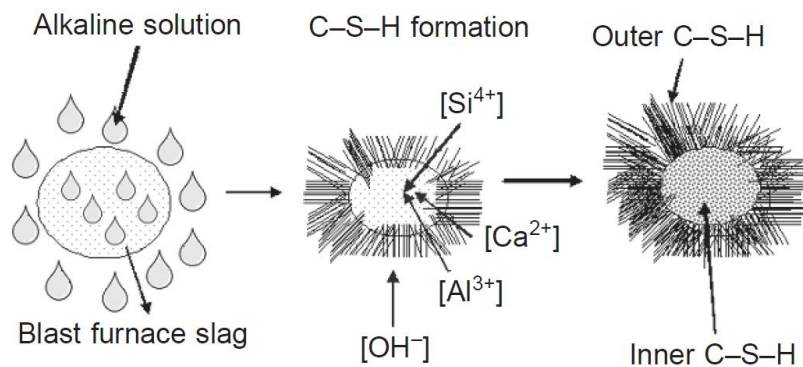


Fig. 2.5: Theoretical model for the reaction mechanism in alkali-activated slag, based upon a model by Glasser in 1990 (Garcia-Lodeiro et al., 2015a, p. 22)

2.3.2. Low-calcium binder chemistry (FA)

According to Garcia-Lodeiro et al. (2015a), the alkali-activation process of low-calcium precursors (like fly ash) is relatively new and therefore less thoroughly understood than the activation of high-calcium binders like blast furnace slag. Duxson et al. (2007) proposed a model (Fig. 2.6) for the process of geopolymerisation, divided into five main stages: (1) dissolution, (2) speciation equilibrium, (3) gelation, (4) reorganization and (5) polymerization and hardening. These processes are coupled and occur simultaneously, although the steps are presented linearly in Fig. 2.6. The activation process begins with the alkali-activated solution that tears into fly ash particles. This results in reaction product at both the in-

and outside of the particle, until the fly ash particle is (almost) consumed. Fig. 2.7a and Fig. 2.7b show partially reacted fly ash particles.

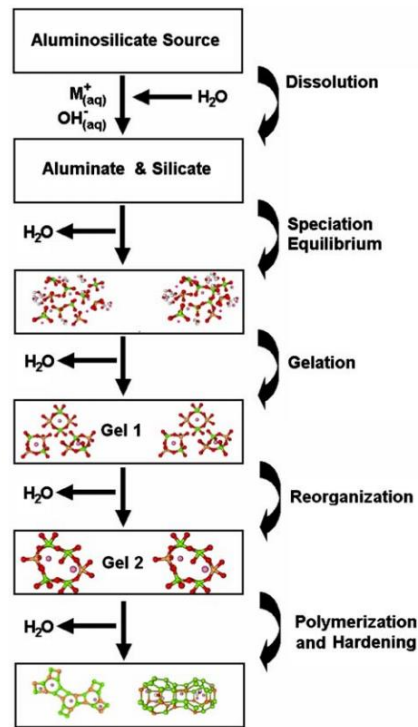


Fig. 2.6: Conceptual model for geopolymerisation (Duxson et al., 2007, p. 2919)

2.3.3. Combined systems

In the previous paragraphs, the two main categories of alkali-activated binders have been discussed. However, low-calcium (eg. fly ash) and calcium-rich (eg. blast furnace slag) precursors can also be mixed to create a binder. This results in a combined system, where a good synergy between mechanical strength and durability can be achieved, according to Provis and Bernal (2014). In their opinion, there is a growing focus on these hybrid systems, because they are characterised by the stable coexistence of the reaction products characteristic of hydration of Portland clinker or alkali-activated BFS (C-S-H gels, as explained in paragraph 2.3.1) and alkali-activated aluminosilicates like fly ash resulting in geopolymeric gel (explained in paragraph 2.3.2). So, coexistence of C-S-H gels and N-A-S-H type of gels is the main microstructural feature of hybrid systems.

Mixing reactive calcium-rich precursors (like slag) with low-calcium materials (like fly ash) seems to be a good method to be able to use low-calcium materials that do not provide sufficient strength development when they would be activated alone, because of lacking reactivity. Provis and Bernal (2014) summarized some interesting results: Li and Liu showed that adding only 4 percent BFS to a 90% fly ash/10% metakaolin mixture, that was cured for 14 days, increased the strength with more than 40%. Kumar et al. (2010) reported that fly ash had more influence in the total reaction product for curing under elevated temperatures (60°C), while blast furnace slag contributed more to the system chemistry when cured at

lower temperatures (27°C). A few of their Scanning Electron Microscopy pictures are shown in Fig. 2.7. So, it is clear that blending different types of precursors can be used to optimize alkali-activated concretes.

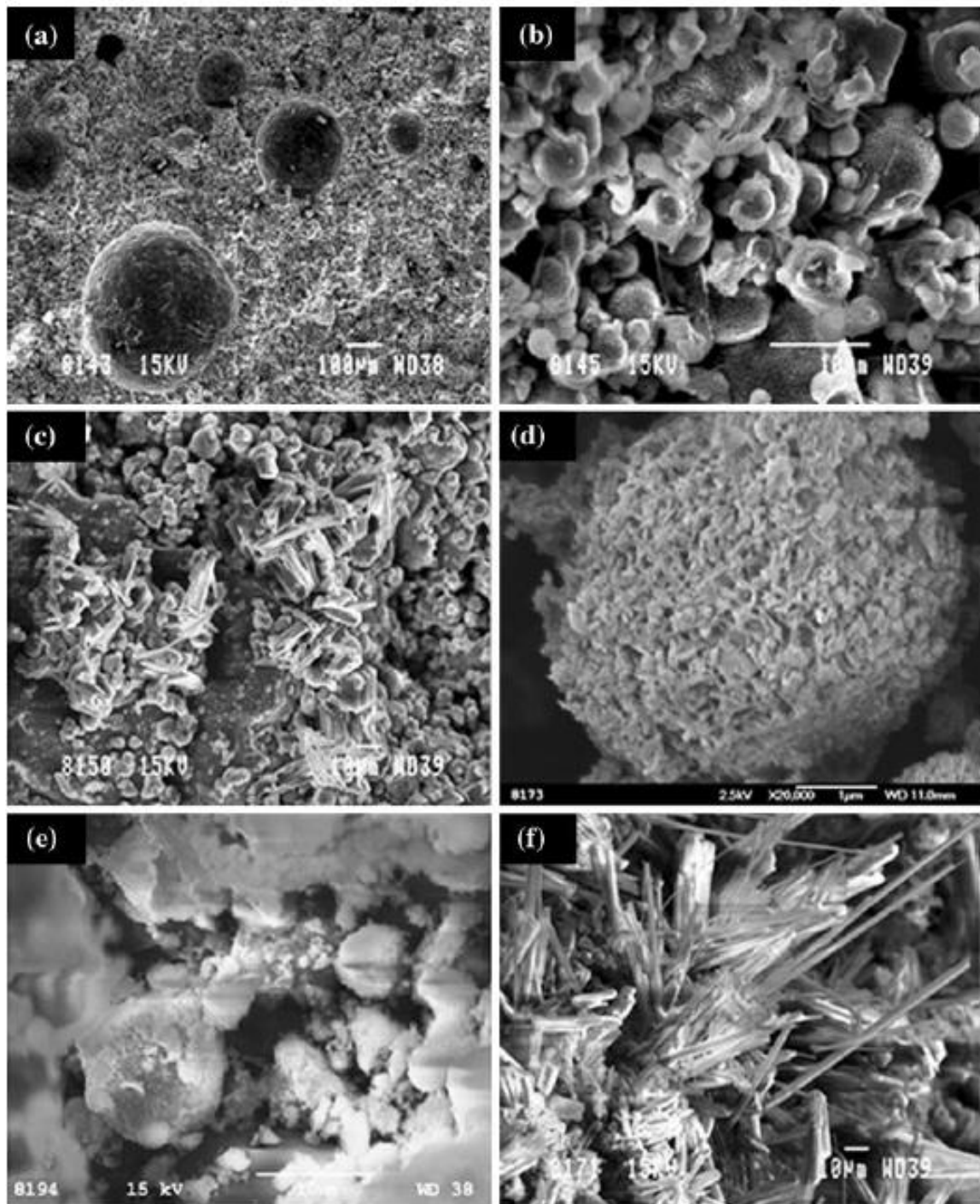


Fig. 2.7: Scanning Electron Microscopy images of alkali-activated concrete, showing (a) a partially reacted cenosphere in fly-ash based geopolymer ; (b) sample with 15% slag showing fly ash cenosphere coated with reaction product; (c) sample with 35% slag showing short prismatic structure; (d) sample with 15% slag showing cenosphere with reaction product on the surface; (e) sample with 25% slag showing dense gel phase and (f) samples with 35% slag showing fibrous products (Kumar et al., 2010, p. 612)

2.4. Benefits of using alkali-activated concrete

Nowadays, there is an increasing focus on sustainability and energy consumption, because of the problems that arise due to global warming. For the building industry, this means that apart from economic efficiency (including quality, costs and time), there are new demands concerning sustainable construction to reduce the environmental impact. Alkali-activated concrete can be a more sustainable alternative for energy-consuming ordinary Portland cement concrete, as was already explained in paragraph 1.1 *Background*. For example, the emitted amount of CO₂ is about 55-75% lower for alkali-activated concrete compared to OPC concrete (Yang et al., 2013), as is shown in Fig. 2.8. The CO₂-footprint of alkali-activated concrete is fairly dependent on the type, concentration and dosage of the activator.

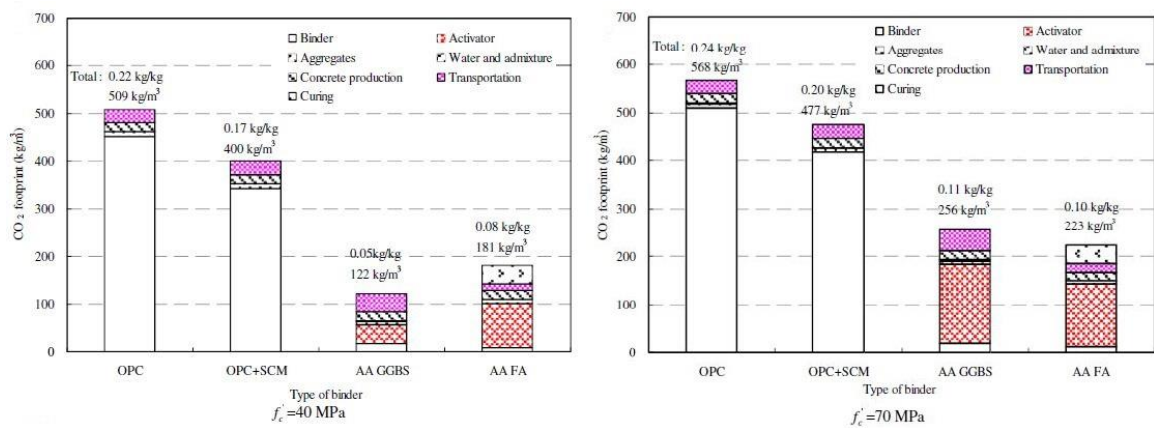


Fig. 2.8: CO₂ footprint for different concrete types.(Yang et al., 2013, p. 269)

Apart from the fact that less CO₂ is emitted during the production of alkali-activated concrete, it is also sustainable that byproducts from several industries can be re-used. In Western Europe, re-using materials like fly ash and blast furnace slag is already applied. Some European countries utilize almost 100% of fly ash and types of slag (Manz, 1997; vom Berg & Feuerborn, 2015), making Europe a world-leader in re-using industrial byproducts. Especially ground granulated blast furnace slag is almost entirely utilized due to its beneficial properties for Portland cement concretes (J. L. Provis, Duxson, et al., 2014).

However, in countries like China and India, characterized by enormous urban and infrastructural developments, electricity is often generated in coal-fired power plants. This results in a lot of available fly ash. Coal ash is even China's largest single source of industrial solid waste (Greenpeace, 2010). *O* shows the current utilization rates of fly ash for the US, India and China. The level of re-use in 2015 is estimated at 50% for the US, 60% for India and about 70% for China (Yao et al., 2015). However, Greenpeace states that, while it is widely believed that over 60% of coal ash is re-used in China, in reality the rate is likely less than half of this. According to them, this impression results from the reporting of false data by the power companies as well as inadequate government control waste (Greenpeace, 2010). In each case it is clear that a significant proportion of fly ash is left-over and could be re-used. Therefore, countries facing huge urban and infrastructural developments (like China and India) are likely to be the primary areas in which alkali-activation technology can be very important and influential (J. L. Provis, Duxson, et al., 2014).

Not only sustainability, but also durability can be a reason to apply alkali-activated concrete. Portland cement concrete is not the optimal solution for all construction applications, as it suffers from durability problems in aggressive environments (Juenger et al., 2011). It is often claimed that alkali-activated concrete has better durability properties than regular OPC concrete. It has a good freezing and thawing resistance and better resistance against acids (J. Provis & van Deventer, 2014; Wang et al., 1995). In 2015, alkali-activated concrete was used for a floor in a milk-powder factory in the Netherlands, as the concrete for this application needs to have a high resistance against acids. With regular OPC concrete, the floor had to be renewed every few years. This is an example of a possible application direction of alkali-activated concrete.

Another advantage of alkali-activated concrete is the fact that it is much easier to produce high-strength concrete with alkali-activated cements than with regular OPC. Alkali-activated slag concrete with a compressive strength of about 70-120 MPa is approximately 10-40% cheaper and saves 60-80% in coal usage when compared to high strength OPC (with added silica fume) concrete (Wang et al., 1995).

Furthermore, alkali-activated concrete is claimed to have better fire resistance than ordinary Portland cement concrete. The residual strength of OPC concrete after a fire of 800-1000°C is about 20-30% because of microstructural destruction and dehydration (Singh et al., 2015). For alkali-activated concrete, especially low-calcium geopolymer concrete, the high permeability acts as an escape route for moisture in the matrix, thereby decreasing the damage during a fire.

However, it is important to emphasize that the physical and chemical properties of alkali-activated concrete vary a lot. For traditional OPC concrete, most properties can be adjusted by modifying the water-cement ratio. This is not the same in alkali-activated concrete. Instead of using Portland cement and water, many different raw materials and alkali activators can be combined to form a binder. Alkali-activated concrete based upon slag has different properties than fly ash-based concrete. A combination of both precursors, or choosing a different activator, results again in different properties. So, the properties of alkali-activated concrete depend largely on the used raw materials, chosen activator and the curing conditions. Thus, it is necessary to investigate how the composition of mixtures affects the properties of alkali-activated concrete.

2.5. Factors that limit the use of alkali-activated concrete

The use of alkali-activated concrete is still limited, despite the fact that a lot of research has been conducted in the past few decades. There are several aspects that make application of alkali-activated concrete difficult. First of all, there is a large variation in properties of alkali-activated concrete, due to the many possible combinations of components (activators and precursors) in the alkali-activated binder (SBRCURnet, 2016). Furthermore, Also, the chemical and physical properties of slag or fly ash are very dependent on the source of the raw materials. So, non-uniformity and local unavailability of raw materials make it hard to use alkali-activated concrete on the scale of regular concrete (Garcia-Lodeiro et al., 2015a).

The absence of specifications and standards is another factor that makes it difficult for the building industry to apply the material. Alkali-activated concrete has a different microstructure than ordinary Portland cement concrete, therefore, assumptions in codes may not be valid for alkali-activated concrete. An additional problem is the limited experience in practice and the fact that little is known about the long term behaviour and durability of the material. The workability of alkali-activated concrete is another challenge. Compared to OPC concrete, alkali-activated concrete seems to harden much faster. Vermeulen and de Vries (2015) reported an open time of about 90 minutes, after which they had to rescue their truck-mixer using a lot of water and aggregate. However, the fact that the material hardens faster than regular OPC concrete is not necessarily a negative thing, for the precast industry this could be an efficient feature.

2.6. Applications

Already in the 1980s and 1990s, a few buildings have been built using alkali-activated slag. These structures were mainly built in countries where frost resistance was an important structural issue, like Russia and Ukraine. Recently, reinforced alkali-activated geopolymer concrete elements have been applied in, for example, Australia, both precast and cast in-situ Aldred and Day (2012). In this paragraph some of these projects, both older and recent projects, will be highlighted.

2.6.1. Projects in the former USSR

Up to 1989, more than 3 million cubic metres of alkali-activated slag concrete was used in the former USSR. Also, national conferences on alkali-activated concrete were held and national standards have been produced. Alkali-activated concrete has been used for floor slabs, foundation piles, road elements, railway sleepers, columns, beams, dams, irrigation canal and centrifugal pipes (Wang et al., 1995). A few of projects, some of them were in use since 1962, have been examined in 1973 and 1984. During this inspection, no structural damage was observed. Furthermore, the frost resistance, strength and impermeability of the concrete had developed significantly during the service years, as is shown in Table 2.4. Wang et al. (1995) even state that ordinary Portland cement concrete, under the same conditions, showed less increase in strength and durability.

Table 2.4: Case studies in the USSR, strength and frost-resistance results (Wang et al., 1995, p. 100)

Application	Service years	Aggregate type	Original strength: MPa	After service		Strength increase: %
				Frost-resistance cycles	Strength: MPa	
Canal surface (under water)	11	Secondary sand rock	15	900	42.6	184
Canal surface (in air)	11	Secondary sand rock	15	900	40.0	167
Water pond	9	Sea sand	25	700	59.5	138
Pile	9	Sea sand	30	600	71.8	139
Road surface	8	Sea sand	16	250	47.6	198
Dam	8	Sea sand	30	570	62.0	107
Pipe	7	River sand	30	—	83.0	177
Floor member	2	Carbonate	90	1115	101.0	11
Floor member	2	Granite	96	1115	122.0	27
Floor member	2	Carbonate	70	1000	110.0	57

Not only parts of buildings have been made using alkali-activated slag concrete, several high-rise buildings were built between 1986 and 1994 by the industrial company Tsentrmetallurgremont in Lipetsk, Russia. One of these buildings, a 24-storey building, is shown in Fig. 2.9. Floor slabs, stairways and other structural elements were pre-cast, the exterior walls were cast in-situ. The concrete for this in-situ elements was transported from the mixing location to the building site with regular concrete trucks, and the concrete has been cured with electrical heating elements.

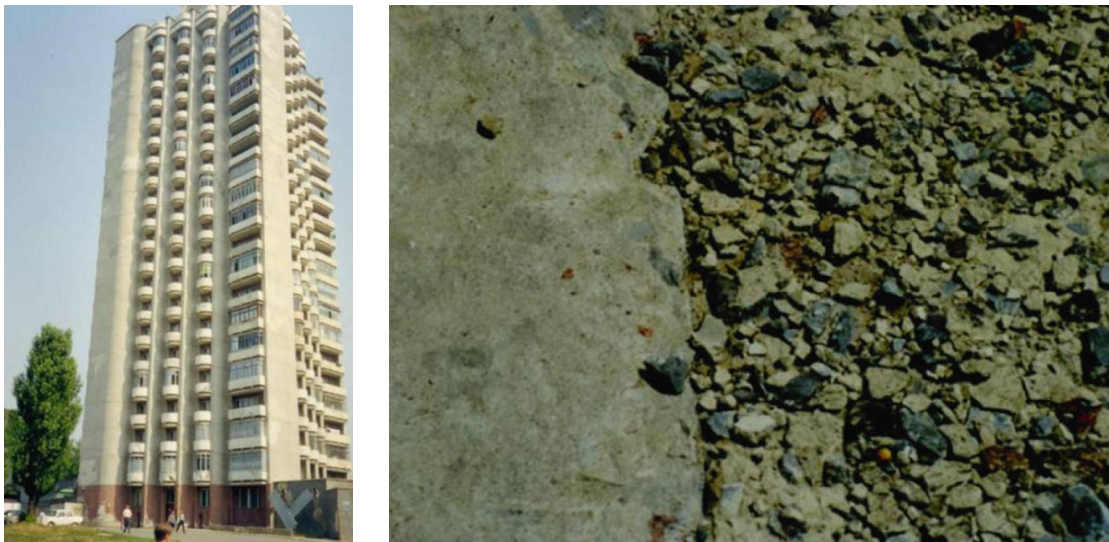


Fig. 2.9: left: 24-storey building in Lipetsk, Russia, built in 1994 with alkali-activated slag concrete, right: Comparison of cast-in-situ alkali-activated slag concrete (left) and ordinary Portland cement concrete road (right) in Ternopol, Ukraine (J. L. Provis, Brice, et al., 2014, p. 316).

Between 1984 and 1990, a 330 meters long cast-in-situ alkali activated slag concrete road and fountain basin were constructed by an industrial enterprise in Ternopol, Ukraine. The road, basin and other equivalent structures built side-by-side with regular ordinary Portland cement concrete were inspected in 1999 (J. L. Provis, Brice, et al., 2014). The comparison can be seen in Fig. 2.9. The structures built with ordinary Portland cement concrete showed serious deterioration, while the road and basin built with alkali-activated slag concrete exhibited good conditions.

2.6.2. Storehouse in Kraków

In Kraków, in 1974, a storehouse has been built using alkali-activated blast furnace slag concrete. The mix composition is shown in Table 2.5. Precast reinforced floor slabs and wall elements have been cast and cured in air at 70 °C for 6 hours, before installing them in the building. The building is shown in Fig. 2.10.

Table 2.5: Mix composition of alkali-activated slag concrete used in Kraków

ground granulated blast furnace slag	300 kg/m ³
mixed aggregates	1841 kg/m ³
Na₂CO₃	18 kg/m ³
water	140 kg/m ³



Fig. 2.10: 6-storey building in Kraków, built with alkali-activated slag concrete in 1974 (J. L. Provis, Brice, et al., 2014, p. 314)

One very interesting aspect of this building is the fact that it has been monitored for many years. And, 27 years after construction, cylinder specimens (diameter 100 mm) were taken from the wall panels and tested on compressive strength and carbonation depth. Furthermore, the microstructure has also been examined from these samples. Table 2.6 shows the test results of compressive tests. It is clear that there is a significant increase in strength from 28 days until 27 years for all specimens. The microstructure showed dense C-S-H binders and no microcracking. Furthermore, no steel corrosion has been observed after 27 years of lifetime.

Table 2.6: Compressive strength of alkali-activated slag concrete cores of a storehouse built in 197 in Krakow, Poland (J. L. Provis, Brice, et al., 2014, p. 315)

Sample	Compressive strength (MPa)	
	28 days	27 years
1	22.1	43.4
2	21.7	41.9
3	21.2	46.2
4	22.3	41.1
5	23.1	45.1
6	22.8	41.6
Average	22.6	43.2

2.6.3. Global Change Institute in Brisbane

The Global Change Institute, part of the University of Queensland, is the first building in the world where alkali-activated geopolymer concrete has been used for structural purpose, according to the Geopolymer Institute (2013). However, in the past buildings have been built using alkali-activated slag, as described in the previous paragraphs. Therefore, this is the first multi-storey building where 'modern' geopolymer concrete, containing fly ash, is used. The four-storey building, shown in Fig. 2.11, features three geopolymer concrete floors made with 33 precast elements. Two beam sizes have been used, both 2.4 meters wide, spanning 10.8 and 9.6 meters respectively. The beams have a curved soffit, and contain pipes for temperature controlled heating of the building (Aldred & Day, 2012).



Fig. 2.11: Render of the Global Change Institute (left) and at the right a geopolymer concrete beam, with a length of 10.8 meters, being craned into position (Aldred & Day, 2012, p. 14).

3

Material and structural properties of alkali-activated concrete

3.1. In general

A thorough understanding of the mechanical properties of alkali-activated concrete is essential for practical applications. This chapter provides an overview of the mechanical properties of AAC and the results reported in literature. The following mechanical properties are discussed: compressive strength, elastic modulus, tensile splitting strength, flexural strength and flexural behaviour of reinforced AAC beams.

The results from Collins and Sanjayan (2001) and Wardhono et al. (2017), also highlighted in paragraph 1.2 *Problem statement*, both show a decline in strength for mixtures with a high amount of blast furnace slag. The slag to fly ash ratio may be a very important factor on the mechanical properties of alkali-activated concrete, according to Ding et al. (2016). They conclude that alkali-activated slag concrete has rapid strength development, whereas fly-ash based concrete generally needs heat curing. Puertas et al. (2000) also state that increasing the slag content in the binder results in higher compressive strengths.

Another important factor for the development of strength is the way of curing. Most researchers consider curing conditions, like temperature, relative humidity and curing time, as an important factor for the development of strength in alkali-activated concrete. However, the effect seems to be different for alkali-activated slag compared to concretes based on fly ash. Thomas and Peethamparan (2015) state that the mechanical strength of alkali-activated fly ash concrete shows a significant effect from curing condition, while in alkali-activated BFS concrete, different curing conditions resulted in no difference in mechanical strength. In contrast to this, Bakharev et al. (1999) investigated that heat treatment considerably accelerates the strength development of alkali-activated slag concrete, but at later ages the compressive strength of the material is reduced compared to concrete cured under ambient conditions. The research by Collins and Sanjayan (2001), as mentioned in paragraph 1.2 *Problem statement*, also shows a significant effect of curing conditions on the compressive strength of alkali-activated slag concrete (Fig. 1.5). The air-exposed sample is characterised by little strength development compared to the sealed and bathed samples.

It seems that the BFS/FA ratio and curing conditions are of paramount importance for the properties and their development over time. Therefore, for each mechanical property, the influence of BFS/FA ratio and curing conditions will be examined. Furthermore, the development of strength or stiffness over time will be discussed, as far as research has been conducted in that specific area. After discussing all these properties, the second last subchapter will deal with flexural strength of reinforced beams, to investigate how alkali-activated concrete behaves when reinforcement is added. In order to be able to use alkali-activated concrete for practical applications, research should not only focus on mechanical properties, but also on more structural elements. The final subchapter summarizes the information that has been retrieved during the literature review with respect to the main research question.

3.2. Compressive strength

The compressive strength of regular Portland-cement concrete is the basis of all codes, based on compressive strength and its correlation with the other properties, most of the material properties of OPC concrete can be estimate quite well. Like in regular OPC concrete, reported AAC compressive strengths range from very low to very high values. Strengths of more than 50 MPa have been widely reported by several authors.

The development of strength is realised by the formation of calciumsilicate or aluminosilicate components in the alkali-activation process. This process depends on a lot of factors, like: chemical composition of raw materials, particle size distribution, type and concentration of activator (Juenger et al., 2011; J. Provis & van Deventer, 2014). Curing conditions like temperature, curing time and relative humidity also play an important role in the development of these calciumsilicate and aluminosilicate gels and thus strength development (Komljenović, 2015).

3.2.1. Influence of BFS/FA ratio

Pure alkali-activated fly ash concrete mixtures are characterized by low strength development. Therefore, elevated temperature curing conditions are needed to improve its early strength development, as suggested by Palomo et al. (1999). However, instead of energy-intensive heat curing, some studies proposed to combine high-calcium BFS with low-calcium fly ashes in order to improve early strength. Puertas et al. (2000) studied the development of compressive strength over time of alkali-activated paste specimens ($1 \times 1 \times 6 \text{ cm}^3$) with different fly ash/slag ratios and activator concentrations NaOH (2 or 10 M) for different curing temperatures, see Fig. 3.1. Some samples were cured at 65°C during the first 5 hours, other specimens were cured at 25°C. After these five hours, all specimens were exposed to ambient temperature and 98% RH. Their study showed that as slag content in the paste increases, the compressive strength also increases.

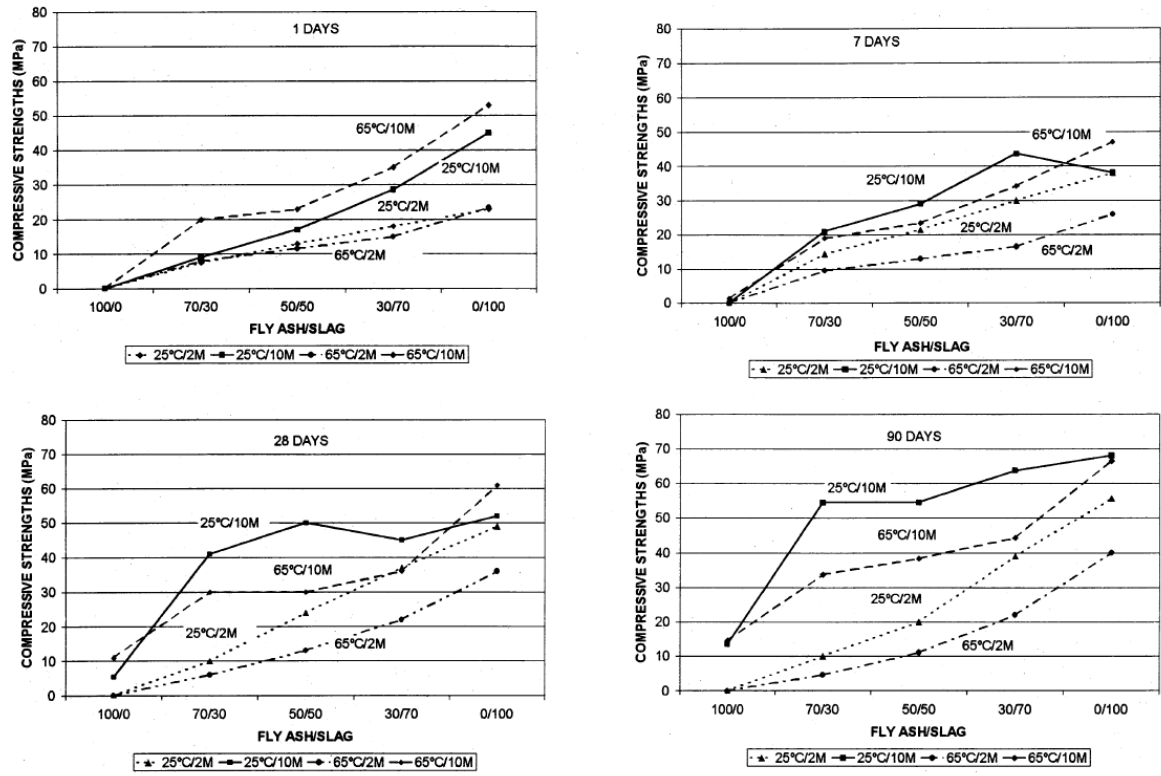


Fig. 3.1: Compressive strengths of alkali-activated mortars, for different fly ash/slag ratios (100/0; 70/30; 50/50; 30/70 and 0/100), curing temperature (65°C or 25°C during the first 5 hours) and activator concentration (NaOH: 2 or 10M) at different ages Puertas et al. (2000)

This same trend was observed by Kumar et al. (2010), as is shown in Fig. 3.2. The figure shows the compressive strength of specimens cured at 27°C for 1–28 days. The compressive strength increases for higher amounts of blast furnace slag, and increases with the age of curing.

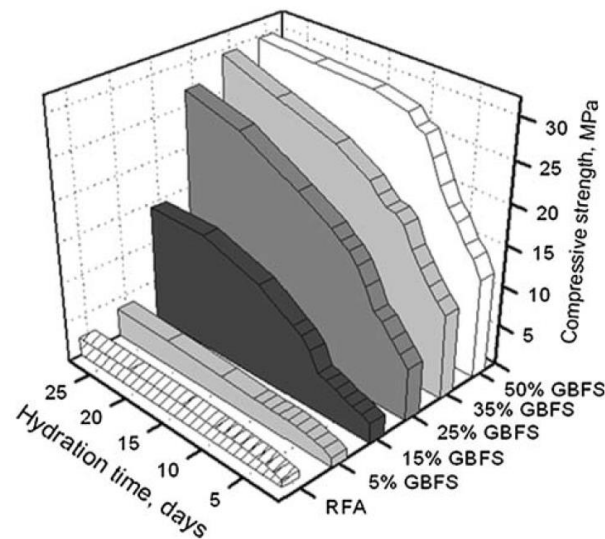


Fig. 3.2: Effect of BFS on the compressive strength, in relation to hydration time at 27°C (Kumar et al., 2010, p. 613)

Lee and Lee (2013) showed a similar result with their study on the behaviour of different slag/fly ash concrete mixes, as is shown in Fig. 3.3. Their results show that the compressive strength at 28 days increases from approximately 15 MPa to 23 MPa by using 15% of slag compared to a 10% fly ash replacement.

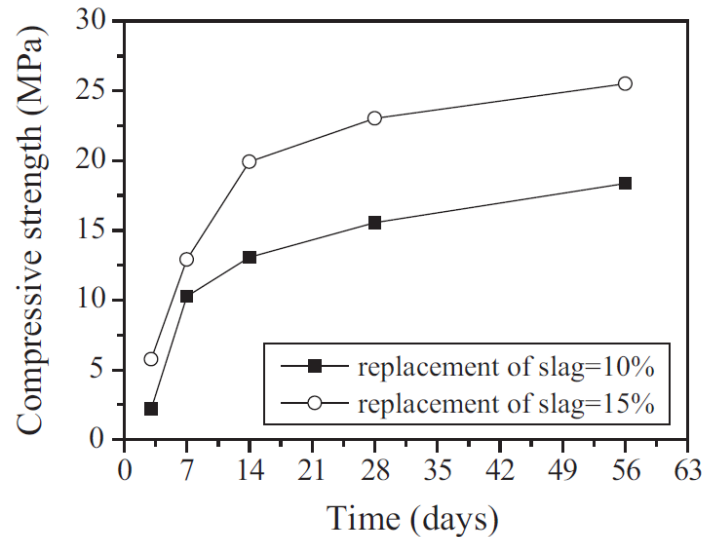


Fig. 3.3: Lee and Lee (2013) investigated the effect of slag on the 28-days compressive strength of alkali-activated BFS/FA concrete, cured until testing, 20°C and 60% RH (Ding et al., 2016, p. 71).

However, a higher amount of slag does not necessarily mean that the compressive strength increases. Fig. 3.4 (left) shows the strength development of S20, S25 and S30 concrete specimens with phosphoric acid (H_3PO_4), this was added in order to slow down the setting of the concrete. In this case, the S30 specimen showed unstable development of compressive strength at larger age compared to the S20 and S25 specimens. Also, the specimen with the highest amount of slag (S30) showed cracks, while the other specimens did not show these surface cracks. Adding phosphoric acid leads to more drying shrinkage, according to Chang et al. (2005), which is the hypothetical reason for these surface cracks. However, the other specimens cast from S20 and S25 mixtures also contained phosphoric acid, but did not show these surface cracks.

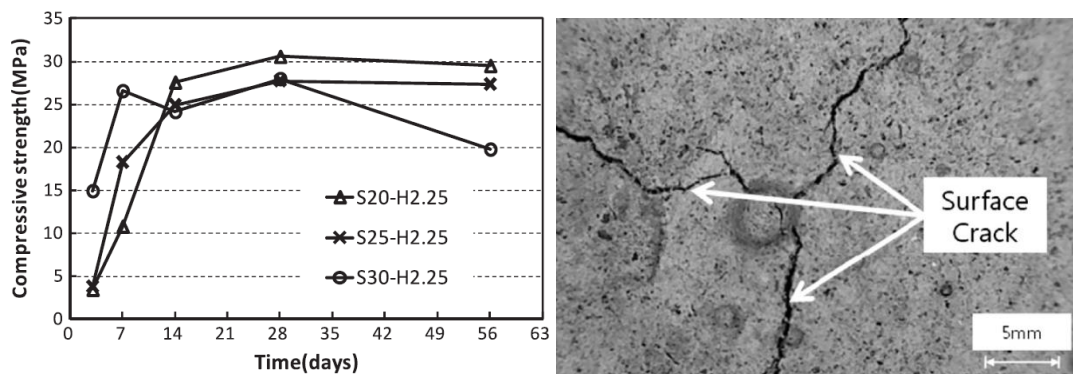


Fig. 3.4: Development of compressive strength over time for S20, S25 and S30 specimens, with added H_3PO_4 , cured until testing, 20°C and 60% RH, and the observed surface cracks (Lee & Lee, 2013, p. 1206)

3.2.2. Influence of curing conditions

As already mentioned in paragraph 1.2 *Problem statement* curing conditions seem to have a major impact on the development of compressive strength for alkali-activated concrete. Curing temperature, curing time (duration) and relative humidity can be distinguished as factors that all seem to influence the properties of AAC.

Kumar et al. (2010) investigated compressive strength development for slag/fly ash concrete mixes and concluded that heat treatment significantly accelerates the strength development of alkali-activated slag (see Fig. 3.5), however, at later ages the compressive strength reduces compared to alkali-activated concrete that is cured at room temperature (Fig. 3.6). In their opinion, the reaction at 27°C is governed by dissolution of C-S-H gel resulting from slag activation, only little interaction of BFS and FA is present. However, at 60°C, the process is regulated by both fly ash and blast furnace slag, and both C-S-H and N-A-S-H gel are formed. So, the higher initial compressive strength in case of room temperature curing can be explained by the higher amounts of resulting C-S-H gel, that improves hardening of the alkali-activated concrete.

The research by Bakharev et al. (1999) reports similar findings, they also concluded that heat-cured alkali-activated slag developed more early strength than samples cured under ambient conditions. However, at later ages the strength of heat-cured samples reduced slightly, and correlates with inhomogeneity in the concrete microstructure. According to them, heat-cured alkali-activated slag has a more open microstructure than OPC. In their opinion, the rate of reaction was much faster than the rate of diffusion, that the hydration products are located close to grains in the slag. This causes relatively open zones in-between, resulting an inhomogeneous microstructure.

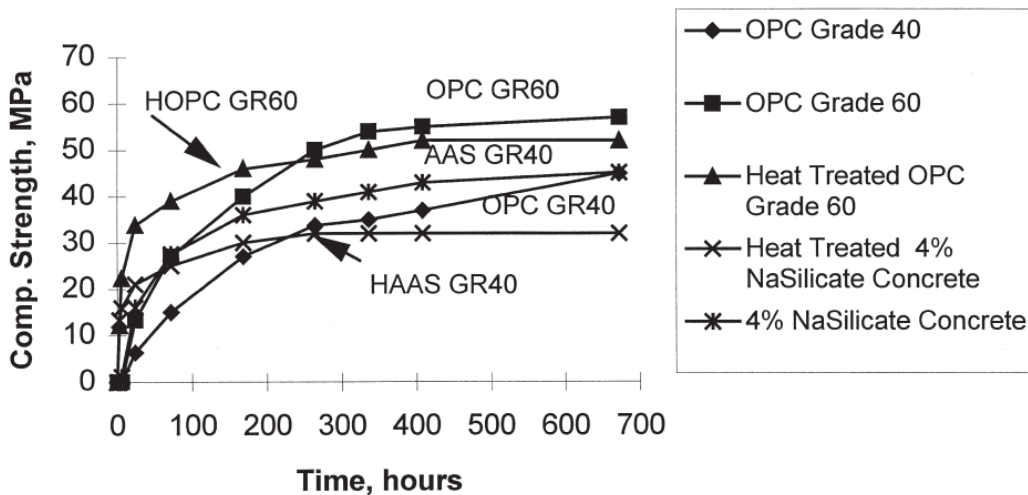


Fig. 3.5: Compressive strength development of heat-cured alkali-activated slag (HAAS GR40) concrete and regular OPC concrete (HOPC GR60) at 65°C, compared with non-heat-cured alkali-activated slag concrete (AAS GR40) and regular OPC (OPC GR40 and GR60) concrete, until the first 700 hours (Bakharev et al., 1999, p. 621)

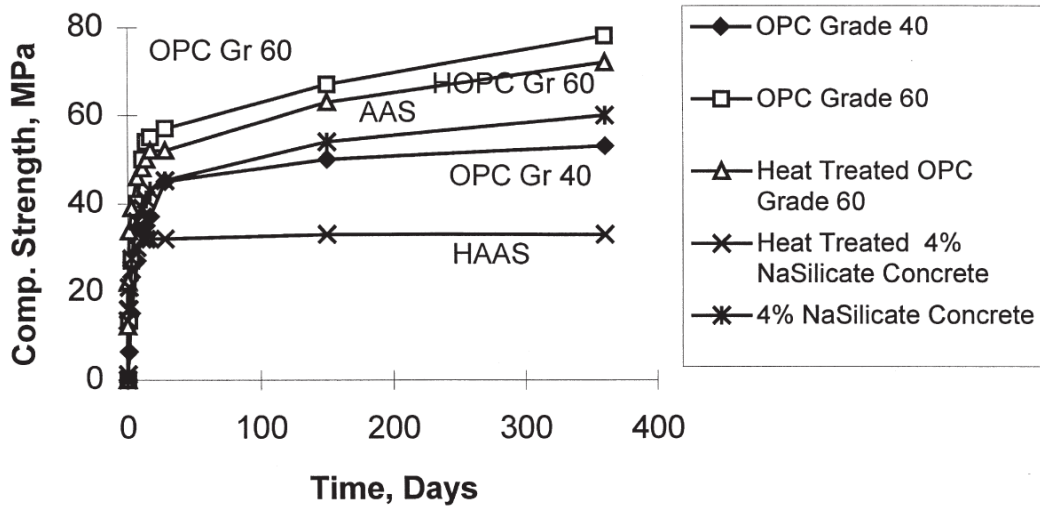


Fig. 3.6: Compressive strength development of heat-cured alkali-activated slag (HAAS GR40) concrete and regular OPC concrete (HOPC GR60) at 65°C, compared with non-heat-cured alkali-activated slag concrete (AAS GR40) and regular OPC (OPC GR40 and GR60) concrete, until the first 400 days (Bakharev et al., 1999, p. 622)

Not only curing temperature is an influential factor in the development of compressive strength, sealing conditions also seem to have some influence. The aforementioned research by Collins and Sanjayan (2001), see paragraph 1.2 *Problem statement* and Fig. 1.5, showed that for bath-cured alkali-activated slag concrete samples, the compressive strength was increasing until 400 days, while sealed specimens did not gain much strength after 91 days. Their research even showed a slight compressive strength decrease for air-exposed samples, possibly due to microcracks that developed.

3.2.3. Development over time

Few studies have investigated the development of compressive strength over time. A study by Wallah and Rangan (2006) for alkali-activated fly ash concrete indicates that, overall, the compressive strength increased over time, see Fig. 3.7. However, the increase is only about 10-20% compared to the 7-day strength, and slight drops in strength are visible.

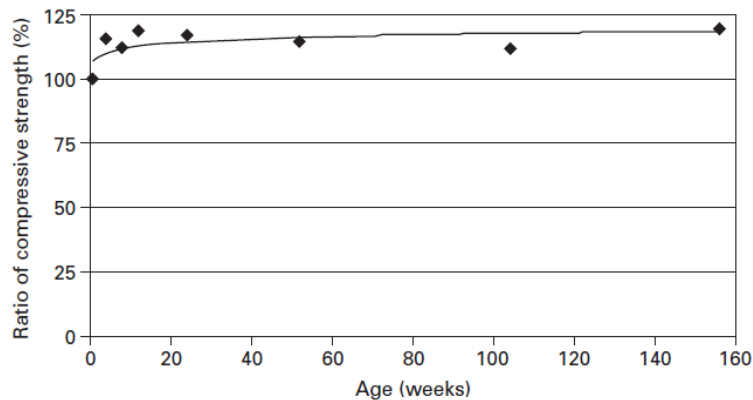


Fig. 3.7: Change in compressive strength of sealed, heat-cured (60 °C for 24 hours) fly ash alkali-activated concrete with age, compared to 7-day compressive strength (Wallah & Rangan, 2006, p. 36). The authors do not specify the conditions after curing, assumed is ambient air-exposure under lab conditions.

The research by Wardhono et al. (2017) see Fig. 3.8, shows no significant development of compressive strength over time for alkali-activated slag concrete. The compressive strength is approximately constant after 28 days. For alkali-activated fly ash concrete, this is not the case. The compressive strength increases over time and is about 48% higher at 540 days when compared to the 28-day strength.

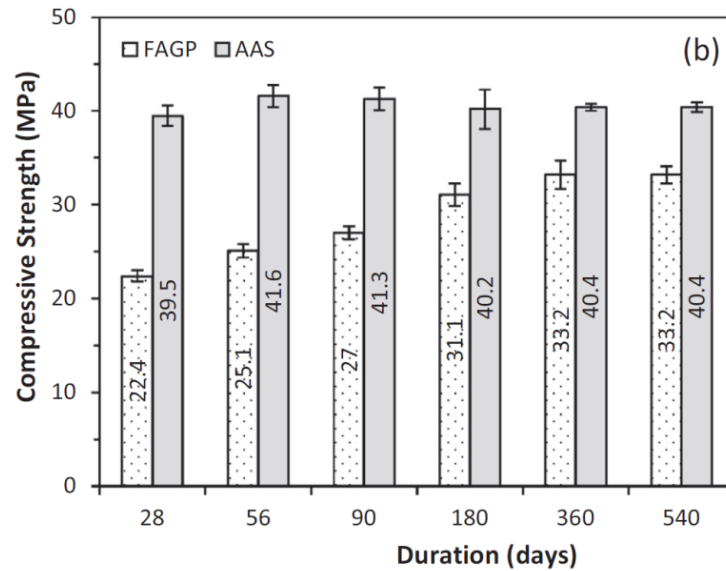


Fig. 3.8: Compressive strength development over time for alkali-activated FA- and BFS-based concrete (Wardhono et al., 2017, p. 275). BFS-samples are demoulded, water-cured (23°C) for 6 days and kept at room temp. until being tested. FA-samples were heat-cured (80°C) using dry oven for 24h, then demoulded and kept at room temp. until testing.

3.3. Modulus of elasticity

The elastic modulus is an important parameter for the design of concrete structures, it gives an indication of the resistance against elastic deformation when a force is applied. Several researchers have investigated the modulus of elasticity for a range of alkali-activated concretes, but the reported results are not very consistent. Most reported results show that the elastic modulus of alkali-activated concrete is slightly lower than that of ordinary Portland cement concrete, for comparable compressive strengths (Collins & Sanjayan, 2001; Lee & Lee, 2013; Singh et al., 2015). But, overall, most of the studies showed an elastic modulus between 10 and 40 GPa, which is comparable to ordinary Portland cement concrete.

In general, the elastic modulus of ordinary Portland cement concrete depends on the type and amount of coarse aggregate fraction. According to Kameswara Rao et al. (1974), the modulus of elasticity for OPC concrete can be accurately predicted by both the elastic modulus and poisson’s ratio of the paste, and the modulus of elasticity and poisson’s ratio of the aggregates. However, in alkali-activated concrete, the microstructure, composition of raw materials and amount of hydration also seem to have a lot of influence on the elastic modulus (Ding et al., 2016; Duxson et al., 2005).

In regular OPC concrete, the modulus of elasticity is highly correlated with compressive strength. In Eurocode 2, Equation 3.1 can be found.

$$E_{cm} = 22000 \left[\frac{f'_c + 8}{10} \right]^{0.3} \quad [Mpa]$$

Equation 3.1: f'_c [MPa] is the specified compressive strength of concrete and E_c the modulus of elasticity (EC2)

For alkali-activated concrete, such an widely applicable expression has not yet been established. Several authors reported a possible equation, however, there is no general consensus yet that these equations are applicable for all types of alkali-activated concrete. As discussed in the previous paragraph, more factors seem to influence the elastic modulus for alkali-activated concrete than in case of regular OPC concrete.

Singh et al. (2015) concluded that the modulus of elasticity of alkali-activated fly ash concrete increases for higher compressive strengths, like in OPC concrete.. Yang et al. (2012) stated that the elastic modulus of alkali-activated slag concrete can be estimated using the corresponding compressive strength, as described in the American building codes (ACI). But, the expressions in Eurocode 2 and CEB-FIB model code overestimate the elastic modulus for alkali-activated slag concrete, as can be seen in Fig. 3.9. Note that the orange line shows the EC2-expression, the authors did not plot the equation in a correct way.

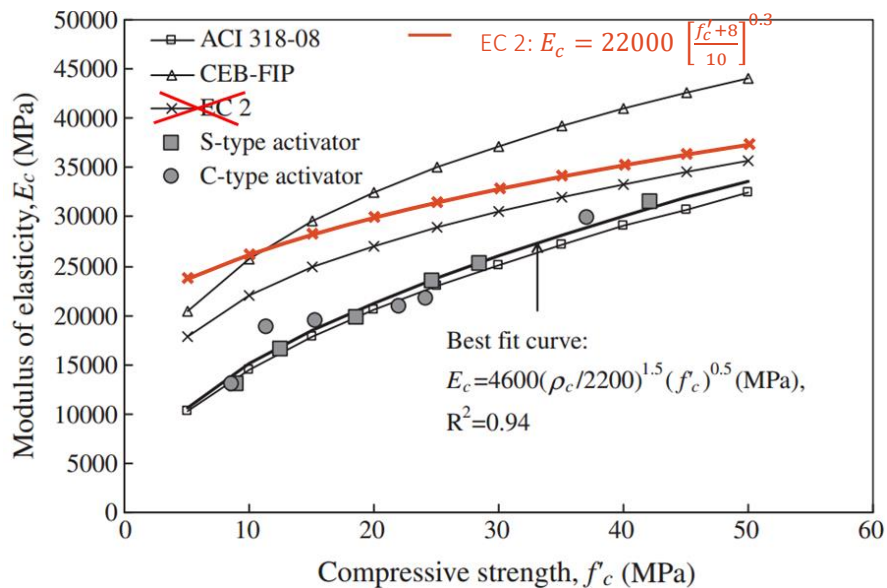


Fig. 3.9: Correlation between compressive strength and modulus of elasticity for alkali activated slag concrete, for S-type activator: $\text{Ca}(\text{OH})_2 + \text{Na}_2\text{SiO}_3$ and C-type activator: $\text{Ca}(\text{OH})_2 + \text{Na}_2\text{CO}_3$. Note that the orange line shows the EC2-expression, the authors did not plot the equation in a correct way. (Yang et al., 2012, p. 509)

It is clear that the expressions that are known for regular OPC concrete cannot be applied directly for alkali-activated concrete. It seems that the elastic modulus of alkali-activated concrete depends on more, or other factors, than in OPC concrete.

3.3.1. Influence of BFS/FA ratio

When comparing the reported results in literature, it is important to consider the ratio of blast furnace slag versus fly ash that is chosen for the conducted experiments. Lee and Lee (2013) found that the elastic modulus of their alkali-activated BFS/FA specimens were approximately 20-40% lower than described in the American concrete codes (ACI), shown in Fig. 3.10. In contrast to this, Sofi et al. (2007) reported that

the ACI codes underestimated the modulus of elasticity they found in their experiments, the elastic modulus is much higher than reported by Lee and Lee. Curing conditions for both studies are comparable, the specimens are cured at room temperature. However, the ratio of slag versus fly ash is different in both studies, and this is a possible reason for the difference in elastic modulus. The primary hydration product of alkali-activated slag is C-S-H gel, which has a higher intrinsic Young's modulus than the N-A-S-H gels that are formed for alkali-activated low-calcium fly ash. Therefore, the elastic modulus is higher in case of higher slag/fly ash ratios.

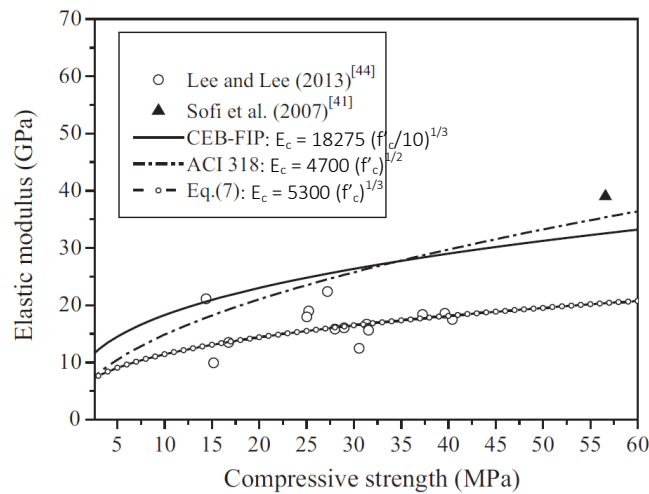


Fig. 3.10: Summary of the relationship between elastic modulus and compressive strength for alkali-activated slag/fly ash concrete (Ding et al., 2016, p. 72). Based upon results for alkali-activated slag/fly ash concrete by Lee and Lee (2013) and Sofi et al. (2007).

Thomas and Peethamparan (2015) state that the model proposed by Lee and Lee for BFS/FA concrete mixes underestimates the modulus of elasticity of their alkali-activated fly ash test results, as plotted in red in Fig. 3.11. According to them, this could be due to the higher water content of those mixes or solely due to the different mix compositions.

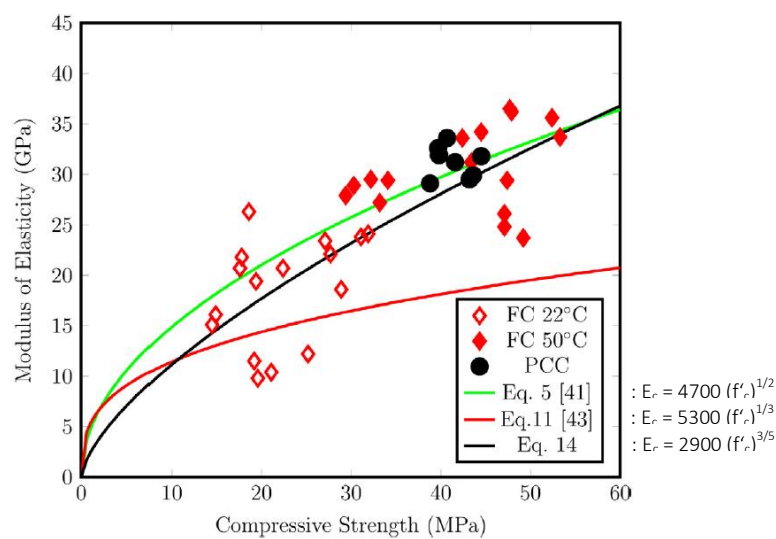


Fig. 3.11: Modulus of elasticity and compressive strength relationship for alkali-activated fly ash concrete, the red line represents the model proposed by Lee and Lee (2013), that underestimates the test results by Thomas and Peethamparan (2015, p. 54).

Ding et al. (2016) collected data from several publications on the correlation between compressive strength and elastic modulus. Fig. 3.12 (left) shows the relationship between elastic modulus and compressive strength for alkali-activated slag concrete. Fig. 3.12 (right) shows the same relationship, but then for alkali-activated fly ash concrete. Both graphs show a high variety in results, although the general trend is that for alkali-activated fly ash concrete values seem to be lower than the values that were found for alkali-activated slag concrete.

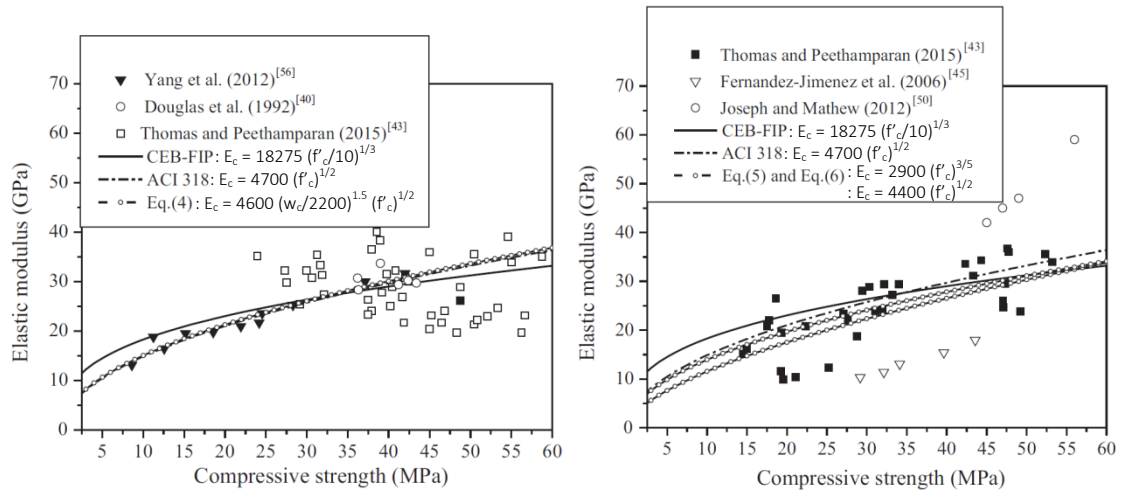


Fig. 3.12: Left: summary of the relationship between elastic modulus and compressive strength for alkali-activated slag concrete (Ding et al., 2016, p. 72). Based upon results for alkali-activated slag concrete published by Yang et al. (2012), E. Douglas et al. (1992) and Thomas and Peethamparan (2015). Right: summary of the relationship between elastic modulus and compressive strength for alkali-activated fly ash concrete (Ding et al., 2016, p. 72). Based upon results for alkali-activated fly ash concrete published by Thomas and Peethamparan (2015), Fernández-Jiménez et al. (2006) and Joseph and Mathew (2012).

Fig. 3.13 summarises all results, including the reported results on mixed slag-fly ash concretes that are shown in Fig. 3.10. It can be seen that there is significant inconsistency in all test data and that the concrete codes cannot directly be applied for alkali-activated concrete.

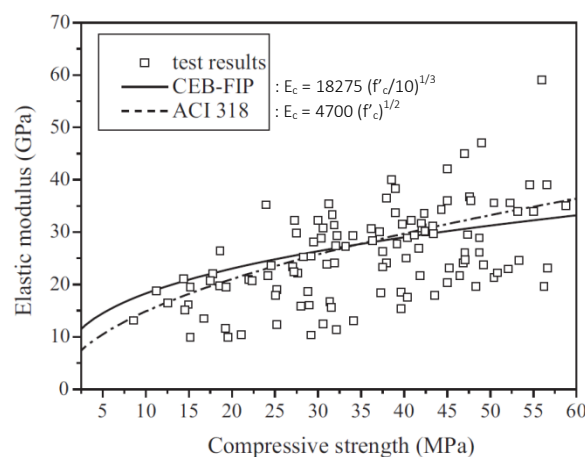


Fig. 3.13: Summary of the relationship between elastic modulus and compressive strength for alkali-activated concrete (Ding et al., 2016, p. 72). Based upon results for alkali-activated slag concrete published by Yang et al. (2012), E. Douglas et al. (1992) and Thomas and Peethamparan (2015); results for alkali-activated fly ash concrete by Thomas and Peethamparan (2015), Fernández-Jiménez et al. (2006) and Joseph and Mathew (2012); results for alkali-activated slag/fly ash concrete by Lee and Lee (2013) and Sofi et al. (2007).

3.3.2. Influence of curing conditions

For alkali-activated fly ash concretes, Wongpa et al. (2010) found that the elastic modulus decreases with increasing curing time. Thomas and Peethamparan (2015) reported that for alkali-activated slag concrete, sealed during curing, the elastic modulus seems to average around 30 GPa, as shown in Fig. 3.14. The results do not show a clear correlation between compressive strength and elastic modulus, as is the case in OPC concrete. Furthermore, for alkali-activated slag concrete (Fig. 3.14) curing temperature does not seem to have a dominant effect on the elastic modulus, both results are quite spread.

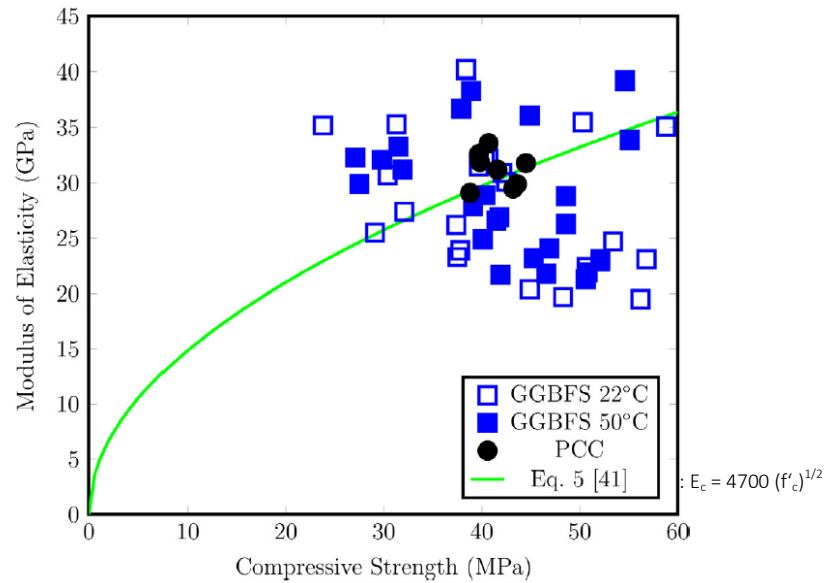


Fig. 3.14: Modulus of elasticity and compressive strength relationship for alkali-activated slag concrete. Half of the specimens were cured for 48 hours at elevated temperature ($50 \pm 0.1^\circ\text{C}$) and the other half were cured at ambient temperature ($22 \pm 1^\circ\text{C}$ and $>95\%$ RH) for 28 days. All specimens remained sealed for the duration of curing to prevent moisture loss, but after curing specimens were demoulded. (Thomas & Peethamparan, 2015, p. 54)

However, for alkali-activated fly ash concrete (Fig. 3.11) the E-modulus of samples that were cured under higher temperatures are higher than of those cured for lower curing temperatures. Hypothetically, higher curing temperatures result in a higher E-modulus for FA-based concrete.

3.3.3. Development over time

Little research has been conducted to show the development of the elastic modulus over time. In paragraph 1.2 *Problem statement*, the research by Wardhono et al. (2017) was mentioned. Their results show a decrease in elastic modulus for alkali-activated slag concrete of 43% between 28 and 540 days, as is illustrated in Fig. 3.15.

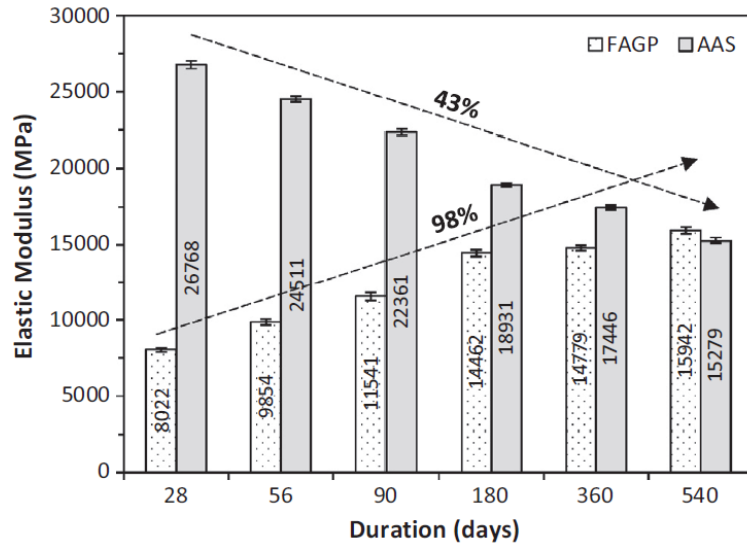


Fig. 3.15: Elastic modulus development over time for alkali-activated FA- and BFS-based concrete (Wardhono et al., 2017, p. 275). BFS-samples are demoulded, water-cured (23°C) for 6 days and kept at room temp. until being tested. FA-samples were heat-cured (80°C) using dry oven for 24h, then demoulded and kept at room temp. until testing

For fly-ash based concrete, Wardhono et al. (2017) found an increase of E-modulus over time. This trend has also been observed by Gunasekara et al. (2017). They measured the E-modulus development over time for four different fly ash concrete mixtures from different power stations in Australia (Fig. 3.16), and noticed also an increase over time.

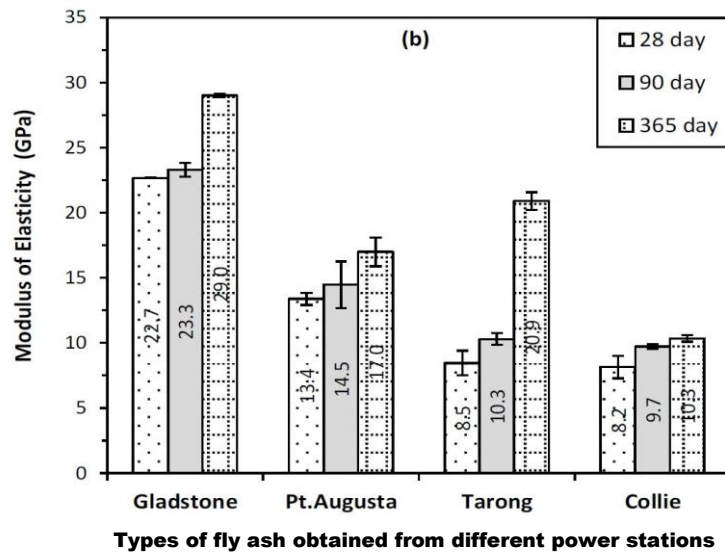


Fig. 3.16: Development of E-modulus over time for alkali-activated class-F fly ash concrete, different types of fly ash obtained from Gladstone, Pt. Augusta, Collie and Tarong power stations in Australia (Gunasekara et al., 2017, p. 5). The samples were kept in a dry oven for 24 hours at 80°C with RH 95%, then demoulded and kept at room temp. until testing.

3.4. Splitting tensile strength

Usually, concrete is not designed to resist direct tension. However, knowledge of the tensile strength is needed in order to estimate the load under which cracks will develop. For example, it is useful to understand the cracking behaviour in order to prevent corrosion of reinforcement for reinforced elements (Neville, 1995). In ordinary Portland cement concrete, the tensile strength is small when compared to the compressive strength. The mean tensile strength, f_{ctm} is related to the cylinder strength, as is shown in the following expressions:

$$\text{Strength classes } \leq \text{C50/60:} \quad f_{ctm} = 0.3f_{ck}^{\frac{2}{3}}$$

$$\text{Strength classes } > \text{C50/60:} \quad f_{ctm} = 2.12 * \ln\left(1 + \frac{f_{cm}}{10}\right)$$

The tensile strength of concrete can be measured by very different types of tests, namely flexural, direct tension and splitting. However, the direct tensile strength is a value that is hardly ever determined by testing, as a direct tensile test is hard to perform (Neville, 1995). Usually, a tensile splitting test or flexural test is performed in order to retrieve the tensile strength. Paragraph 3.5 Flexural strength will deal with the flexural strength, this paragraph is about the tensile splitting strength. For regular concrete, the tensile strength is determined from the tensile splitting strength using the following relationship:

$$f_{ctm} = 0.9f_{ct,sp}$$

For alkali-activated concrete, the tensile strength is also small when compared to the compressive strength. However, some studies indicate that alkali-activated concretes show relatively higher tensile and flexural strengths than would be predicted from OPC concretes for similar compressive strength (Lee & Lee, 2013; J. L. Provis, Bílek, et al., 2014; Thomas & Peethamparan, 2015). Several authors (Lee & Lee, 2013; Sofi et al., 2007) reported a hypothetical formula between compressive strength and tensile strength, however, there is no general consensus yet that these equations are applicable for all types of alkali-activated concrete.

3.4.1. Influence of BFS/FA ratio

Ryu et al. (2013) showed that the splitting tensile strength to compressive strength ratio for alkali-activated fly ash concrete at 28 days ranged between 7.8 and 8.2%, which is similar to that of OPC concrete for comparable compressive strengths. The equation mentioned in Eurocode 2 fits their results well. However, Thomas and Peethamparan (2015) state that the tensile strength is notably higher than that of ordinary Portland cement concrete for comparable compressive strength, for both alkali-activated fly ash and slag concrete.

Ding et al. (2016) summarized data from several publications on the correlation between splitting tensile strength and compressive strength. Fig. 3.17 (left) shows the relationship between splitting tensile strength and compressive strength for alkali-activated slag concrete. Fig. 3.17 (right) shows the same relationship, but then for alkali-activated fly ash concrete.

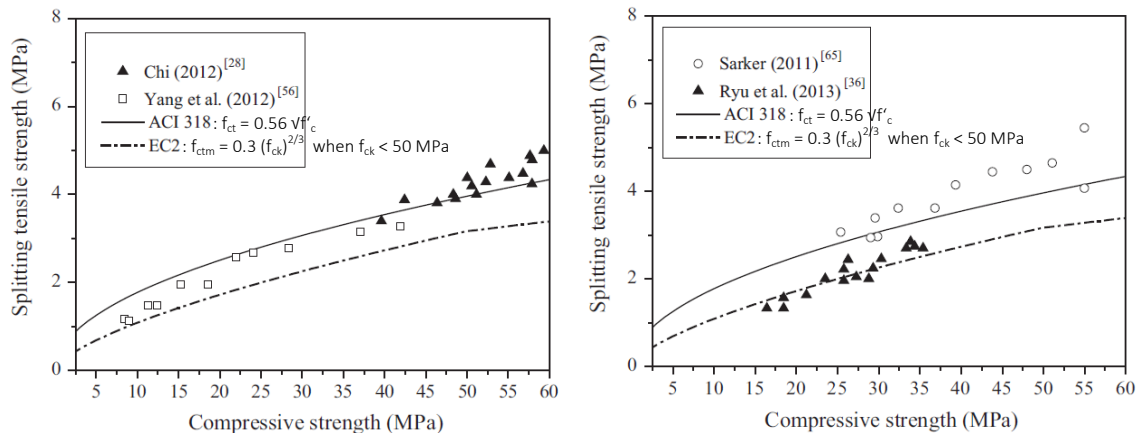


Fig. 3.17: Left: summary of the relationship between compressive strength and splitting tensile strength for alkali-activated slag concrete by Ding et al. (2016, p. 74). Based upon results for alkali-activated slag concrete published by Chi (2012) and Yang et al. (2012). Right: summary of the relationship between compressive strength and splitting tensile strength for alkali-activated fly ash concrete by Ding et al. (2016, p. 74). Results published by Prabir Kumar Sarker (2011) and Ryu et al. (2013).

For slag-based concrete, it is clear that the ratio between splitting tensile strength and compressive strength is higher than the relationship that is presented in in the concrete Eurocode. However, for alkali-activated fly ash concrete, the results are more spread. Ryu et al. (2013) found that the ratio between splitting tensile strength and compressive strength is approximately similar to that of ordinary Portland cement concrete. Prabir Kumar Sarker (2011) reported that the splitting tensile strength of alkali-activated fly ash concrete is generally higher than regular Portland cement concrete for the same compressive strength. According to Sarker, this could be due to the fact that geopolymer concrete has a denser interfacial transition zone (ITZ) between the aggregates and paste compared to a regular cement matrix. In his opinion, the stronger ITZ contributed to the higher splitting tensile strength and bond strength of geopolymer concrete. However, it may be questioned if all fly ash-based mixtures have this denser ITZ, as the results from Ryu et al. do not show this higher ratio between tensile splitting strength and compressive strength.

For alkali-activated concrete that contains both fly ash and blast furnace slag, the results do not show a significant higher ratio between tensile and compressive strength. Fig. 3.18 shows the relationship between splitting tensile strength and compressive strength for alkali-activated fly ash/slag concrete, from two different researches. There is no consistent trend, both higher and lower tensile to compressive strength ratios have been found.

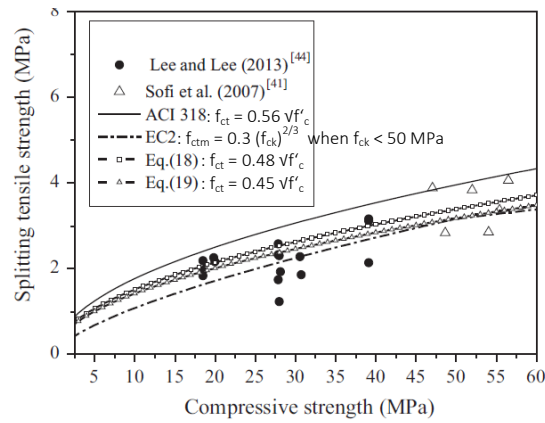


Fig. 3.18: Summary of the relationship between compressive strength and splitting tensile strength for alkali-activated slag/fly ash concrete by Ding et al. (2016, p. 74). Based upon results for alkali-activated slag concrete published by Lee and Lee (2013) and Sofi et al. (2007).

It can be concluded that it is not clear if the amount of slag or fly ash has a significant influence on the splitting tensile strength of alkali-activated concrete, although it seems that often alkali-activated slag concrete is characterized by a higher ratio between splitting tensile strength and compressive strength when compared to regular OPC concrete.

3.4.2. Influence of curing conditions

According to Thomas and Peethamparan (2015), the splitting tensile strength of alkali-activated fly ash concrete is sensitive for curing conditions. For samples cured at ambient temperature, they measured that the average splitting tensile strength is $19.4 \pm 2.8\%$ of the compressive strength, while this ratio is $16.5 \pm 1.9\%$ when the samples were cured at elevated temperature (48h at 50°C). So, either the compressive strength is relatively high for samples cured at elevated temperature compared to ambient curing, or the tensile splitting strength is relatively low for samples cured at elevated temperature.

In contrast to this, for alkali-activated slag concrete, the two curing different conditions resulted in no significant difference in splitting tensile strength. This can also be seen in Fig. 3.19 (left).

ID	Curing condition	f'_c (MPa)	f_{ct} (MPa)	E (GPa)
PCC1	28 d @ 22 °C	39.5	5.9	33.1
PCC2	28 d @ 22 °C	40.9	6.2	32.7
FC1	28 d @ 22 °C	16.2	2.9	17.7
FC2	48 h @ 50 °C	31.5	6.1	28.8
FC3	28 d @ 22 °C	28.9	6.7	21.5
FC4	48 h @ 50 °C	47.7	7.6	26.0
FC5	28 d @ 22 °C	22.9	3.8	22.6
FC6	48 h @ 50 °C	50.3	7.5	35.5
FC7	28 d @ 22 °C	21.3	4.1	10.5
FC8	48 h @ 50 °C	40.9	6.5	30.9
GGBFS1	28 d @ 22 °C	33.7	6.8	34.2
GGBFS2	48 h @ 50 °C	29.5	6.1	31.7
GGBFS3	28 d @ 22 °C	44.7	7.2	26.2
GGBFS4	48 h @ 50 °C	44.0	7.4	28.2
GGBFS5	28 d @ 22 °C	46.7	6.3	27.0
GGBFS6	48 h @ 50 °C	45.6	7.7	25.4
GGBFS7	28 d @ 22 °C	35.0	6.3	27.9
GGBFS8	48 h @ 50 °C	37.7	6.2	28.9
GGBFS9	28 d @ 22 °C	45.7	8.3	22.4
GGBFS10	48 h @ 50 °C	48.7	7.4	22.9
GGBFS11	28 d @ 22 °C	52.6	8.4	33.5
GGBFS12	48 h @ 50 °C	50.8	7.7	33.5

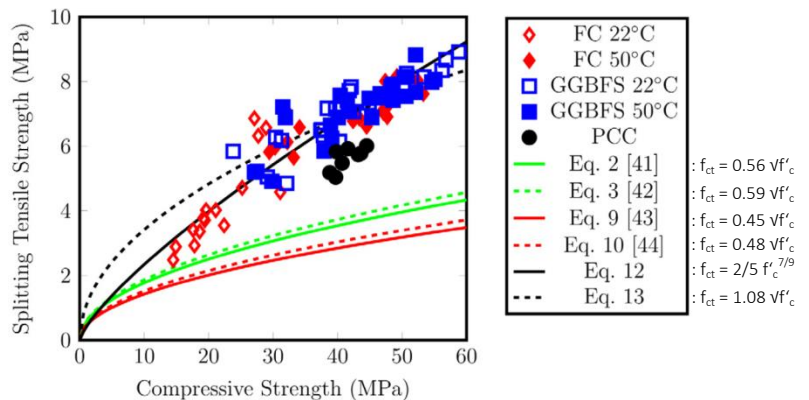


Fig. 3.19: Left: summary of results on alkali-activated concrete by Thomas and Peethamparan (2015, p. 53). Right: Splitting tensile strength vs. compressive strength of alkali-activated class C fly ash and BFS for different curing conditions, along with proposed models (eq. 12 and 13) and existing models proposed by Lee and Lee (2013, eq. 9) and Sofi et al. (2007, eq. 10). Results from Thomas and Peethamparan (2015, p. 53)

Another research, by Chi (2012), shows however that different types of curing condition had a significant influence on splitting tensile strength of alkali-activated slag concrete. The splitting tensile strength was the highest for samples cured at 60°C with RH 80%, followed by the samples that were air-exposed. The lowest values were found for samples that had saturated limewater curing.

3.4.3. Development over time

The research by Wardhono et al. (2017), as already mentioned in paragraph 1.2 *Problem statement*, shows little tensile strength development over time for alkali-activated slag concrete (see Fig. 3.20), but a significant increase in strength for fly ash-based concrete. In their opinion, the tensile strength of alkali-activated concrete is very dependent on the bond between gel and aggregate. The interface between these two elements is important because it shows a different microstructure than the hardened paste in-between. Wardhono et al. observed that the alkali-activated slag concrete had a dense gel matrix with little microcracks in the first 90 days, however, microcracking increased over time. Together with a reducing density of the gel matrix, this is the hypothetical cause for the lack of strength development over time, according to them.

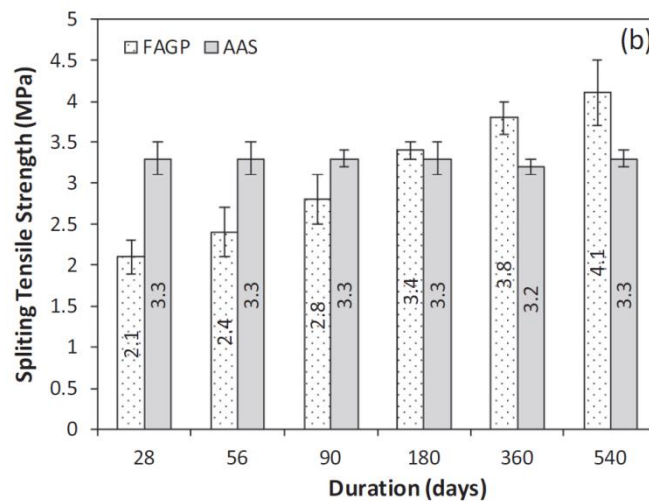


Fig. 3.20: Splitting tensile strength development over time for alkali-activated FA- and BFS-based concrete (Wardhono et al., 2017, p. 275). BFS-samples are demoulded, water-cured (23°C) for 6 days and kept at room temp. until being tested. FA-samples were heat-cured (80°C) using dry oven for 24h, then demoulded and kept at room temp. until testing.

Fig. 3.21 shows the splitting tensile strength development over time for four different types of alkali-activated fly ash concrete by Gunasekara et al. (2017). These results show the same trend as the results for FA-based concrete from Wardhono et al. (2017), Fig. 3.20, splitting tensile strength increases over time.

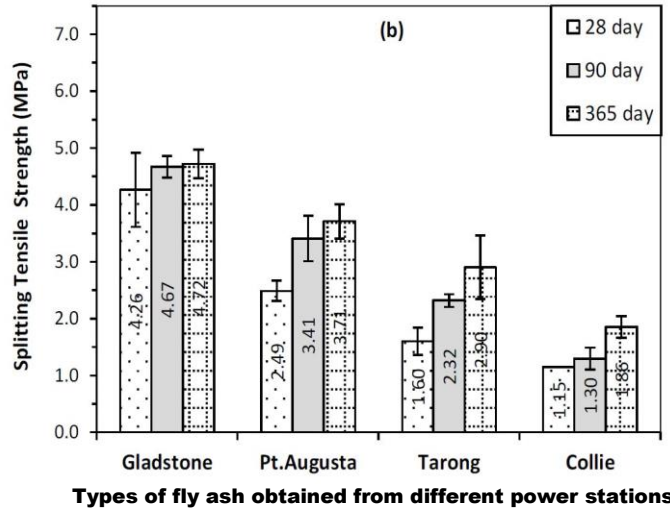


Fig. 3.21: Development of splitting tensile strength over time for alkali-activated class-F fly ash concrete, different types of fly ash obtained from Gladstone, Pt. Augusta, Collie and Tarong power stations in Australia (Gunasekara et al., 2017, p. 5). The samples were kept in a dry oven for 24 hours at 80°C with RH 95%, then demoulded and kept at room temp. until testing.

3.5. Flexural strength

Whereas paragraph 3.4 *Splitting tensile strength* dealt with the tensile splitting strength, this paragraph is about flexural strength. For regular concrete, the relationship between tensile strength and flexural strength can be determined using Equation 3.2:

$$f_{ctm,fl} = (1.6 - h[m]) * f_{ctm} \geq f_{ctm}$$

Equation 3.2: Relationship between flexural strength and tensile strength for regular Portland cement concrete, in which $f_{ctm,fl}$ is the flexural strength in MPa, h the height of the specimen in meters and f_{ctm} the mean tensile strength in MPa (Eurocode 2)

For alkali-activated concrete, such detailed expressions have not yet been established. A lot of researchers state that the flexural strength of AAC is significantly higher than would be expected from the mentioned formulas for Portland cement concrete for similar compressive strengths, as is also the case for tensile splitting strength. Fig. 3.22 shows the relationship between flexural and compressive strength for different types of alkali-activated concrete. J. L. Provis, Bílek, et al. (2014) obtained the data from a variety of literature sources. It is clear that almost all of the data for AAC exhibit higher flexural strengths than are given by the expressions for Portland cement concrete.

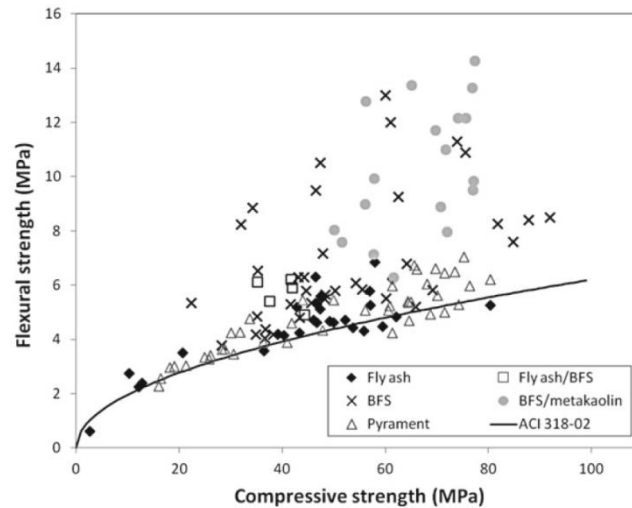


Fig. 3.22: Relationship between flexural and compressive strength of alkali-activated concretes, synthesized from various precursors as marked, at ages between 4 h and 1 year, with the relationship for OPC concretes as specified in ACI 318-02 shown for comparison. The data for alkali-activated concretes are taken from Häkkinen (1993), Diaz-Loya et al. (2013), Bernal et al. (2012), Sofi et al. (2007), Husbands et al. (1994), Fernández-Jiménez et al. (2006), Collins and Sanjayan (1999), Douglas et al. (1991) and Wu et al. (2011). Graph by J. L. Provis, Bílek, et al. (2014, p. 283)

3.5.1. Influence of BFS/FA ratio

Ding et al. (2016) collected data from two publications about the flexural strength of alkali-activated fly ash concrete. Fig. 3.23 shows the load deflection curves for both alkali-activated fly ash concrete and Portland cement control concrete. Pan et al. (2011) tested several specimens cured at 60°C in a three-point bending test. Their results show that the descending branch of the curve was much steeper for alkali-activated fly ash concrete than for regular concrete of similar compressive strength. According to them, the alkali-activated fly ash concrete showed more brittle behaviour than the OPC control concrete. P.K. Sarker et al. (2013) conclude the same, the failure modes they observed for the alkali-activated fly ash concrete specimens were generally more brittle than those of the control concrete specimens. As shown in Fig. 3.23, the peak load of the alkali-activated concrete specimens was generally higher, and again the descending part of the load–deflection curve is steeper. So, alkali-activated fly ash concrete has a higher brittleness than regular Portland cement concrete, according to these results. However, this is not that remarkable, as the strength of AAC is generally higher than that of OPC concrete, resulting in higher brittleness.

From literature review, it cannot be concluded whether this is only the case for fly ash-based concrete, or also for alkali-activated slag concrete. No specific results on slag-based concrete have been found.

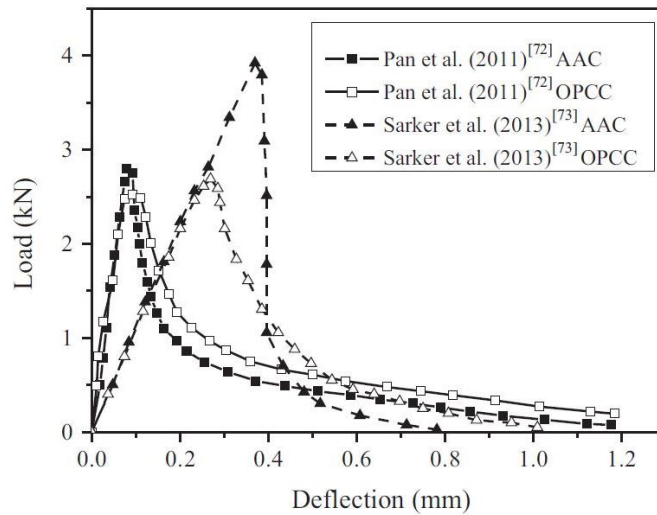


Fig. 3.23: Load-deflection curves of OPC concrete and heat cured (60°C) alkali-activated fly ash concrete, subjected to three-point bending at 28d (Ding et al., 2016). Results from Pan et al. (2011) and P.K. Sarker et al. (2013)

3.5.2. Influence of curing conditions

There is little information on the influence of curing on flexural strength of alkali-activated concrete. However, in paragraph 3.4.2 *Influence of curing conditions*, it was shown that there seems to be some influence of curing conditions on the splitting tensile strength of alkali-activated concrete. And because both splitting tensile strength and flexural strength are closely related to the direct tensile strength of concrete, it seems logical to assume that curing conditions can also influence the flexural strength of alkali-activated concrete.

3.5.3. Development over time

In paragraph 1.2 *Problem statement*, the research by Wardhono et al. (2017) was mentioned. Their results show a decrease in flexural strength for alkali-activated slag concrete of about 13% between 28 and 540 days, as is illustrated in Fig. 3.24. For alkali-activated fly ash concrete, they found an increase in flexural strength over time.

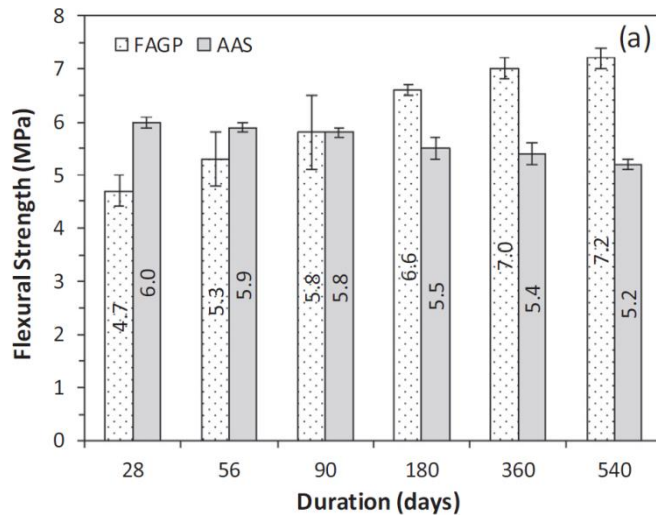


Fig. 3.24: Flexural strength development over time for alkali-activated FA- and BFS-based concrete (Wardhono et al., 2017, p. 275). BFS-samples are demoulded, water-cured (23°C) for 6 days and kept at room temp. until being tested. FA-samples were heat-cured (80°C) using dry oven for 24h, then demoulded and kept at room temp. until testing.

In *Kennispaper Geopolymeerbeton*, a Dutch publication about alkali-activated concrete, a decrease of flexural strength over time was also mentioned. Four mixtures were investigated, all four showed a decrease of flexural strength between 28 and 250 days. However, as this is not a scientific paper, there are not a lot of details about the way of curing. It is even not clear from the paper whether the samples were made from alkali-activated fly ash paste, mortar or concrete.

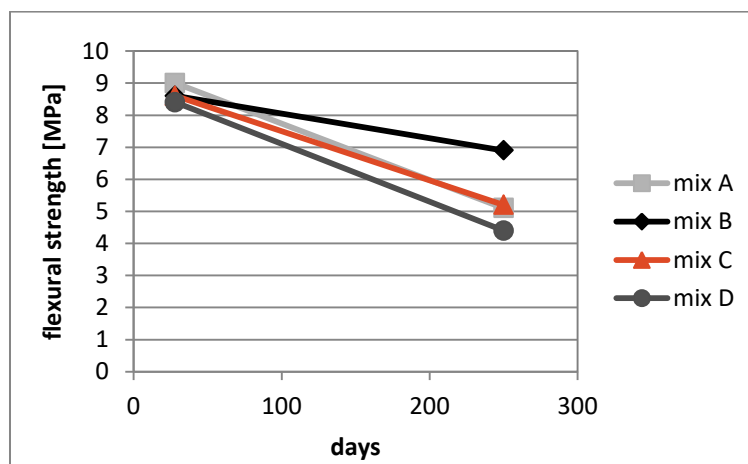


Fig. 3.25: Development of flexural strength for alkali-activated fly ash paste, mortar or concrete over time (SBRCURnet, 2016, p. 9).

Nevertheless, also this result proves that it is important to investigate the long term behaviour and strength development of alkali-activated concrete.

3.6. Flexural behaviour of reinforced beams

Sumajouw et al. (2005) investigated the flexural behaviour of sixteen steel-reinforced alkali-activated fly ash concrete beams for several reinforcement ratios (0.64-2.69%). They concluded that the behaviour and strength of reinforced alkali-activated fly ash beams is similar to that of OPC concrete beams. Furthermore, as expected, the flexural capacity increased when the reinforcement ratio was higher. In

their opinion, the flexural strength of these geopolymer beams could be calculated using the Australian standards for concrete structures (AS 3600).

Kumaravel and Thirugnanasambandam (2013) observed that the failure modes and crack patterns (Fig. 3.26) for reinforced alkali-activated fly ash concrete beams were similar to the regular concrete control beams. In the compressive zone concrete crushing occurred, but first reinforcement steel yielded. However, the pictures (Fig. 3.26) of the beams after failure seem to show a higher degree of concrete compressive failure than the AAC beams. Kumaravel and Thirugnanasambandam reported that the ultimate load capacity of alkali-activated fly ash beams was about 15% higher than the regular concrete control beams (Table 3.1). But, the compressive strength of AAC was about 26 MPa, whereas the OPC control concrete had a compressive strength of 23.5 MPa.

Table 3.1: Summary of test results. (Kumaravel & Thirugnanasambandam, 2013)

S. No	Beam Code	Ist Crack Load (kN)	Service Load (kN)	Yield Load (kN)	Ultimate Load (kN)		Max. Deflection (mm)	
					Experimental	Numerical (ANSYS)	Experimental	Numerical (ANSYS)
1	RCC-I	12.50	28.34	40.50	42.50	40.00	72.00	70.00
2	RCC-II	12.00	29.00	41.50	43.50	40.00	75.00	70.00
3	GPC-I	15.00	30.67	45.00	46.00	45.00	75.00	75.00
4	GPC-I	15.00	32.00	46.50	48.00	45.00	78.00	75.00

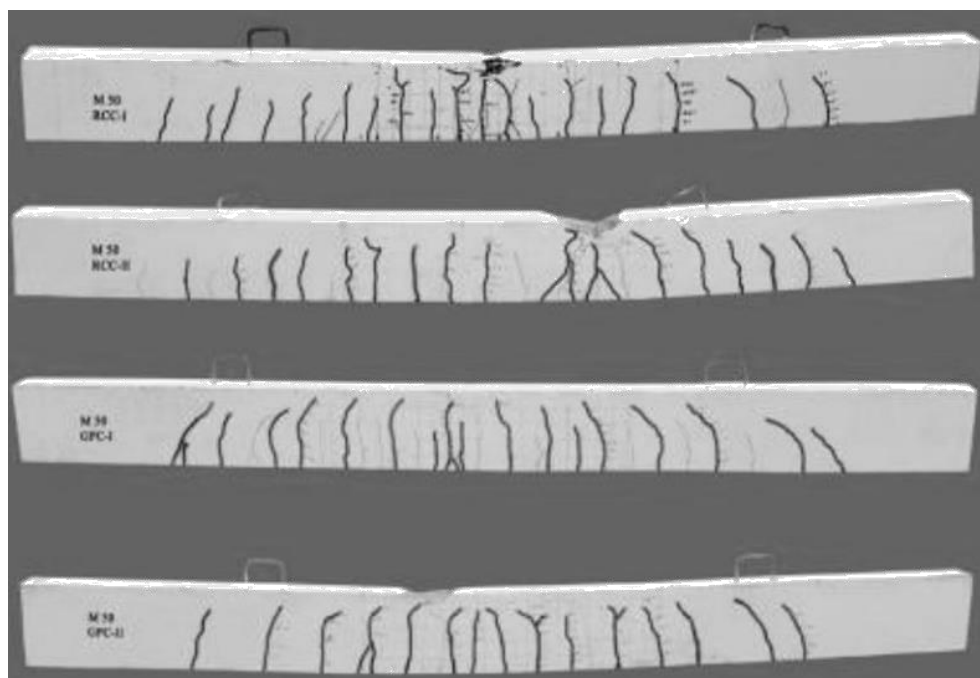


Fig. 3.26: Crack pattern of regular concrete control beams (the two on top) and alkali-activated fly ash beams (two beams at bottom of picture). (Kumaravel & Thirugnanasambandam, 2013, p. 3)

Shah and Shah (2017) investigated the behaviour of both plain and reinforced beams in four-point bending tests. They tested beams with 30% slag and 70% FA, beams with only FA as a binder precursor and OPC concrete control beams. The failure pattern of alkali-activated concrete was very similar to OPC concrete, but the load carrying capacity of the AAC beams was about 50% higher than that of the OPC concrete beams for beams with flexural reinforcement (Table 3.2). The AAC beams also had larger

displacement when compared to the OPC concrete beams. So, generally speaking, the AAC beams were characterized by higher deformation capacity before failure, resulting in a higher load capacity compared to the OPC specimens.

Table 3.2: Results of four-point bending tests on AAC beams and OPCC beams (Shah & Shah, 2017, p. 320). The authors did not specify the type of curing for OPC concrete beams, but it is assumed that these beams were air exposed.

		OPC Beams	100F0S12M		70F30S12M	
		Normal curing (base values)	open air curing	90°C oven curing	open air curing	60°C oven curing
Compressive strength of cubes on 28 th day (from same mix) in N/mm ²		34.7	33.70	51.6	52.31	52.80
Plain Beams	Peak Load (kN)	17.8	14% less	2% less	11% less	13% less
	Displacement (mm)	1.2	23% more	3% less	19% more	18% more
Flexural reinforcement only	Peak Load (kN)	46.31	45% more	26% more	56% more	54% more
	Displacement (mm)	1.9	4.26 times	3.32 times	4.7 times	7.13 times
Flexural and shear reinforcement	Peak Load (kN)	65.8	16% more	3% more	15% more	16% more
	Displacement (mm)	6.5	98% more	36% more	68% more	83% more

In their experiments, Shah and Shah also investigated the effect of oven curing. Part of the specimens was cured for 24 hours in a 60°C oven, the other beams were kept in ambient temperature. The effect of oven-curing was negligible, see Table 3.2.

3.7. Conclusion

There is no sound explanation for the observed strength and stiffness reduction of alkali-activated concrete yet. Little research has been conducted regarding the engineering properties of alkali-activated concrete, and especially not in the development of properties over time. It is clear from the literature research that strength and stiffness reduction has only been observed in concrete mixtures that contain blast furnace slag, and this behaviour has not been reported for fly ash based concrete. The research by Wardhono et al. (2017) shows this very explicitly, see Fig. 3.15. The E-modulus for 100% alkali-activated blast furnace slag concrete is decreasing over time, while the stiffness of 100% alkali-activated fly ash concrete shows an increase over time.

Furthermore, curing conditions also seem to influence the strength and stiffness development over time, although the effect seems to differ for each different type of mixture. The research by Collins and Sanjayan (2001), shows a significant effect of curing conditions on the development of compressive strength over time for alkali-activated slag concrete (Fig. 1.5). The exposed sample is characterised by little strength development compared to the sealed and bathed samples. Also, the exposed samples (50% RH and 23°C) showed surface cracks from the first day onwards, as is shown in Fig. 3.27. These surface cracks have also been reported by Lee and Lee (2013), as is shown in Fig. 3.4. In their research, concrete specimens with 30% slag exposed to 20°C and 60% RH until testing, also showed surface cracks.

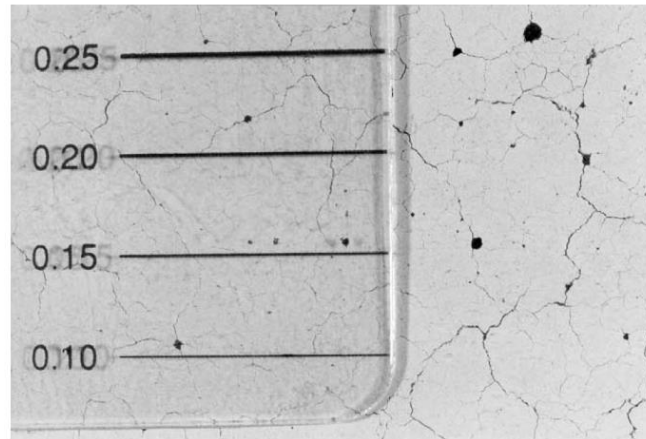


Fig. 3.27: Microcracks on alkali-activated slag (100%) concrete exposed to 50% RH and 23°C from day 1 onwards (Collins & Sanjayan, 2001, p. 348)

So, both curing conditions and the amount of blast furnace slag seem to have influence on the development of strength over time. Although Fig. 1.5 shows that curing conditions have influence on the overall development of strength over time, it may be questioned whether the way of curing is the main cause of a decrease in strength or stiffness at a certain point. In the research by Collins and Sanjayan (2001), the exposed samples were constantly kept in 50% RH and 23°C, from the first day onwards. During the process, these conditions did not change, but a small decreasing trend in compressive strength is visible after approximately 56 days. Wardhono et al. (2017) water-cured their alkali-activated blast furnace slag concrete samples for six days, but after this the samples were exposed until testing. So, again, the conditions did not change over time after taking them out of the curing room, but at a certain moment over time the strength stops to develop, as is illustrated in Fig. 3.28. This implies that something related to the material is changing, because the “curing” conditions are still the same. Also, strength and stiffness reduction have only been reported for alkali-activated concrete that contains blast furnace slag. Hypothetically, the amount of blast furnace slag could be a factor that has influence on the observed strength and stiffness decrease over time, although it is clear that also curing conditions affect the development of strength and stiffness over time.

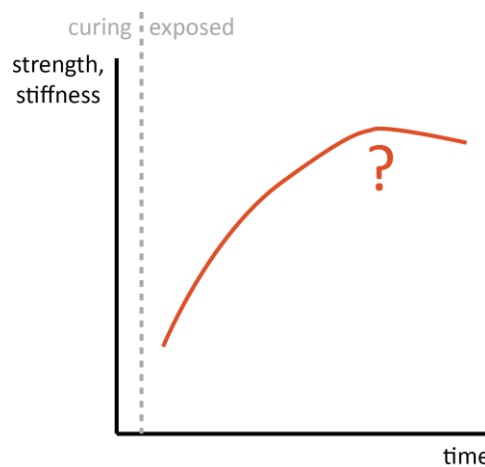


Fig. 3.28: The change in curing conditions is at a different moment over time compared to the moment over time when strength or stiffness stops to develop, according to the reported results in literature, indicating something is happening with the material.

The surface cracks observed by both Collins and Sanjayan (2001) and Lee and Lee (2013) could have influence on the strength of the material. However, these cracks were already observed directly after hardening, as reported by Collins and Sanjayan (2001). Therefore, if this would be the main cause of a lack of strength or stiffness development, this would also influence the early-age test results, and not only the long-term behaviour. So, this does not explain a sudden drop in strength or stiffness.

Some authors state that microcracking inside the material could be an important factor for the lack of strength and stiffness development (Collins & Sanjayan, 2001). Combined with the increasing volume of the hardening paste, this might lead to a reduction in strength (Thomas & Peethamparan, 2015). Wardhono et al. (2017) also name the propagation of cracks and the related reduction of gel matrix density as a hypothetical cause for the lack of strength development and drastic decrease of elastic modulus they observed. In their study, they included SEM (Scanning Electron Microscope) images that show the microstructure at certain ages of the concrete over time, Fig. 3.29 shows the images for their alkali-activated fly ash concrete and Fig. 3.30 for alkali-activated blast furnace slag concrete. In their opinion, the fly ash concrete showed a non-compact heterogeneous microstructure in the first 90 days, but over time the microstructure became denser, consistent with on-going gel formation. However, they point out that the alkali-activated slag concrete showed a dense gel matrix with little microcracks in the first 90 days, but over time, these cracks developed and the packing density of the gel matrix reduced. According to them, this could be the hypothetical reason for the lack of strength and stiffness development over time observed for the alkali-activated slag concrete specimens.

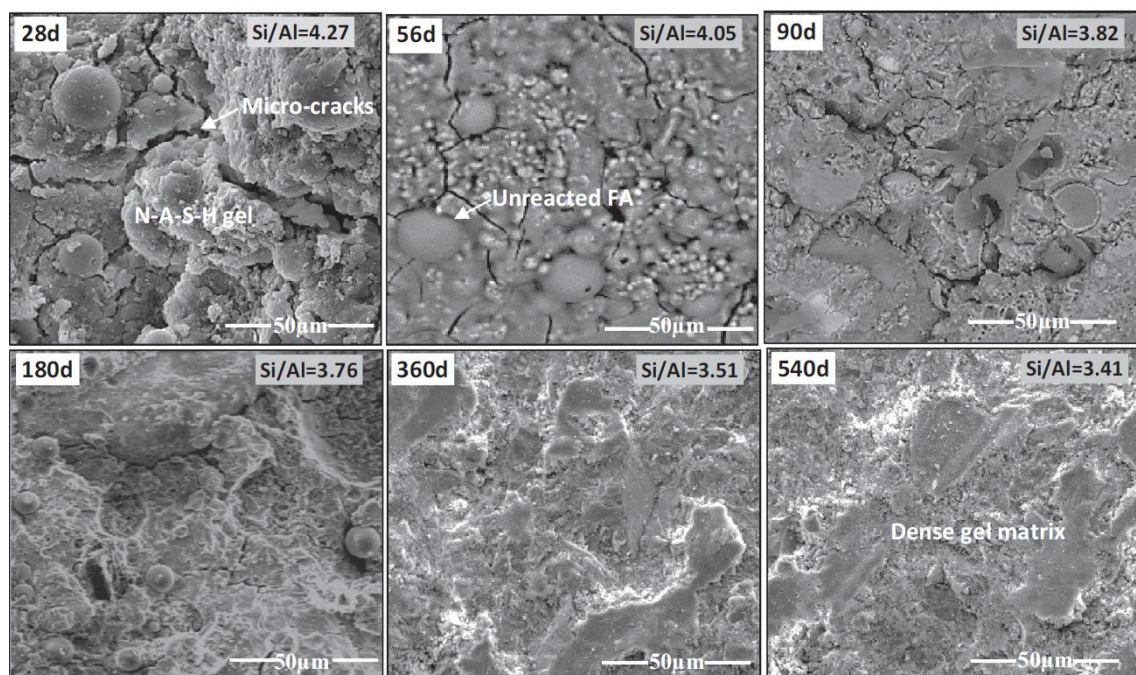


Fig. 3.29: Microstructural development of alkali-activated fly ash (100%) concrete (Wardhono et al., 2017, p. 277)

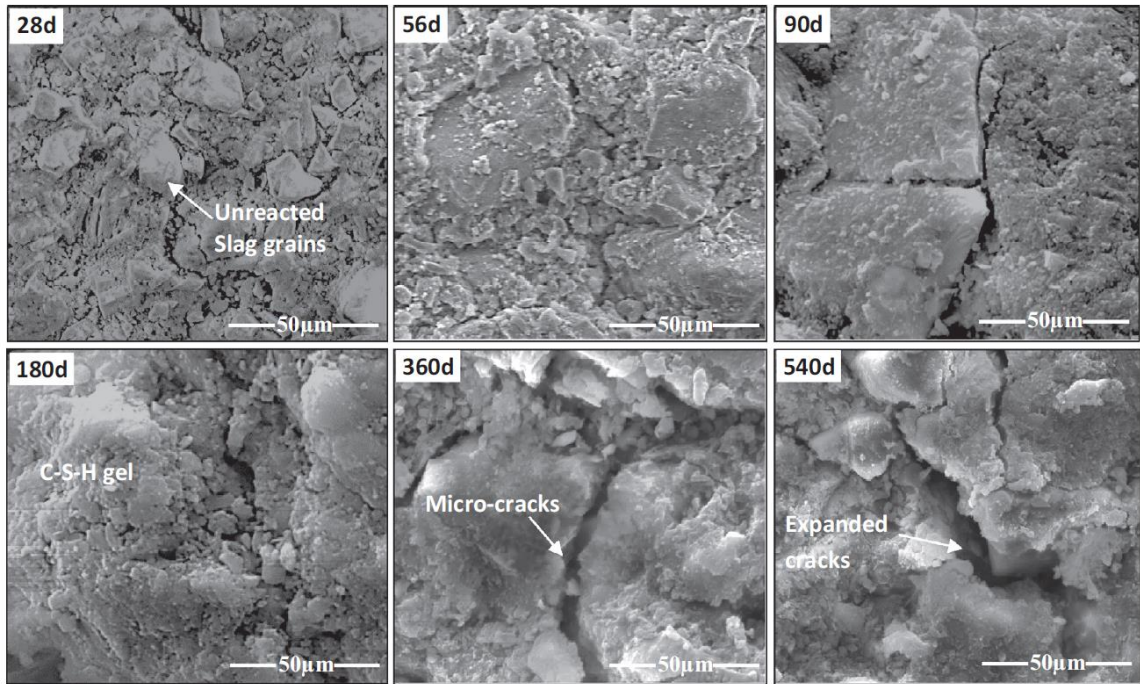


Fig. 3.30: Microstructural development of alkali-activated blast furnace slag (100%) concrete (Wardhono et al., 2017, p. 277)

However, this is the only hypothesis that has been reported in literature, possibly due to the fact that in general not a lot of research has been conducted regarding the development of engineering properties over time for alkali-activated concrete. Therefore, further research on the reported lack of strength and stiffness development is needed, to investigate this phenomenon.

4

Approach and methodology

4.1. Plan

4.1.1. Research objectives and goals

As shown in the previous chapter, a few researchers have reported results that indicate a decrease of strength or stiffness over time for alkali-activated concrete containing blast furnace slag. In order to use alkali-activated concrete for practical applications, the observed decrease might not be a very desirable phenomenon and should be well-understood. Therefore, the goal of this research is to give more insight in the development of strength and stiffness for alkali-activated concrete mixtures containing blast furnace slag and investigate if a decrease of strength and stiffness over time can also be found for the TU Delft alkali-activated concrete mixtures.

So, part of this research is a comparison study of engineering properties of alkali-activated concrete, for different BFS/FA ratios. This leads to the following sub-objectives:

- Give insight in the elastic modulus development of alkali-activated concrete for different BFS/FA ratios, over time.
- Give insight in the compressive strength development of alkali-activated concrete for different BFS/FA ratios, over time.
- Give insight in the tensile splitting strength development of alkali-activated concrete for different BFS/FA ratios, over time.
- Give insight in the flexural strength development of alkali-activated concrete for different BFS/FA ratios, over time.
- Give insight in the performance of reinforced alkali-activated concrete beams for different BFS/FA ratios, over time.

These objectives will be investigated in an experimental manner. For each sub-objective, tests will be conducted to investigate the development over time.

4.1.2. Parameters

The development of strength and stiffness over time for alkali-activated concrete containing blast furnace slag is the main focus of this research. Therefore, the two main parameters for the experimental part of the research are time and the amount of blast furnace slag.

Blast furnace slag / fly ash ratio

Hypothetically, the amount of slag could play an important role in the reported results on lack of strength and stiffness development for alkali-activated concrete. Therefore, half of the specimens will be casted with a binder based upon a BFS/FA ratio of 100:0, named S100, developed by Microlab - TU Delft.

The other half of the specimens will be casted with a hybrid mixture, with 50% blast furnace slag and 50% fly ash, named S50 by the Microlab - TU Delft. The research by Wardhono et al. (2017) showed clearly different results for a 100% slag mixture, compared with a 100% fly ash concrete mixture. Therefore, it is interesting to see the development of strength and stiffness over time for a mixture with both raw materials, and investigate if strength or stiffness reduction also occurs for this S50 mix. Another reason to use the S50 mixture is the fact that a combination of slag and fly ash seems most suitable for practical applications. Mixtures with only slag have bad workability and short setting time in general, while mixtures with only fly ash are characterized by a very slow strength development.

Time

The parameter time is included in the research in order to discover the development of several mechanical properties of alkali-activated concrete. In order to get a good indication of the strength and stiffness development, the properties should be tested at several ages. Furthermore, it is important to investigate the “long-term” behaviour, and not only consider the strength and stiffness up to 28 days. Therefore, it is decided that the experiments will be conducted at 28, 56 and 91 days.

Curing conditions

Although curing conditions may not be the direct cause or mechanism causing a lack of strength or stiffness development over time, it is clear that curing has a significant influence on the overall strength development. That is reported by a lot of researchers, and also clear from Fig. 1.5. Hypothetically, exposing the samples to ‘severe’ drying in an early stage could cause the surface cracks reported in literature, due to drying shrinkage. However, in order to be able to investigate the strength and stiffness development of alkali-activated concrete over time and the possibly related material changes, surface cracks are not very desirable for research purposes.

The experience with alkali-activated concrete at the TU Delft indicates that, in case of wet curing, the duration of curing is an important factor to consider. As shown in Fig. 4.1, S50 samples that have been cured for 28 days show no cracks, whilst short-time curing (1, 3 or 7 days) resulted in more surface cracks. In order to eliminate the effect of these surface cracks (that are hypothetically caused by the way of curing), all samples will be wet-cured (20°C and 95% RH) for 28 days.

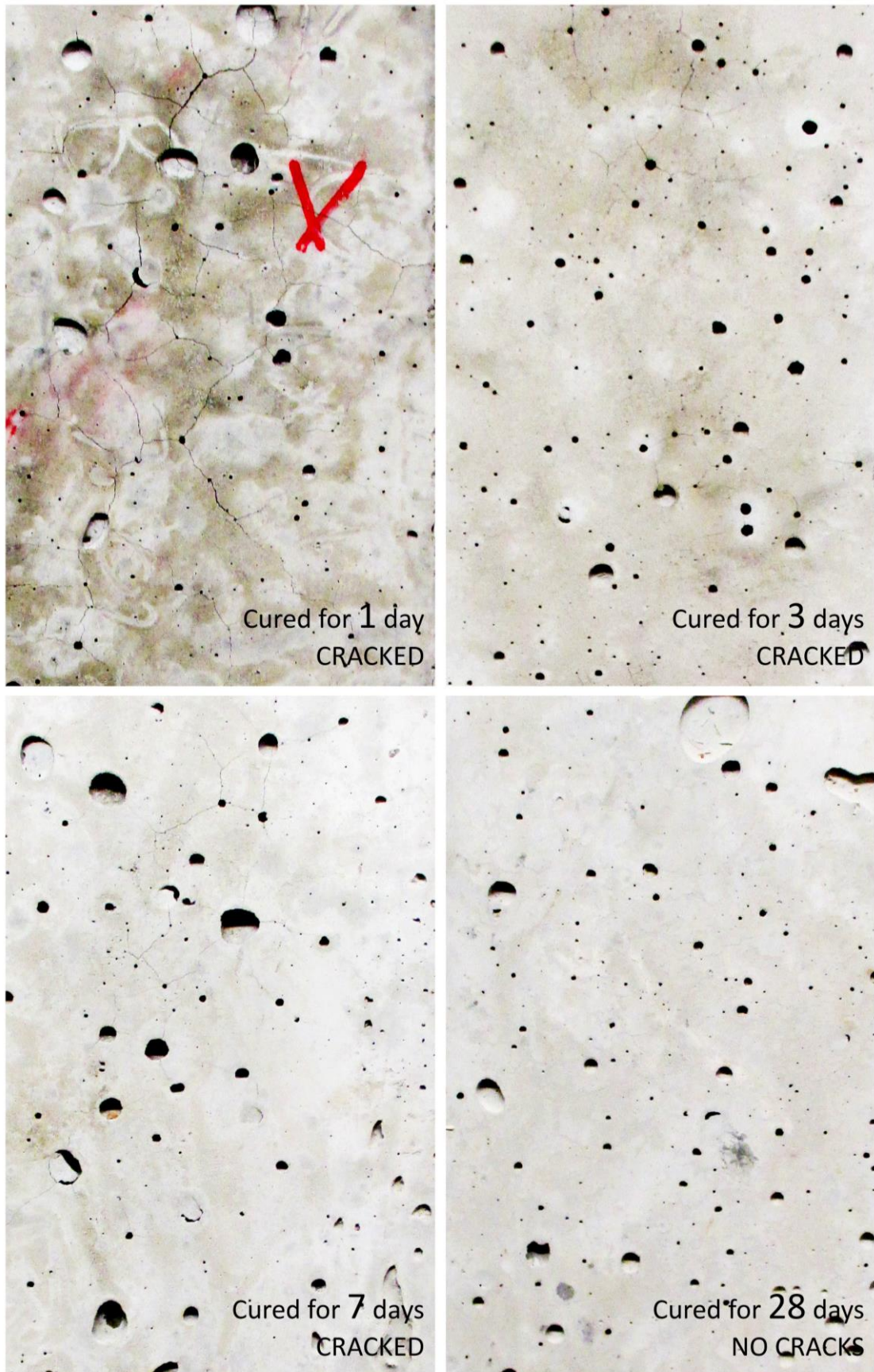


Fig. 4.1: Cracks visible in casted surface of S50 specimens that were cured for 1, 3 or 7 days. No cracks visible in the specimens that were cured for 28 days. All specimens are casted with the S50 mixture (50% FA, 50% BFS). (Aldin et al., 2017)

4.2. Approach

For the experimental part of this research, the experimental programme was separated into two main parts; one focusing on the mechanical properties of alkali-activated concrete, while the other experiments concentrate on the structural behaviour of reinforced beams subjected to four-point bending. The experimental programme is shown in Fig. 4.2.

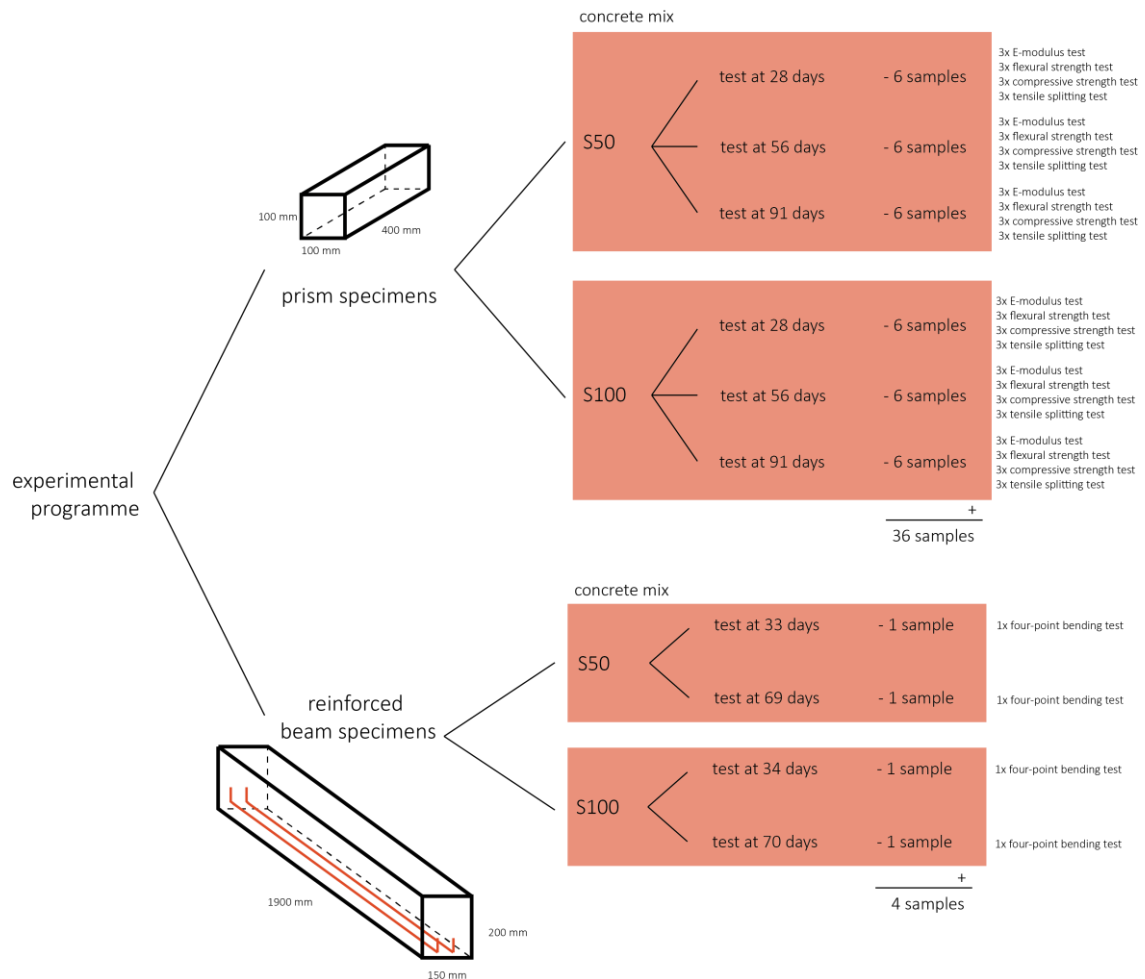


Fig. 4.2: Overview of experimental programme.

4.3. Method

4.3.1. Materials and mixture designs

Table 4.2 shows the concrete mixture designs as applied in this research, based on previous studies in the Microlab - TU Delft. Fly ash and blast furnace slag are the precursors (raw materials) that have been used, their chemical compositions are shown in Table 4.1. Two different concrete mixtures have been casted, the S50 and S100 mixture. The S100 concrete mixture contains only blast furnace slag as a precursor, the S50 concrete mixture is characterised by a 50%/50% BFS/FA precursor ratio. The precursors have been activated by an alkaline solution. The alkaline solution was made by mixing anhydrous pellets of sodium

hydroxide with deionized water and commercial sodium silicate solution (27.5 wt.% SiO₂, 8.25 wt.% Na₂O). Both concrete mixtures are characterised by a water/binder ratio of 0.53. No admixtures have been added.

Table 4.1: Chemical composition of BFS and FA used, based upon X-ray fluorescence results by Nedeljković et al (2017).

[%]	SiO ₂	Al ₂ O ₃	CaO	Mg	Fe ₂ O ₃	SO ₃	Na ₂	K ₂	TiO	P ₂ O	L.O.I.
BFS	34.4	11.53	39.1	7.81	1.42	1.6	0.23	0.58	-	-	1.15
FA	54.2	23.32	4.23	1.62	8.01	0.6	0.85	1.97	1.23	0.54	1.37

Table 4.2: TU Delft alkali-activated concrete mixtures.²

	S50	S100
for 1 m ³ concrete:	[kg]	[kg]
low calcium fly ash (FA)	200	0
blast furnace slag (BFS)	200	400
sand (0-4 mm)	784	784
gravel (4-8 mm)	435,5	435,5
gravel (8-16 mm)	522,5	522,5
alkaline solution	212	212
w/b ratio	0.53	0.53

4.3.2. Casting and curing procedures – prisms specimens

The preparation of all prism specimens was divided over three different days, to spread the amount of tests in the weeks after the castings (Table 4.3). The mixing of concrete was carried out using a 40L concrete mixer, in batches of 25L. All materials were weighed and divided in buckets, per batch (see Fig. 4.3a). First, the dry materials (blast furnace slag and/or fly ash, fine and coarse aggregates) were mixed for 3 minutes. Meanwhile, the sodium-hydroxide solution was added to the waterglass and continuously stirred (see Fig. 4.3b). Then, the alkaline activator was added to the dry mix (Fig. 4.3c), and mixing continued for another 3 minutes. After this, the mixture was glossy and well-mixed. Then, the concrete was poured into a wheelbarrow (Fig. 4.3d). The workability of the S50 concrete mixture (Fig. 4.3e) was satisfactory, the open time was about 20 minutes. The S100 concrete mixture had almost no workability, it was immediately hardening (Fig. 4.3f).

Table 4.3: Casting of prism specimens - batches

material needed:	casting day I				casting day II				casting day III			
	16th of May - total 100L S50, 4 batches				18th of May - total 100L S100, 4 batches				23th of May - total 75L S50 + 25L S100			
	I: 25L S50	II: 25L S50	III: 25L S50	IV: 25L S50	I: 25L S100	II: 25L S100	III: 25L S100	IV: 25L S100	I: 25L S50	II: 25L S50	III: 25L S50	IV: 25L S100
FA	[kg]	[kg]	[kg]	[kg]	[kg]	[kg]	[kg]	[kg]	[kg]	[kg]	[kg]	[kg]
BFS	5.00	5.00	5.00	5.00	0.00	0.00	0.00	0.00	5.00	5.00	5.00	0.00
sand (0-4)	19.60	19.60	19.60	19.60	19.60	19.60	19.60	19.60	19.60	19.60	19.60	19.60
gravel (4-8)	10.89	10.89	10.89	10.89	10.89	10.89	10.89	10.89	10.89	10.89	10.89	10.89
gravel (8-16)	13.06	13.06	13.06	13.06	13.06	13.06	13.06	13.06	13.06	13.06	13.06	13.06
alkaline sol.	5.30	5.30	5.30	5.30	5.30	5.30	5.30	5.30	5.30	5.30	5.30	5.30

² There where in this thesis "TU Delft alkali-activated concrete mixtures" is mentioned, it is meant to be referred to Arbi et al. (2015), Arbi et al. (2016) and Nedeljković (2014).



Half of the concrete mixture was then poured in the pre-oiled moulds (Fig. 4.3g and h), that were positioned on the vibrating table. During the first casting day, oil was used, but the second and third casting Vaseline was applied, because it proved to be much easier during un moulding.

When all moulds were half full, the concrete was vibrated for about 20 seconds. After this, the rest of the concrete was poured in the moulds and another 20 seconds of vibrations were applied (Fig. 4.3i). The moulds were covered with plastic (Fig. 4.3j). After one day, all specimens were un moulded (Fig. 4.3k) and placed in the fog room where they have been cured (22° and 99% RH) until 28 days, see Fig. 4.3l. After the 28-day curing period, the specimens were moved from the curing room to laboratory conditions (20°C and 55% RH). Comparison photos of the surfaces of S50 and S100 concrete can be found in 0.

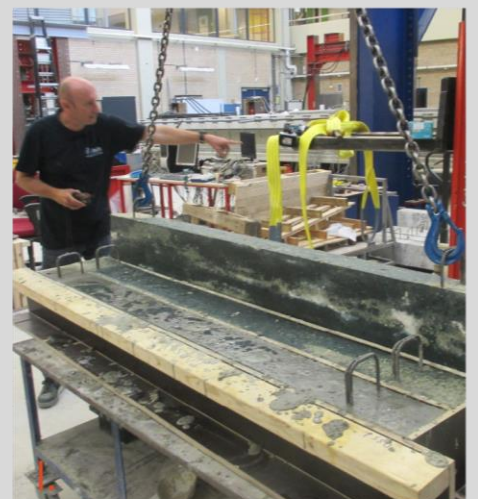
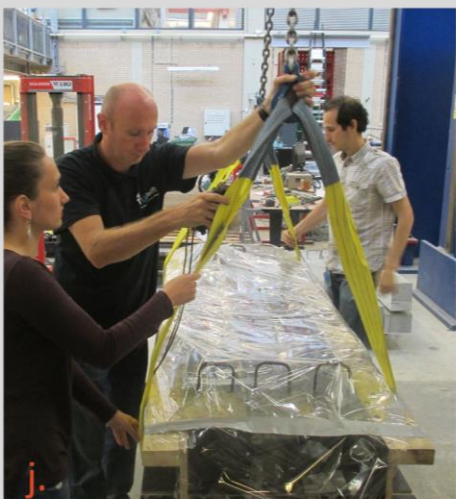
4.3.3. Casting and curing procedures – reinforced beams

All reinforced beams have been casted at the same day. In the weeks before the casting day, the moulds were prepared and the reinforcement was made. All beams were reinforced with 3 bars $\varnothing 8$ as tensile reinforcement at the bottom, and 2 bars $\varnothing 8$ at the top, as practical reinforcement (Fig. 4.4). The reinforcement drawings are attached in *Appendix C – Reinforcement drawings*. Also, a calculation of the expected failure load was made, the calculation is attached in *Appendix D – Calculation of reinforced beams*. After the reinforcement and the moulds were ready, spacers have been casted from alkali-activated paste (see Fig. 4.5a) and placed in the moulds (Fig. 4.5b). The mixing of concrete was carried out using a 220L mixer (Fig. 4.5d) for S50 concrete, in batches of 100L (Table 4.4). For the S100 concrete, smaller batches were chosen, because of the fast hardening time. The S100 beams were casted using a 40L concrete mixer (Fig. 4.5e) in batches of 25L. All materials were weighed and divided in buckets, per batch (Fig. 4.5c). First, the dry materials (blast furnace slag and/or fly ash, fine and coarse aggregates) were mixed for 3 minutes. Meanwhile, the waterglass and sodium-hydroxide were mixed. Then, the alkaline activator was added to the dry mix and mixing continued for another 3 minutes. The mixture was well-mixed after this procedure. Then, the concrete was poured into a wheelbarrow and transported to the moulds, prepared with Vaseline, on the vibrating table (Fig. 4.5f). The workability for both mixtures was the same as described in paragraph 4.3.2 *Casting and curing procedures – prisms specimens*. Half of the concrete was then poured into the moulds. Per beam, also three cubes (Fig. 4.5g) of 150 x 150 x 150 mm³ were casted, to determine the compressive strength when testing the beam.

Table 4.4: Casting of reinforced beams – batches

CASTING THURSDAY 29th of JUNE								
A: 300L S50 - 3 x 100 L				B: 160 L S100 - 4 x 40L				
	A1: 100L S50	A2: 100 L S50	A3: 100 L S50	B1: 40L S100	B2: 40L S100	B3: 40L S100	B4: 40L S100	
	[kg]	[kg]	[kg]	[kg]	[kg]	[kg]	[kg]	[kg]
FA	20.00	20.00	20.00	0.00	0.00	0.00	0.00	0.00
BFS	20.00	20.00	20.00	16.00	16.00	16.00	16.00	16.00
sand (0-4)	78.40	78.40	78.40	31.36	31.36	31.36	31.36	31.36
gravel (4-8)	43.55	43.55	43.55	17.42	17.42	17.42	17.42	17.42
gravel (8-16)	52.25	52.25	52.25	20.90	20.90	20.90	20.90	20.90
alkaline sol.	21.20	21.20	21.20	8.48	8.48	8.48	8.48	8.48

Fig. 4.3 (opposite page): Preparation of the prism specimens



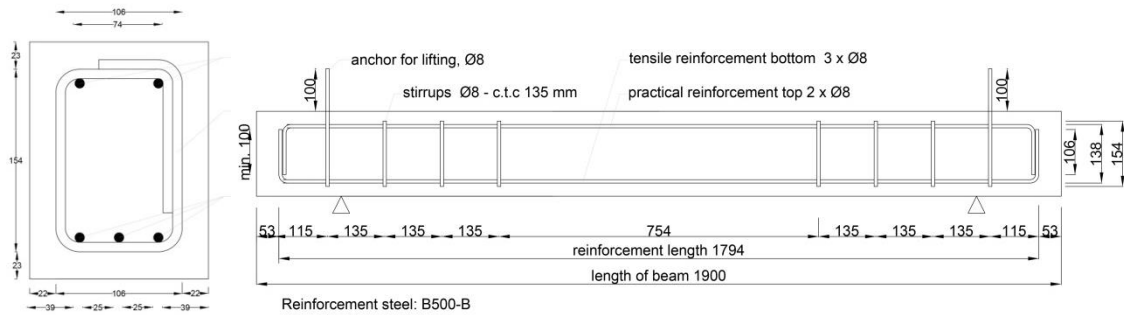


Fig. 4.4: Cross-section and side-view of reinforced alkali-activated concrete beams.

When all moulds were half filled, the concrete was vibrated for about 20 seconds. Then, the rest of the concrete was poured in the moulds and another 20 seconds of vibrations were applied. However, for S100, the batch size was too small to fit a full mould, so there was a full “stop” between the casting moments, in which the new batch was prepared. All filled moulds (beams and cubes) were covered with plastic (Fig. 4.5h and i). After one day, all specimens were un moulded (Fig. 4.5j, k and l) and placed in the fog room where they have been cured (22° and 99% RH) for 28 days. After the 28-day curing period, all specimens were moved from the curing room to laboratory conditions (20°C and 55% RH) and were kept there until testing.

4.4. Testing procedures

4.4.1. Flexural test

The three-point bending tests have been performed in accordance with NEN-EN 14651+A1, except for the fact that the prism size was 100x100x400 mm³ instead of 150x150x550-700 as specified in the NEN-standard. The tests have been performed using the Instron machine in the Microlab - TU Delft, with a speed of 0.5 micron/sec. A notch of 25 mm was made at midspan, for all samples, using wet-sawing. After this, the samples were dried for at least 6 hours before testing. Two Linear Variable Data Transformers (LVDTs) were placed, one on each side of the specimen (Fig. 4.6, left), measuring length change. After reaching the maximum force, the test was continued until the force was about one-third of the maximum-reached force. Then, the flexural strength was calculated from the maximum sustained load using Equation 4.1:

$$f_{flex} = \frac{M}{W} = \frac{\frac{1}{4} * F * L}{\frac{1}{6} * b * h^2} = \frac{\frac{1}{4} * 387 * F}{93750}$$

Equation 4.1: f_{flex} is the flexural strength in MPa. M is the moment in Nmm, using the maximum sustained load (F, in N) and the spanning length L, in mm. W is the section modulus, in mm³, using the width and height (minus notch depth) of the specimen.

Fig. 4.5 (opposite page): Preparation of the reinforced beam specimens.



Fig. 4.6: Left: three-point bending test setup. Right: Compressive strength test set-up.

After the flexural tests, six cubes ($100 \times 100 \times 100 \text{ mm}^3$) were sawn from each three specimens, illustrated in Fig. 4.7. These cube specimens have been used to determine the tensile splitting and compressive strength, as is explained in the following subparagraphs.

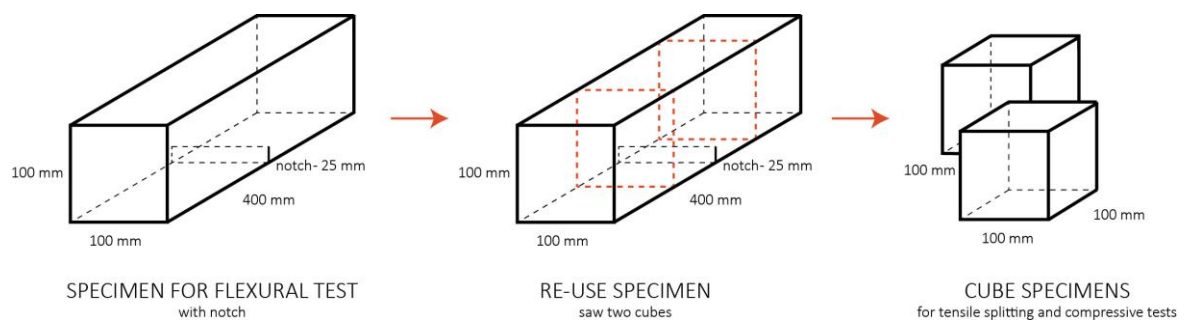


Fig. 4.7: Specimen re-use process.

4.4.2. Compression test

The compressive strength test has been performed in accordance with NEN-EN 12390-3, however, cube specimens of $100 \times 100 \times 100 \text{ mm}^3$ were used. These cubes were sawn from the specimens that were first used for flexural tests, using wet-sawing, as explained in paragraph 4.4.1 *Flexural test*. After this, the samples were dried for at least 2 hours before testing. The tests have been performed using the CYBER-TRONIC machine in the TU Delft Macrolab (Fig. 4.6, right), with a loading rate of 6.5 kN/sec. All cube specimens have been positioned so that the load is applied perpendicularly to the direction of casting. The compressive strength of the concrete was then obtained from the maximum load sustained by the specimen, divided by the cross-sectional area of the concrete specimen.

4.4.3. Splitting tension test

The splitting tension tests have been performed in accordance with NEN-EN 12390-6, however, cube specimens of $100 \times 100 \times 100 \text{ mm}^3$ are used instead of cylindrical specimen. According to NEN-EN 12390-6, the results obtained from testing cube specimens of concrete are likely to be about 10% higher than that

obtained from testing a cylindrical specimen of the same concrete. The cubes were sawn from the specimens that were first used for flexural tests, using wet-sawing, as explained in paragraph 4.4.1 *Flexural test*. After this, the samples were dried for at least 2 hours before testing. All cube specimens were positioned in the 'CYBER-TRONIC' machine so that the load is applied perpendicularly to the direction of casting. Small wooden slats were placed in the middle of the top and bottom surfaces of the specimens (see Fig. 4.8, left), in order to concentrate the load and cracking pattern. Then, the specimen was loaded until failure with a loading rate of 1.1 kN/sec. The splitting tensile strength was calculated from the maximum sustained load using Equation 4.2:

$$f_{ct} = \frac{2 * F}{\pi * L * d}$$

Equation 4.2: f_{ct} is the splitting tensile strength in MPa. F is the maximum sustained load in N. L is the length of the line of contact of the specimen, in mm, and d is the designated cross-sectional dimension in mm.



Fig. 4.8: Left: Splitting tensile strength test set-up. Right: Elastic modulus test set-up.

4.4.4. Elastic modulus test

The elastic modulus has been determined in accordance with ISO 1920-10:2010 (ISO, 2010). However, the specimens have not been re-immersed in water for 12 h, before testing. The specimen size was 100 x 100 x 400 mm³, so the height/width ratio is 4, that fits the limits of the ISO code. LVDT's were placed on the specimen, four horizontal and four vertical, to measure horizontal and vertical displacement (see Fig. 4.8, right). The tests have been performed using the TONI-BANK machine in the TU Delft Macrolab. First, the specimen was loaded using displacement-control, until a stress of 5 MPa was achieved. Then, the machine was switched to strain-controlled loading, with a speed of 0.001/s, until one-third of the maximum strength (determined before from compressive tests). Then this cycle was repeated once or twice more. The output is a series of force vs. displacement data, obtained by the LVDT's. These results were translated to strain vs. stress curves from which the E-modulus can be determined using linear regression between the two stress levels (5 MPa and one third of maximum strength).

4.4.5. 4-point bending test – reinforced beams

All beams were tested in a test machine with a capacity of 100 kN. The beams were simply supported over a span of 1500mm, and subjected to two concentrated loads placed symmetrically on the span. The distance between the loads was 500mm, as can be seen in Fig. 4.9.

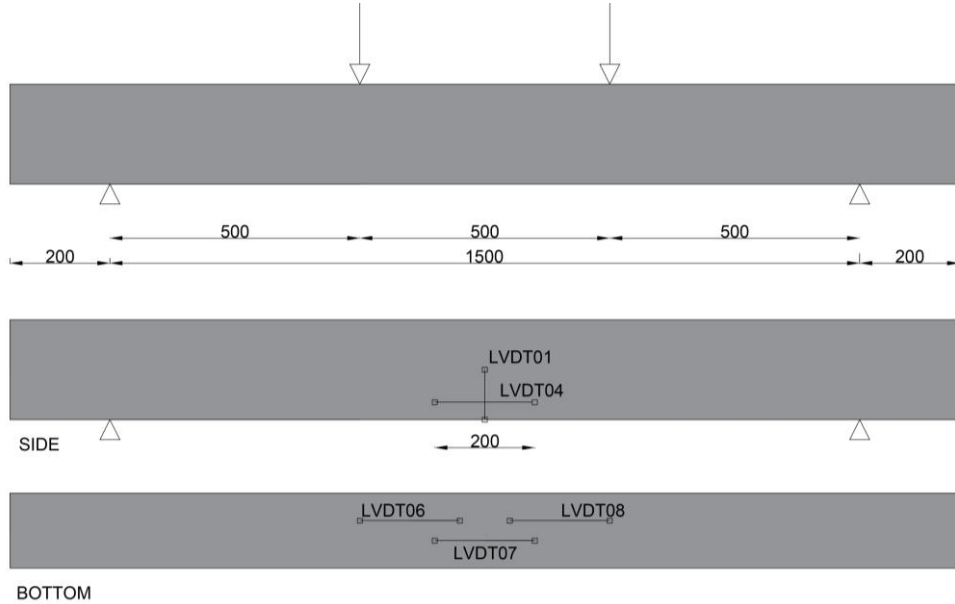


Fig. 4.9: Schematical representation of test set-up

One side of the beam was painted white, with an irregular pattern of black dots on top of it (Fig. 4.10, left), for the purpose of image analysis (for other researches in the TU Delft Macrolab). Linear Variable Data Transformers (LVDTs) were placed at several locations on the beam, three at the bottom, one at the side and one to measure vertical deflection. For measuring the vertical deflection, a substructure was attached to the beam, spanning from support to support at the height of the neutral axis (Fig. 4.10, right). Load and the deflection data were electronically recorded, data was sent to the computer two times per second. The specimens were tested under a displacement controlled force, with a speed of 0.01 mm/sec. After every step of 5 kN, the process was paused. Cracks were marked and measured, photos were taken. When the force reached approximately 60 kN, the speed was increased to 0.05 mm/sec.



Fig. 4.10: Test set-up. Left: painted side of beam for image analysis. Right: LVDTs to measure deformation.

5

Results

5.1. In general

This chapter presents results of the conducted experiments. First, all investigated mechanical properties will be presented. The second part of the chapter shows the results from the four-point bending test on reinforced beams.

5.2. Mechanical properties

Table 5.1 shows an overview of all mechanical properties that have been tested over time, for the S100 concrete mixture (100% slag, no fly ash). In Table 5.2, all results on the S50 mixture (50% slag, 50% fly ash) are summarized. It is clear that some properties show a decrease over time. In the following subparagraphs, the development of each mechanical property will be presented graphically.

Table 5.1: Mechanical properties of S100 concrete mixture (100% slag, no fly ash). Specimens have been cured (20°C and 95% RH) for 28 days. After this, the samples were exposed to laboratory conditions (20°C and 55% RH) until testing. NB: compressive strength and splitting tensile strength have been tested on 100x100x100 mm³ cubes, instead of regular 150x150x150 mm³ cubes.

S100	compr. strength			elastic modulus			poisson's ratio			spl. tens. strength			flexural strength		
	days	[Mpa]	SD	average	[Gpa]	SD	average	[-]	SD	average	[Mpa]	SD	average	[Mpa]	SD
28	91,63	1,76	93,45		0,41	32,96		0,003	0,157	5,46	0,27	5,38		0,58	6,22
	92,75			32,50			0,153			5,23			6,55		
	92,84			33,29			0,157			5,11			5,56		
	96,31			33,08			0,160			5,72			6,57		
	93,74														
47	99,84	3,36	95,98	32,41	1,23	31,91	0,141	0,013	0,146	5,39	0,35	5,42	6,87	0,25	6,60
	93,71			30,51			0,137			5,78			6,39		
	94,39			32,82			0,161			5,09			6,53		
74										4,79	0,90	5,43			
										6,07					
91	94,56	4,63	97,96	30,41	1,89	28,55	0,149	0,01	0,15	4,67	0,09	4,77	6,06	0,26	5,76
	96,09			28,62			0,140			4,84			5,63		
	103,23			26,63			0,158			4,80			5,60		

Table 5.2: Mechanical properties of S50 concrete mixture (50% slag, 50% fly ash). Specimens have been cured (20°C and 95% RH) for 28 days. After this, the samples were exposed to laboratory conditions (20°C and 55% RH) until testing. NB: compressive strength and splitting tensile strength have been tested on 100x100x100 mm³ cubes, instead of regular 150x150x150 mm³ cubes.

S50	compr. strength			elastic modulus			poisson's ratio			spl. tens. strength			flexural strength		
	days	[Mpa]	SD	average	[Gpa]	SD	average	[-]	SD	average	[Mpa]	SD	average	[Mpa]	SD
28	76,13	2,32	75,25	26,57	0,39	26,42	0,136	0,017	0,152	4,60	0,40	4,67	4,56	0,14	4,66
	77,00			25,98			0,170			4,30			4,61		
	72,62			26,73			0,149			5,10			4,82		
49	76,46	5,34	71,54	21,44	0,08	21,40	0,141	0,019	0,156	3,90	0,20	4,02	4,43	0,20	4,59
	64,88			21,46			0,178			3,88			4,52		
	75,19			21,31			0,150			3,99			4,82		
	69,62									4,30					
72	74,50	4,87	72,77							3,88	0,24	3,95			
	77,09									3,72					
	63,40									3,97					
	72,10									3,88					
	75,42									4,42					
74,12			3,85												
91	74,89	3,39	71,77	19,28	0,56	18,36	0,167	0,013	0,183	3,58	0,24	3,60	-	0,20	3,93
	74,11			18,00			0,175			3,50			4,16		
	68,99			18,15			0,203			3,99			3,88		
	73,53			17,90			0,181			3,32			3,77		
	67,31			18,45			0,189			3,43			-		
	-			-			-			-			3,76		

5.2.1. Compressive strength

Fig. 5.1 shows a graphical representation of the compressive strength development for both the S50 and S100 concrete mixtures. The results for S100 on compressive strength show an increase of about 4% between 91 and 28 days. For the S50 concrete mixture, a decrease of approximately 4% was observed.

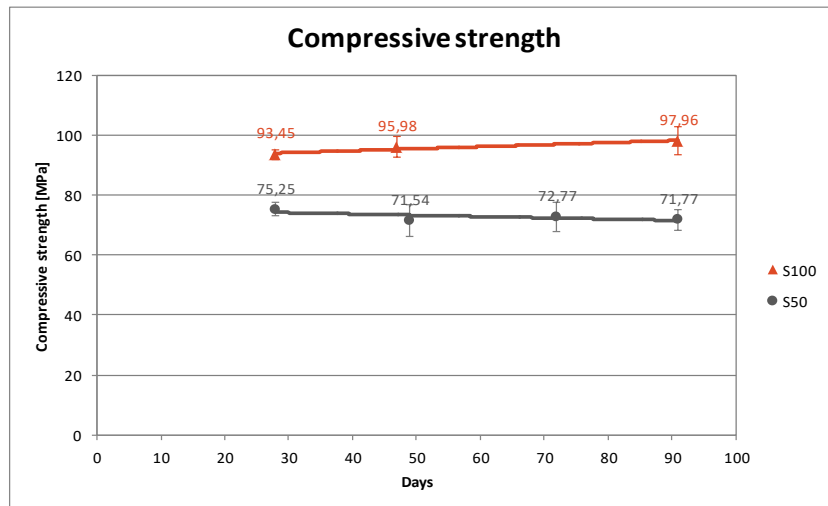


Fig. 5.1: Development of compressive strength over time for alkali-activated concrete. The graph shows the development over time for both S100 (100% slag) and S50 (50% slag and 50% fly ash) concrete mixtures. Specimens have been cured (20°C and 95% RH) for 28 days. After this, the samples were exposed to laboratory conditions (20°C and 55% RH) until testing. Compressive strength has been tested on 100x100x100 mm³ cubes, instead of regular 150x150x150 mm³ cubes.

5.2.2. Tensile splitting strength

An overview of the development of tensile splitting strength for both mixtures is shown in Fig. 5.2. It is clear that both concrete mixtures show a decrease of tensile splitting strength over time. The splitting tensile strength of S100 concrete dropped with 11% between 91 and 28 days. For S50, this decrease is about 22%.

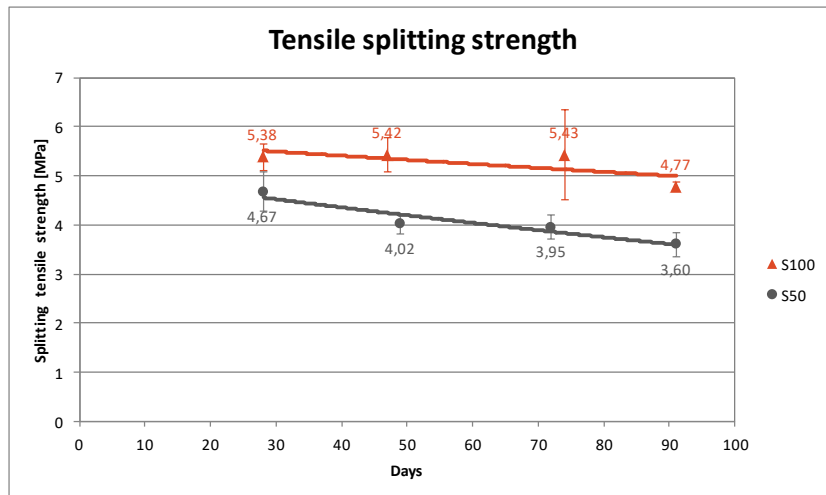


Fig. 5.2: Development of tensile splitting strength over time for alkali-activated concrete. The graph shows the development over time for both S100 (100% slag) and S50 (50% slag and 50% fly ash) concrete mixtures. Specimens have been cured (20°C and 95% RH) for 28 days. After this, the samples were exposed to laboratory conditions (20°C and 55% RH) until testing. Tensile splitting strength has been tested on 100x100x100 mm³ cubes, instead of regular 150x150x150 mm³ cubes.

5.2.3. Flexural strength

Fig. 5.3 shows the development of flexural strength over time for both alkali-activated concrete mixtures. The flexural strength of the S100 concrete decreased 7% between 91 and 28 days. For S50 concrete, this decrease is more, about 15%.

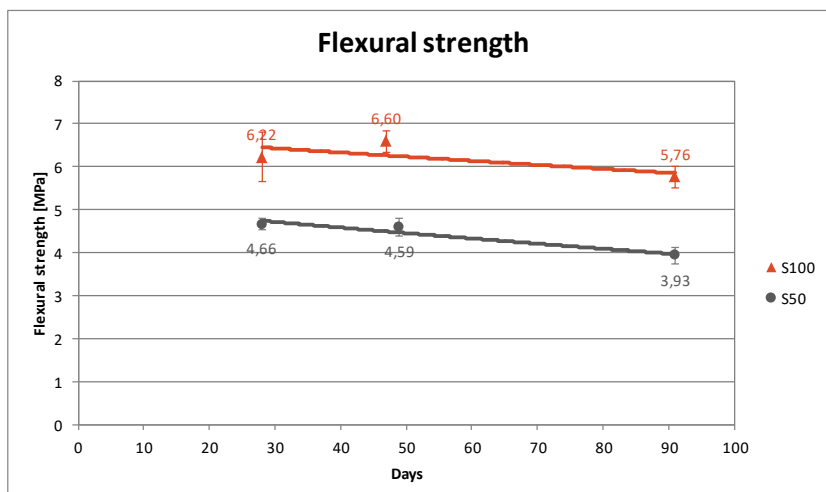


Fig. 5.3: Development of flexural strength over time for alkali-activated concrete. The graph shows the development over time for both S100 (100% slag) and S50 (50% slag and 50% fly ash) concrete mixtures. Specimens have been cured (20°C and 95% RH) for 28 days. After this, the samples were exposed to laboratory conditions (20°C and 55% RH) until testing.

5.2.4. Elastic modulus and poisson's ratio

In Fig. 5.4, the development of elastic modulus for both mixtures is presented. These results show the highest decrease over time, approximately 13% for S100 concrete and more than 30% for the S50 concrete mixture.

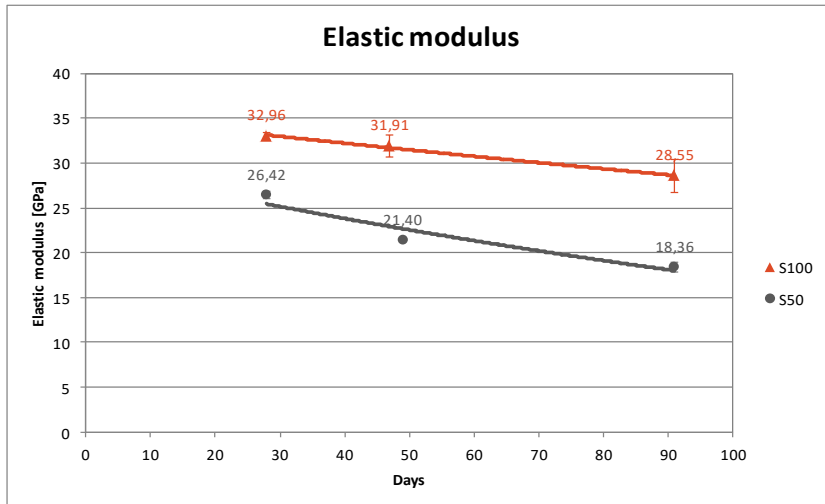


Fig. 5.4: Development of elastic modulus over time for alkali-activated concrete. The graph shows the development over time for both S100 (100% slag) and S50 (50% slag and 50% fly ash) concrete mixtures. Specimens have been cured (20°C and 95% RH) for 28 days. After this, the samples were exposed to laboratory conditions (20°C and 55% RH) until testing.

Fig. 5.5 shows the development of poisson's ratio over time, for both mixtures. The results show an increase for S50 concrete, and relatively constant values for the S100 concrete mixture. However, the standard deviation is quite big, between approximately 9-12%. This might be due to the fact that the method of determining poisson's ratio is not very precise, because of damaged equipment.

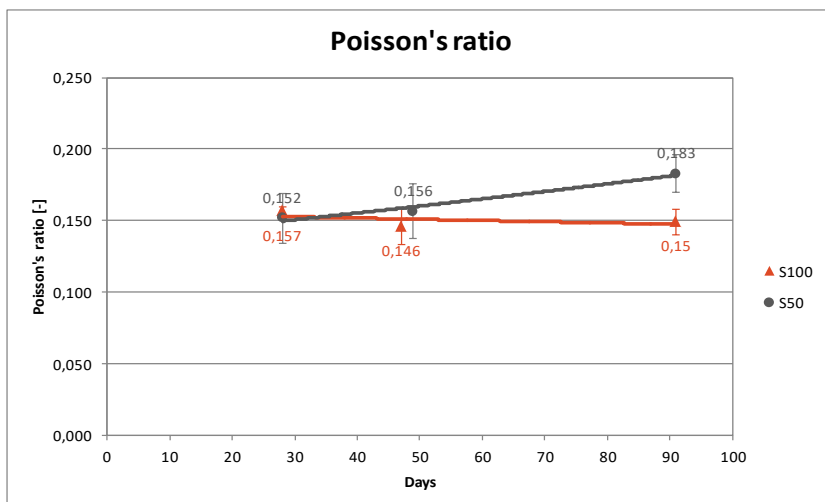


Fig. 5.5: Development of poisson's ratio over time for alkali-activated concrete. The graph shows the development over time for both S100 (100% slag) and S50 (50% slag and 50% fly ash) concrete mixtures.

5.3. Bending capacity of reinforced beams

Table 5.3 gives an overview of all beam test results. All the beams failed in a flexural mode, no shear failure occurred. The location of the failure zone was in the constant moment zone (between the loads) for all beams, as expected. In all cases, the cracks at the mid-span widely opened near failure. For three beams (S50-33d, S100-34d and S100-70d), reinforcement failure was observed before compressive failure of the concrete occurred. However, for the S50-69d beam, crushing of the concrete in the compression zone occurred before failure of the reinforcement. The failure load for this beam is also irregular (about 12 percent lower) when compared to the other three beams in which reinforcement failed. However, compressive strength is comparable to the other S50 beam.

Table 5.3: The table shows results for both S100 (100% slag) and S50 (50% slag and 50% fly ash) concrete beams. Compressive strength has been tested on 150x150x150 mm³ cubes. Specimens have been cured (20°C and 95% RH) for 28 days. After this, the samples were exposed to lab conditions (20°C and 55% RH) until testing.

Beam	Testing age [days]	Tens. reinf. ratio [%]	Compr. strength [MPa]	Average	Failure load [kN]	Max. deflection jack [mm]	Max. defl. LVDT01 [mm]	Ultimate moment [kNm]	Failure Type
S50	33	0.61	80.32	75.1	67.4	32.5	27.4	16.9	Reinf.
			78.31						
			66.62						
S50	69	0.61	81.73	77.1	58.8	35.2	34.3	14.7	Concr. compr.*
			70.87						
			78.61						
S100	34	0.61	91.20	86.6	67.6	30.1	33.1	16.9	Reinf.
			81.94						
S100	70	0.61	88.04	83.7	66.3	37.4	35.0	16.6	Reinf. (even broke)
			71.24						
			91.79						
OPC concrete	33	0.61		45.7	59.1	17.7	10.8	14.8	Concr.

*The failure mechanism for beam S50-69d is different from the other three beams, compressive failure was observed.

The OPC beam had an average cube compressive strength of approximately 45 MPa, this implies that the beam is characterized by concrete class C30/37 ($f_{cm} = f_{ck,cube} - 8 = 37$ MPa), and an elastic modulus of 32 GPa. This value is comparable to the E-modulus of S100, as is shown in Table 5.1, but higher than value for E-modulus as found for S50 concrete (Table 5.2).

Fig. 5.6 shows the load versus mid-span deflection curves for the two S50 beams tested at different ages. The mid-span deflection was measured using an LVDT, however, because it was out of range during the test, it was chosen to plot the deformation of the jack as well. In the graphs, the flexural behaviour of an OPC concrete control beam was also plotted. This beam has exactly the same dimensions, reinforcement and cover as the alkali-activated beams, but lower compressive strength. The OPC concrete beam was casted and tested by TU Delft master student Zhekang Huang. From the graph, it is clear that the alkali-activated beams deflected more than the OPC concrete beam, for the same load. The overall stiffness of AAC is a bit lower, the first part of the graph is steepest for the regular OPC concrete beam. The S50 concrete beam tested at 69 days is less stiff and deflects more than the S50-33d beam.

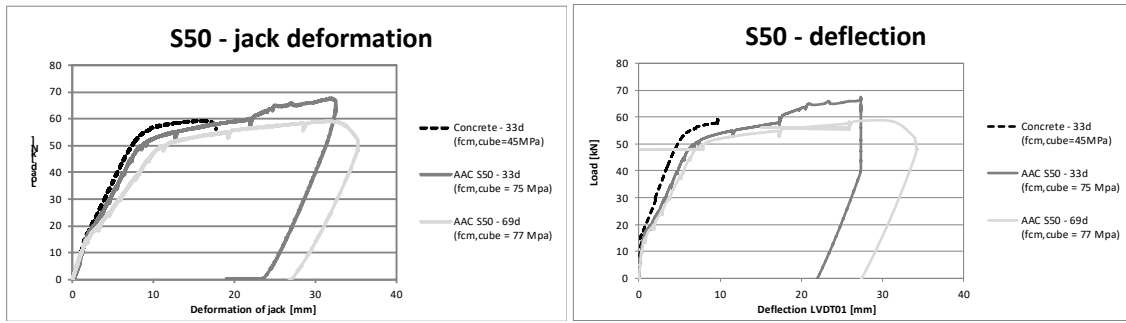


Fig. 5.6: Relationship between load and deformation for beams subjected two four-point bending tests, left graph shows jack deformation and right graph shows deflection as measured by LVDT01. The graph shows the test results for S50 (50% slag and 50% fly ash) concrete, at two different ages, and regular OPC concrete (results by master student Zhekang Huang). S50 specimens have been cured (20°C and 95% RH) for 28 days. After this, the samples were exposed to laboratory conditions (20°C and 55% RH) until testing. OPC concrete was kept in the mould for 33 days (covered with plastic) in lab conditions and then un moulded.

Fig. 5.7 shows the load versus deflection curves for the two S100 beams tested at two different ages and the OPC concrete control beam by Zhekang Huang. Again, the S100 alkali-activated beams deflected more than the regular OPC concrete beam, for the same load. Also, the stiffness of S100-70d is a bit lower, the first part of the graph is steepest for regular OPC concrete and S100-33d. The S100 concrete beam tested at 70 days shows less stiffness and more deflection than the S100 beam tested at 34 days.

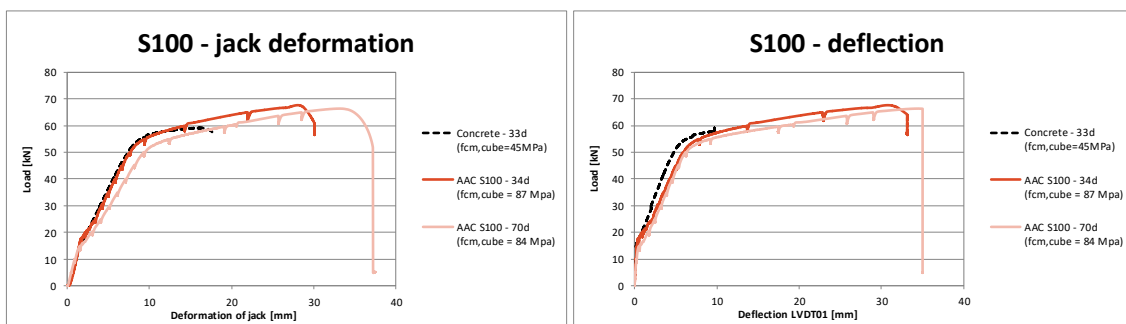


Fig. 5.7: Relationship between load and deformation for beams subjected two four-point bending tests, left graph shows jack deformation and right graph shows deflection as measured by LVDT01. The graph shows the test results for S100 (100% slag and no fly ash) concrete, at two different ages, and regular OPC concrete (results by master student Zhekang Huang). S100 specimens have been cured (20°C and 95% RH) for 28 days. After this, the samples were exposed to laboratory conditions (20°C and 55% RH) until testing. OPC concrete was kept in the mould for 33 days (covered with plastic) in lab conditions and then un moulded.

For all four beams, the flexural capacity was higher than expected based on the conducted theoretical calculations. In *Appendix D – Calculation of reinforced beams*, the theoretical calculations are compared with the test results.

Fig. 5.10 and Fig. 5.11 show the crack patterns of all four alkali-activated concrete beams after failure. The cracking pattern of the regular OPC concrete control beam by Zhekang Huang is shown in Fig. 5.8. The crack patterns for the S50 and S100 are comparable to the OPC concrete beam. The crack spacing is also similar, see Table 5.4. Only one beam, S100-34d exhibited more cracks, so a smaller crack spacing, than the other beams. For this beam, compressive strength was also higher compared to the other beams. Alkali-activated concrete shows bigger crack widths than OPCC, but also a different failure mode (reinforcement failure for three out of the four AAC beams, concrete compressive failure for OPCC beam).

Table 5.4: Number of cracks in the constant moment area for alkali-activated S50 and S100 beams and OPC concrete control beam by Zhekang Huang.

Beam	Testing age [days]	Nr. of cracks* [-]	Crack spacing [mm]
S50	33	5	100.0
S50	69	7	71.4
S100	34	5	100.0
S100	70	5	100.0
OPC concrete	33	5	100.0

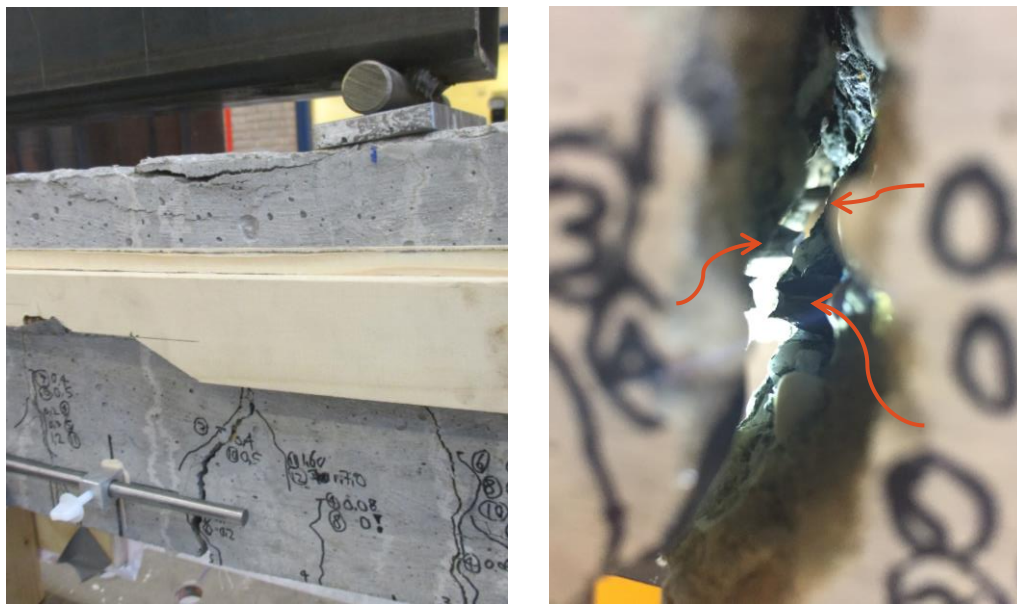
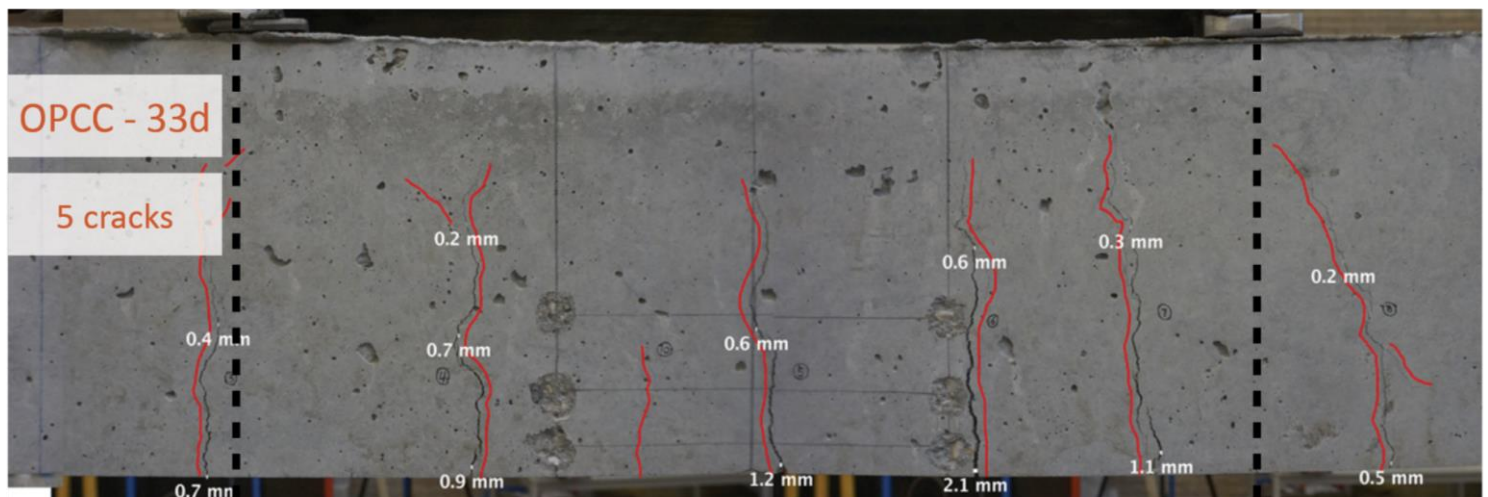


Fig. 5.9: Left: concrete compressive failure for beam S50-69d. Right: three broken tensile reinforcement bars for beam S100-70d.

Fig. 5.8: Crack patterns in ordinary Portland cement concrete. Dotted lines indicate the constant moment area. Results and photo by Zhekang Huang.



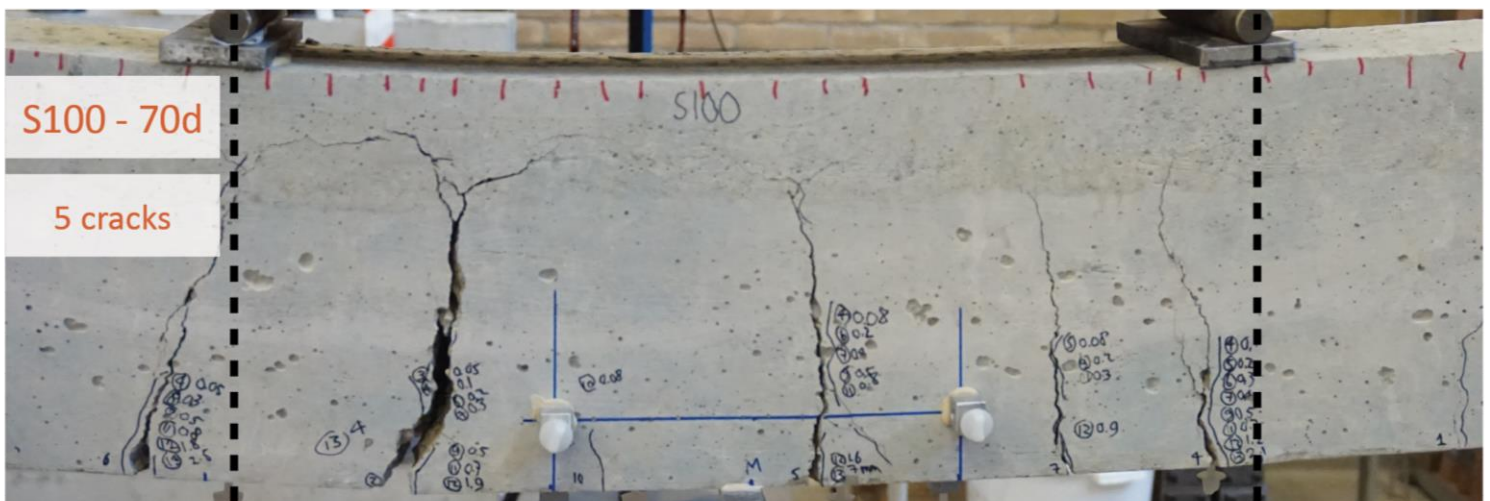
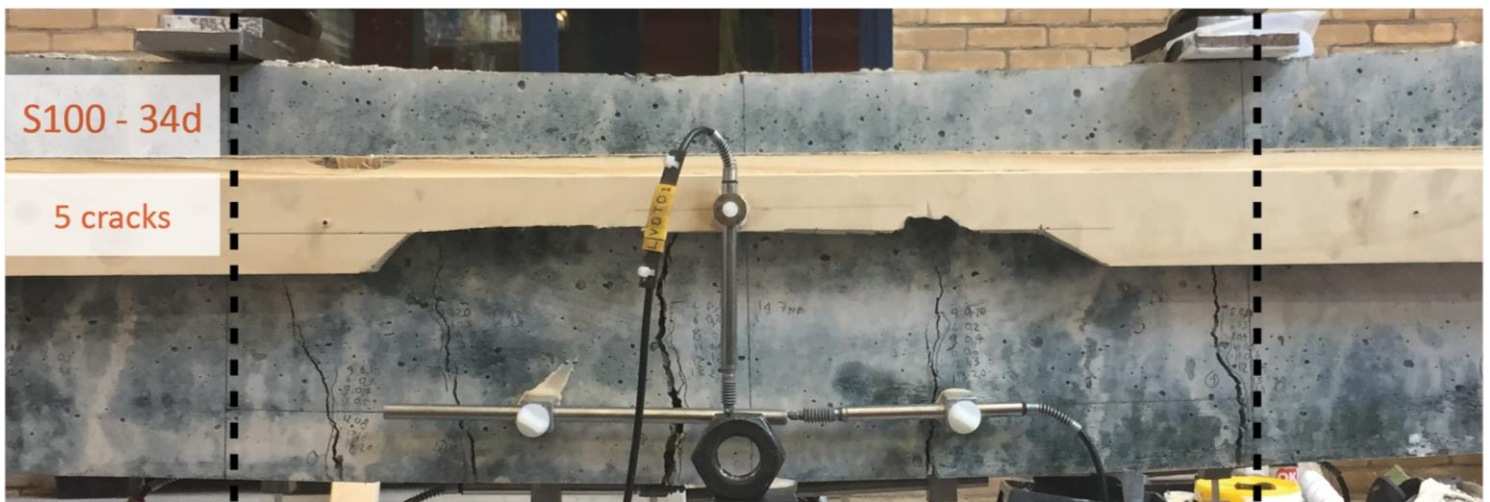
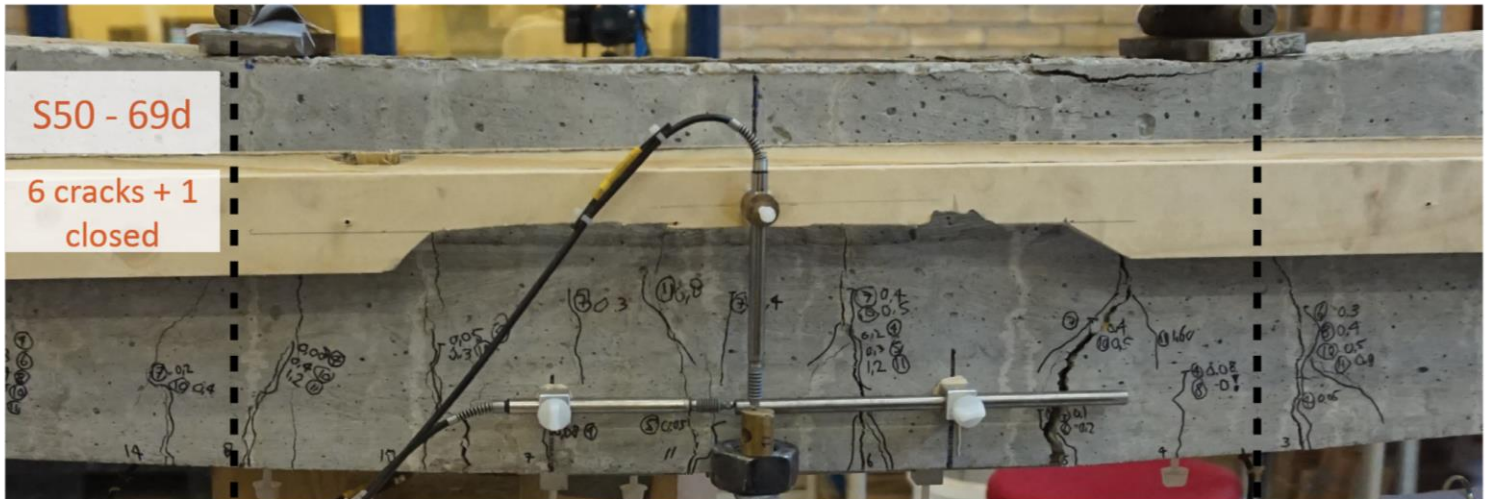


Fig. 5.10: Crack patterns in alkali-activated beams, after failure. Dotted lines indicate the constant moment zone.

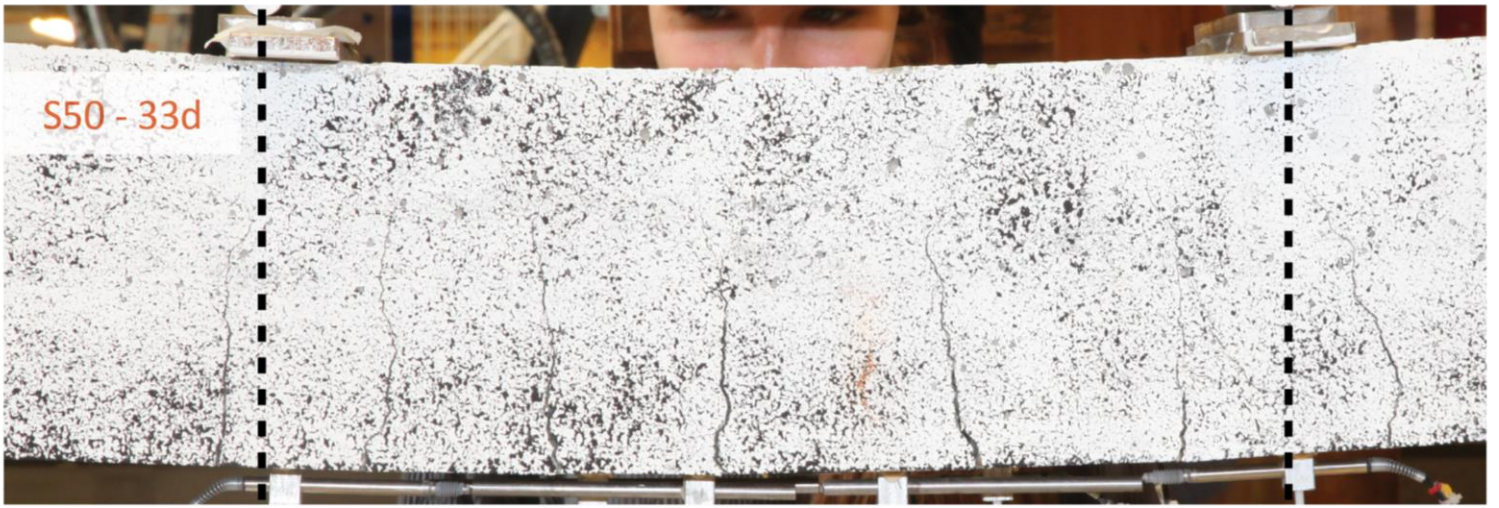


Fig. 5.11: Crack patterns in alkali-activated beams, after failure. Dotted lines indicate the constant moment zone.

Fig. 5.12 and Fig. 5.13 show graphical representations of the propagation of cracks and load-deflection behaviour during the four-point bending tests, for alkali-activated concrete and the OPCC results from Zhekang Huang. These figures show that all crack results are very similar, except for the fact that the propagation of cracks in the OPCC beam stopped earlier because of concrete compressive failure, and the deflection was still small compared to the alkali-activated concrete beams.

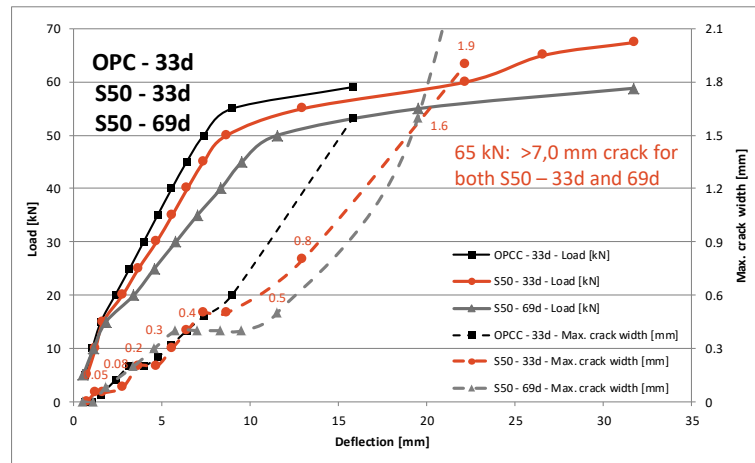


Fig. 5.12: Development of cracks during four-point bending tests on S50 beams at 33 and 69 days and comparison with regular OPCC beam, results by Zhekang Huang. S50 specimens have been cured (20°C and 95% RH) for 28 days. After this, the samples were exposed to laboratory conditions (20°C and 55% RH) until testing. OPC concrete was kept in the mould for 33 days (covered with plastic) in lab conditions and then un moulded.

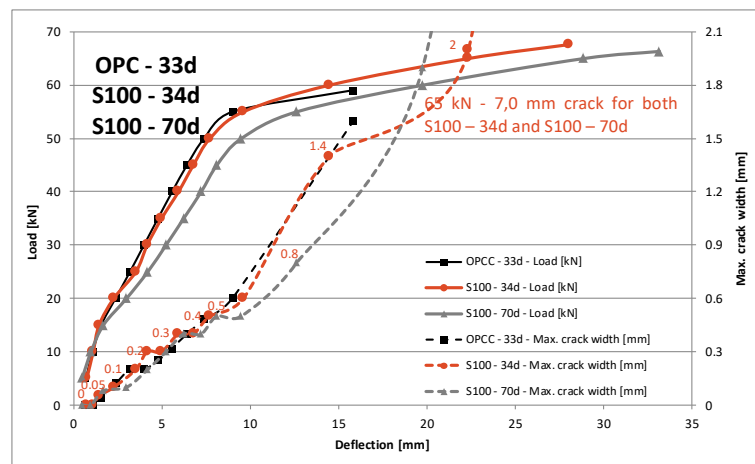


Fig. 5.13: Development of cracks during four-point bending tests on S100 beams at 34 and 70 days and comparison with regular OPCC beam, results by Zhekang Huang. S100 specimens have been cured (20°C and 95% RH) for 28 days. After this, the samples were exposed to laboratory conditions (20°C and 55% RH) until testing. OPC concrete was kept in the mould for 33 days (covered with plastic) in lab conditions and then un moulded.

In general, the structural and cracking behaviour (crack spacing and width), seems to be similar for reinforced AAC and OPC concrete, except for the fact that reinforced AAC showed higher deflections. This is attributed to the relatively lower stiffness; AAC exhibits more ductile behavior (higher rotational capacity) than OPC concrete.

6

Discussion

6.1. In general

In this chapter, the acquired results will be reviewed with respect to the research question. First of all, it is clear that most of the obtained results show a decrease of strength or stiffness for alkali-activated concrete over time, at least for the used curing conditions (20°C and 95% RH for 28 days). Fig. 6.1 shows the relative change of properties for S50 concrete, relative to the strength or stiffness at 28 days. All four properties (compressive strength, splitting tensile strength, flexural strength and E-modulus) show a decrease over time. The highest decrease was found for the elastic modulus, the lowest for compressive strength.

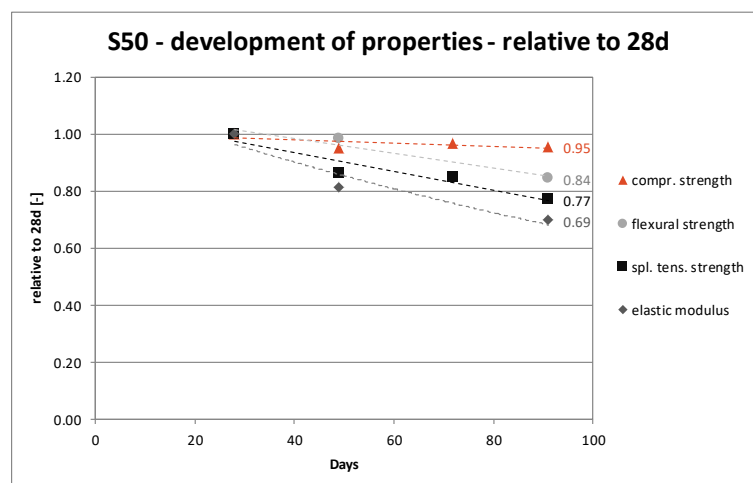


Fig. 6.1: The graph shows the (relative) development of strength and stiffness over time for the S50 (50% slag and 50% fly ash) alkali-activated concrete mixture. Specimens have been cured (20°C and 95% RH) for 28 days. After this, the samples were exposed to laboratory conditions (20°C and 55% RH) until testing.

In Fig. 6.2, the relative change of properties is plotted for S100 (100% slag) concrete. For S100, the results also show the highest decrease over time for the elastic modulus, a slight increase for compressive strength.

So, the results are quite consistent, S50 concrete shows a higher degree of decrease over time than S100 for all four tested properties (compressive strength, splitting tensile strength, flexural strength and E-

modulus). This can clearly be seen when Fig. 6.1 and Fig. 6.2 are compared. The degree of decrease is also consistent in S50 and S100 concrete. Compressive strength shows almost no decrease (or even an increase for S100), flexural strength shows a higher decrease over time, followed by splitting tensile strength and elastic modulus, that shows the highest decrease over time for both the S50 and S100 concrete mixtures.

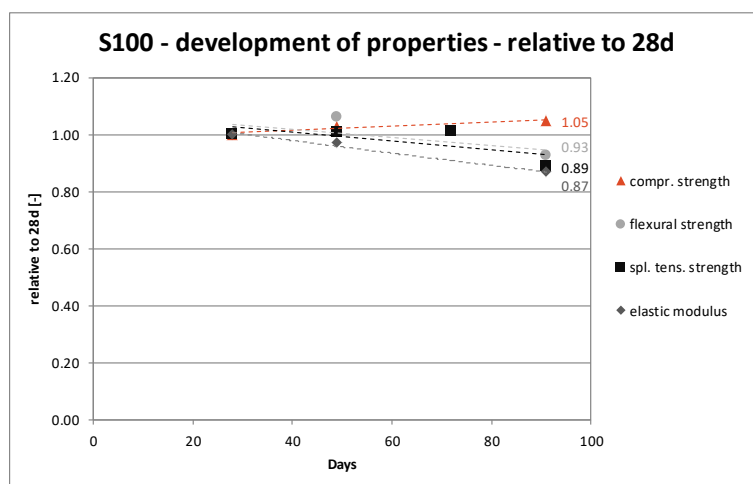


Fig. 6.2: The graph shows the (relative) development of strength and stiffness over time for the S100 (100% slag) alkali-activated concrete mixture. Specimens have been cured (20°C and 95% RH) for 28 days. After this, the samples were exposed to laboratory conditions (20°C and 55% RH) until testing.

Based on these results, it is obvious that the decrease is not directly related to the amount of BFS. If the amount of slag would be the only reason for the decrease over time, it would be logical to assume that S100 shows a higher degree of decrease than S50 concrete, which has not been observed. So, it cannot be concluded that a higher slag content in the binder is causing the decrease over time, as the S50 concrete with 50% fly ash and 50% slag shows a higher degree of decrease than the S100 concrete that contains only blast furnace slag as a binder precursor. However, based on the results in literature (Wardhono et al., 2017), it seems that fly ash is not causing a decrease of strength or stiffness over time, as mixtures with only fly ash as a binder precursor do not show a decrease of properties over time. Now, the main question is of course, what could be the cause of the strength and stiffness loss over time?

Essentially, alkali-activated concrete consists of two main components: the aggregates and the paste in between. It is not likely that the properties of the aggregate will change over time. Furthermore, the bond between those two components, the interface, can also contribute to the development of strength and stiffness over time (Fig. 6.3). At least one of these aspects is changing over time, resulting in a drop of strength and stiffness, possibly due to (micro)cracks. Therefore, it is hypothesized that either the paste, or the bonding zone between the paste and aggregate is changing over time.

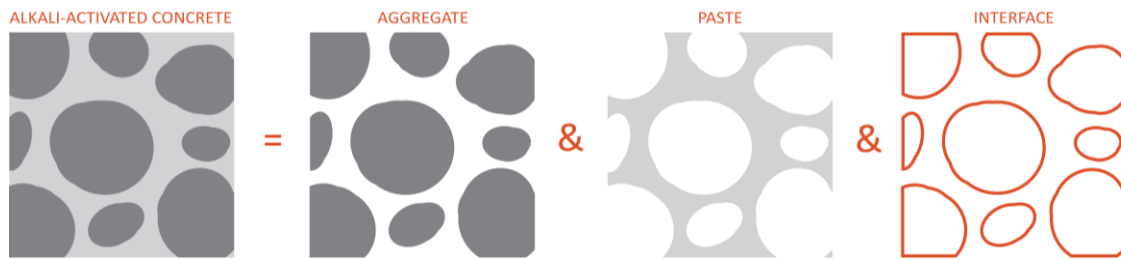


Fig. 6.3: Essential components of alkali-activated concrete.

Apart from changes in the material itself, it could also be that the properties of the material are not negatively influenced, but that eigenstresses occur due to shrinkage gradient. This then results in a lower strength of the specimens, but as long as it does not cause (micro)cracking, the observed decrease might be only temporary. If the conditions outside and inside the material are equal again, a higher value could probably be found.

6.2. Influence of drying

All the samples were wet-cured for 28 days and then exposed to laboratory conditions, while tests were performed at different ages (28, 56 and 91 days). It might be that exposing the samples to dry after the wet-curing period has influence on the strength development. During the experimental phase, some extra specimens have been casted. When all samples were taken out of the curing room (20°C and 95% RH) after 28 days, two 100x100x400 mm³ samples of S50 concrete and two similar S100 specimens were kept in the curing room. After 92 days, they were taken out and tested. The E-modulus is the property that showed the strongest decrease over time, for both S50 and S100 concrete, therefore it was decided to determine E-modulus on these samples that were cured for 92 days. After this, one of the samples was sawn into cubes and used for splitting tensile strength tests, as this is the second-most influenced property. The results of the E-modulus tests are shown in Fig. 6.4.

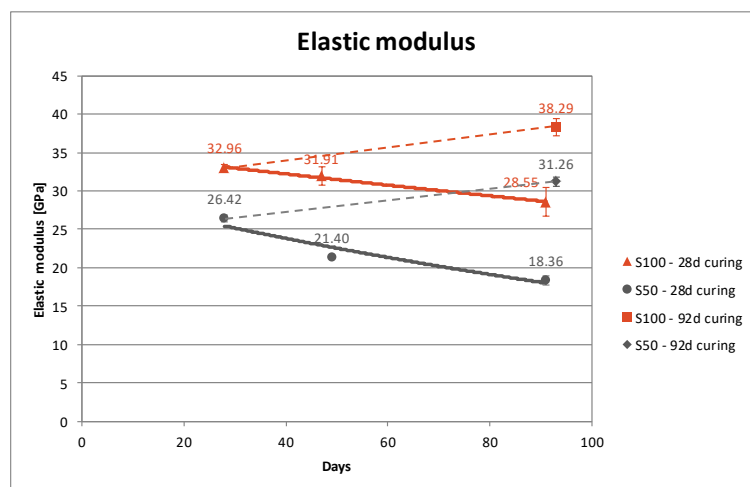


Fig. 6.4: Development of elastic modulus over time for alkali-activated concrete. The graph shows the development over time for both S100 (100% slag) and S50 (50% slag and 50% fly ash) concrete mixtures. Specimens have been cured (20°C and 95% RH) for 28 days or 92 days (see labels). After this, the samples were exposed to laboratory conditions (20°C and 55% RH) until testing.

Fig. 6.4 shows that the elastic modulus increased with more than 15% for S100 and S50 concrete between 92 and 28 days, for the samples that were kept in the curing room for 92 days. Fig. 6.5 shows the results from the splitting tensile strength tests. Similarly, an increase in strength is visible, splitting tensile strength increased with 3% and 10% for S100 and S50 concrete, respectively.

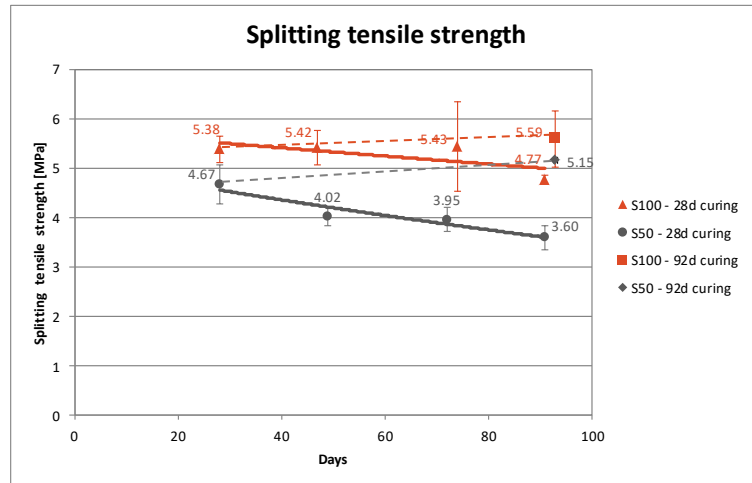


Fig. 6.5: Development of splitting tensile strength over time for alkali-activated concrete. The graph shows the development over time for both S100 (100% slag) and S50 (50% slag and 50% fly ash) concrete mixtures. Specimens have been cured (20°C and 95% RH) for 28 days or 92 days (see labels). After this, the samples were exposed to laboratory conditions (20°C and 55% RH) until testing. Splitting tensile strength has been tested on 100x100x100 mm³ cubes, instead of regular 150x150x150 mm³ cubes.

These results indicate that the drop of strength and stiffness that has been observed might be related to the process of drying. Samples that were taken out after 28 days of wet-curing show a decrease over time, while samples that are taken out of the curing after 92 days show an increase when compared to the 28 day properties. After taking the 92d-cured samples out of the curing, E-modulus has been measured at different moments over time for both a S50 and a S100 concrete sample, to investigate if the same reduction trend can be observed. Fig. 6.6 shows the decrease in E-modulus for both the samples that were cured for 28d and 92d, and a similar trend can be seen.

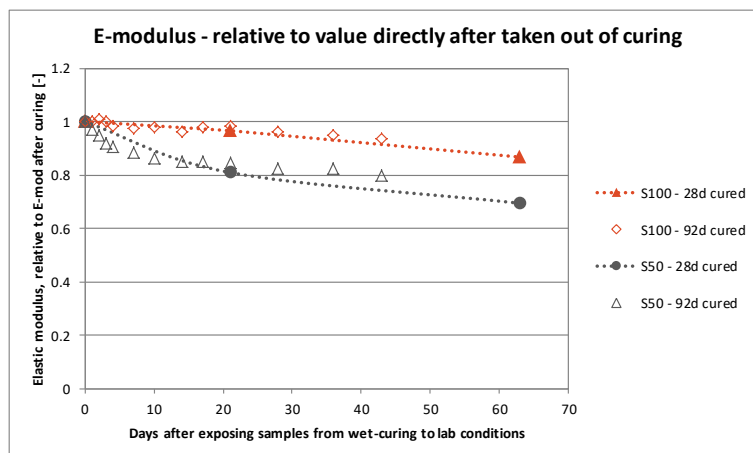


Fig. 6.6: Relative development of elastic modulus over time for alkali-activated concrete, compared to the value for E-modulus on the day that the sample was taken out of wet-curing conditions. The graph shows the development over time for both S100 (100% slag) and S50 (50% slag and 50% fly ash) concrete mixtures. Specimens have been cured (20°C and 95% RH) for 28 days or 92 days (see labels). After this, the samples were exposed to laboratory conditions (20°C and 55% RH) until testing moment.

For the S50 and S100 sample, weight loss was also measured, after the wet-curing period of 92 days. The result is shown in Fig. 6.7, left. The results show a higher weight loss for S50 concrete when compared to the S100 sample. Also, data for CEM III/B concrete is plotted in this graph (Mors, 2011), showing that that the weight loss for the S100 is comparable to slag-rich CEM III/B concrete, whereas S50 loses more moisture. In Fig. 6.7 (right) the relation between E-modulus and weight loss is shown. A linear relation can be observed, which implies that there is a strong influence of moisture loss on the E-modulus. When the samples are exposed to drying, after being wet-cured for a certain amount of time, the E-modulus reduces over time.

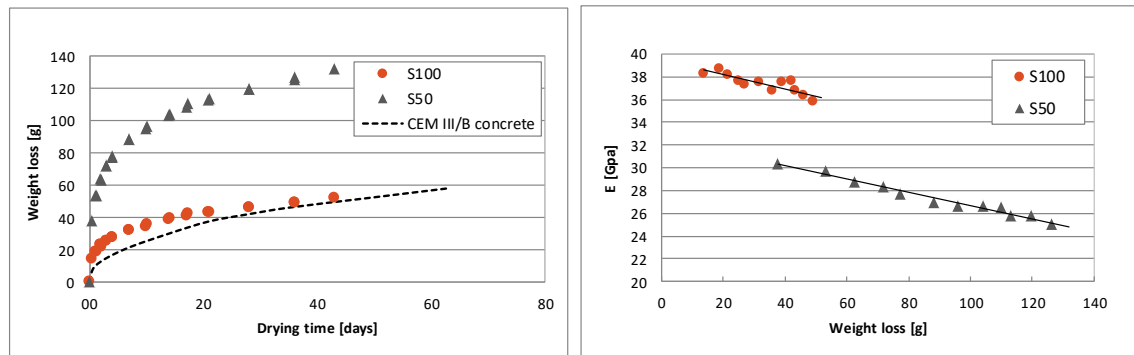


Fig. 6.7: Left: weight loss for one S50 and one S100 AAC sample that have been wet-cured (20°C and 95% RH) for 92 days. After this, the samples were exposed to laboratory conditions (20°C and 55% RH). Also plotted is weight loss for a CEM III/B concrete sample (with the same dimensions), wet-cured for 28 days and then exposed to drying, data from Mors (2011). Right: Relationship between E-modulus and weight loss for the same S50 and S100 samples.

This phenomenon is also observed in regular OPC concrete. Monteiro and Kuhmar Mehta (2006) state that concrete specimens that are tested in wet conditions show about 15 percent higher elastic modulus than the corresponding specimens tested in a dry condition, disregarding any difference in mix proportions or curing age. Monteiro and Kuhmar Mehta mention that the E-modulus decreases because the interfacial transition zone (ITZ) loses strength due to microcracking. This could also be the case for alkali-activated concrete. Yet, a bigger decrease than 15% is visible in the results on elastic modulus in this research. Hypothetically, alkali-activated concrete loses more moisture than OPC concrete because (almost no) water is required to form reaction products in the alkali-activation process. In slag-based systems (BFS), water is (partly) consumed in the activation process, but for geopolymer binders (FA) this is not the case, no water is needed to harden. This is also consistent with the results, S50, containing less BFS than S100, shows a higher decrease of E-modulus over time, probably less water was used during the hardening process. However, initially, both mixes had the same amount of water. Another reason might be a lower porosity and finer pore structure of S100 concrete, which is, therefore, also losing less water compared to S50 (Nedeljković et al., 2017). However, in regular OPC concrete the compressive strength is about 15 percent higher when specimens are tested in a dry condition, compared to testing under wet conditions, because the paste matrix gains strength due to an increase in the van der Waals force of attraction in hydration products (Monteiro & Kuhmar Mehta, 2006). Nevertheless, the results on AAC show contradictory behaviour. Compressive strength is almost constant over time for S100 concrete, and even decreasing for S50. Therefore, it seems that the decrease in elastic modulus cannot be explained

only by moisture loss. Probably some additional changes in the microstructure of S50 and S100 are present.

6.3. ESEM analysis of microstructure

To check if any difference in microstructure was visible, it was decided to investigate the microstructure of the specimens with ESEM (Environmental Scanning Electron Microscope) in the Microlab - TU Delft. Thin sections were cut out of intact rest pieces from sawing the cubes, for all four concrete types (S50-28d cured, S50-92d cured, S100-28d cured and S100-92d cured), see Fig. 6.8. A small sample of these sections was taken out, in order to fit the ESEM machine. The small samples were polished with different grain sizes (from rough to fine) and then examined with ESEM on the same day. Fig. 6.9 shows a few of the images that were acquired during the observation with ESEM. The exact location of the shown images is indicated in *Appendix F – Location of ESEM images*.

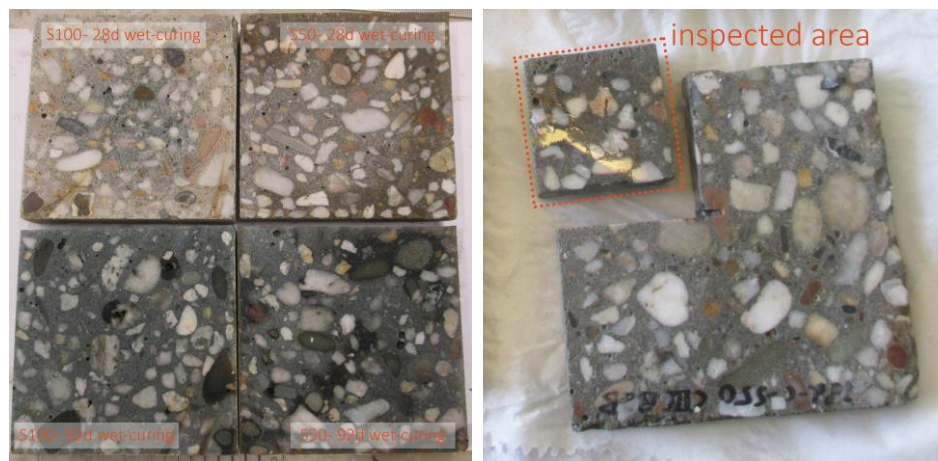


Fig. 6.8: left: Comparison of wet-sawn cross-sectional surfaces for S50 and S100 concrete, cured for 28d or 92d. Right: sawn specimen from section.

The ESEM analysis did not show clear differences between the samples that were cured for 28 days or 92 days. Fig. 6.9 shows small microcracks (with a width of approximately $5\ \mu\text{m}$), both in the paste as well as in the interface between aggregate and paste. Also, there was no convincing difference between the microstructure at the edge (hypothetically more drying occurred there) and the inside of the sample. Some locations showed a bit more microcracks, some spots almost none. The analysis of ESEM images can be quite subjective when zoomed in on a certain location. To conclude, there seems to be no significant difference in microstructure for samples with different curing duration and strength/stiffness development, based on these ESEM analysis. Therefore, the hypothesis of Wardhono et al. (2017), developing cracks (Fig. 3.30) in the gel matrix and reducing packing density, cannot be confirmed with these results. However, it could be that the surfaces look similar because with ESEM analysis only a very thin layer of the material (a few μm) is investigated. While preparing the samples, sawing and grinding, drying (cracks) may have already occurred in the wet-specimens that were cured for 92 days, resulting in similar images that were acquired for the dried specimens that were taken out of the curing at 28 days.

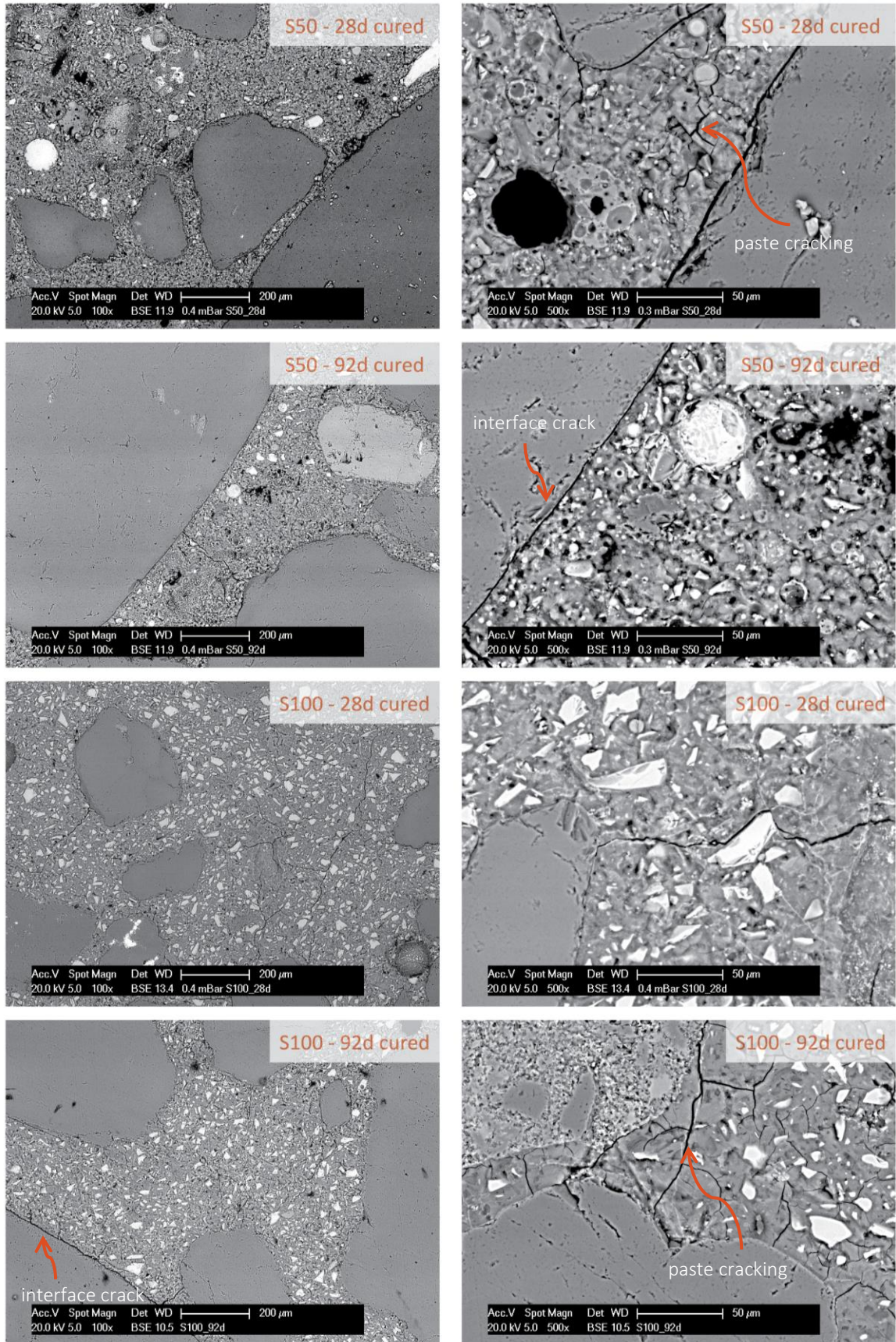


Fig. 6.9: ESEM images for S100 (100% slag) and S50 (50% slag and 50% fly ash) concrete. The two columns have different magnification factors. Specimens have been cured (20°C and 95% RH) for 28 days or 92 days (see labels). After this, the samples were exposed to laboratory conditions (20°C and 55% RH) until the images were made. The exact location of the shown images is indicated in *Appendix F – Location of ESEM images*.

6.4. Size effects

If drying would cause a decrease of properties over time, it would be expected that the outer layer is affected first, as drying starts from the outside. This implies that small samples would show a stronger decrease of strength over time than large samples, because drying has relatively more effect on small samples, illustrated in Fig. 6.10.

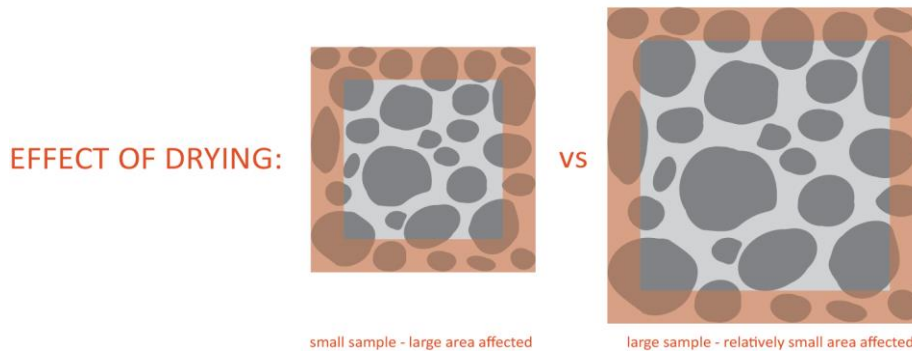


Fig. 6.10: Drying may cause a size effect when samples of different sizes are compared at similar ages.

To investigate this hypothesis, results of cube tests on $100 \times 100 \times 100 \text{ mm}^3$ samples have been plotted against the test results on $150 \times 150 \times 150 \text{ mm}^3$ cubes that have been casted simultaneously with the reinforced beams. This is shown in Fig. 6.11. The results do not explicitly confirm the hypothetical size effect that can be caused due to drying. For S100, the results on bigger samples are even lower. A possible reason for this is the casting procedure and short workable time of the S100 mixture. Namely, $150 \times 150 \times 150 \text{ mm}^3$ cubes were casted only after casting the beams, whereas the $100 \times 100 \times 400$ prisms were cast immediately after mixing. No clear conclusions can be made on the effect of size (in combination with drying) with respect to the observed reduction in strength and stiffness for alkali-activated concrete.

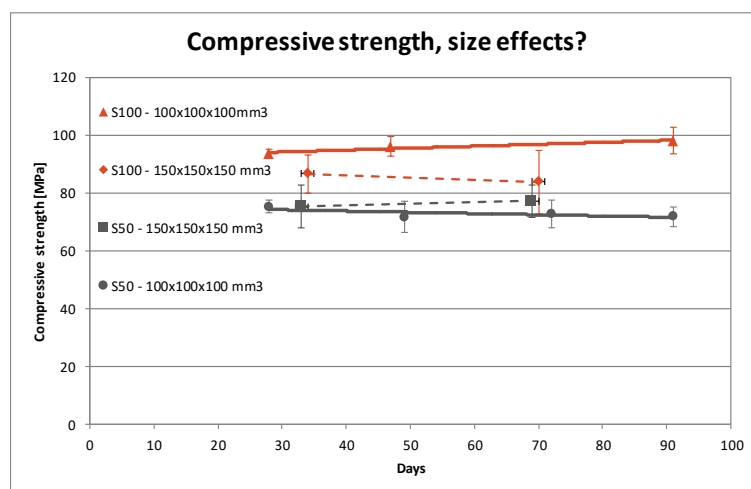


Fig. 6.11: Comparison of results on compressive strength for cubes of $150 \times 150 \times 150 \text{ mm}^3$ and $100 \times 100 \times 100 \text{ mm}^3$ (as indicated) for both S100 (100% BFS) and S50 (50% BFS and 50% FA) concrete. Specimens have been cured (20°C and 95% RH) for 28 days. After this, the samples were exposed to laboratory conditions (20°C and 55% RH).

6.5. Bending capacity of reinforced beams

The results on the bending capacity of reinforced beams showed a contradictory phenomenon for S50 concrete. When testing the reinforced specimen at 33 days, the failure mode was reinforcement failure, no concrete crushing in the compressive zone occurred yet. The failure load of the reinforced S50 beam that was tested at 69 days was approximately 13% lower, and concrete compressive failure was observed (Fig. 5.9, left), instead of reinforcement failure. However, compressive tests on cubes (150x150x150 mm³) indicate that the compressive strength of the S50 concrete increased with time, as is shown in Table 6.1. Note that the opposite trend is observed for 100x100x100 mm³ compression specimens, as was shown in Fig. 5.1 and Fig. 6.1.

The general properties of both beams are exactly the same (dimensions, reinforcement), and compressive strength is about the same, so the same failure mode would be expected. This means that the results imply that something is different.

Table 6.1: Comparison of the results from the S50 concrete beams tested at 33 days and 69 days.

	Testing age	Tens. reinf. ratio	Compr. Strength	Failure load	Max. deflection jack	Ultimate moment	Failure
Beam	[days]	[%]	[MPa]	[kN]	[mm]	[kNm]	
S50	33	0.61	75.1	67.4	32.5	16.9	<i>Reinf.</i>
S50	69	0.61	77.1	58.8	35.2	14.7	<i>Concr. compr.*</i>

*The failure mechanism for beam S50-69d is different from the other three tested beams, compressive failure was observed.

The beam tested at 69 days showed compressive failure, while the compressive strength tested on cubes was comparable to cubes tested at 33 days. This indicates that the compressive strength of the top zone in the beam might have had different properties than the tests on cubes showed. Right before failure, the compressive zone height (x_u) is very small, so different material properties in this top layer can have impact on the failure mode of the reinforced beams. Fig. 6.12 shows two possible explanations of how the top layer of concrete can differ amongst the two beams. It could be the case that due to vibrating during casting, aggregates are not evenly distributed across the concrete cross section. This results in a different compressive strength for this small top layer than expected based on the cube tests. Another reason could be that, like discussed in the previous paragraphs, some phenomenon that has to do with drying causes a decrease of properties over time. This is justified by the reduction of compressive strength for the 100x100x100 mm³ samples.

If the graphs in Fig. 5.6 and Fig. 5.7 are carefully observed, it seems that the stiffness of the S50 and S100 beam tested at 69 and 70 days is lower than for the beams tested at 33 and 34 days. The first part of the force-displacement graph for the beams tested at 69 and 70 days is less steep. This implies that the E-modulus is also decreasing over time. But, as only one beam is tested for each mixture and moment over time, these observations and hypothesis might not be representative for a big batch. Based on the current results with only one tested beam per condition, no final conclusions can be drawn on the cause of the different failure mode. A recommendation would be to cut the specimens, and investigate the cross section to observe if there is any difference between the beams.

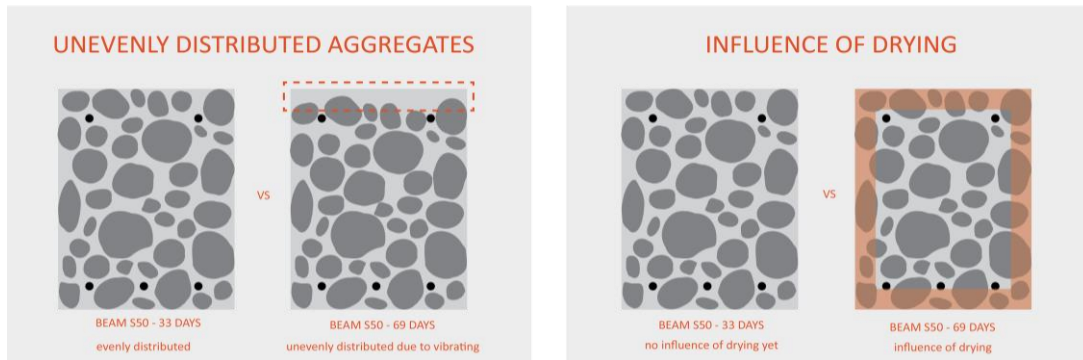


Fig. 6.12: Possible explanations for the different failure mode and capacity of the S50 concrete beam tested at 33 days (reinforcement failure, no concrete crushing) when compared to the beam tested at 69 days (concrete crushing in the compressive zone).

6.6. Comparison with regular OPC concrete

6.6.1. Effect of drying on the development of strength and stiffness for OPC concrete

Fig. 6.13 shows development of compressive strength over time for American OPC type I, II and III cement³ concretes, wet-cured for seven days and then exposed to drying. From this graph, it is clear that the behaviour observed in this study (for the chosen AAC mixtures and curing conditions) is not comparable to the development of strength for OPC concrete, where an increase over time is observed, although the samples are exposed to drying.

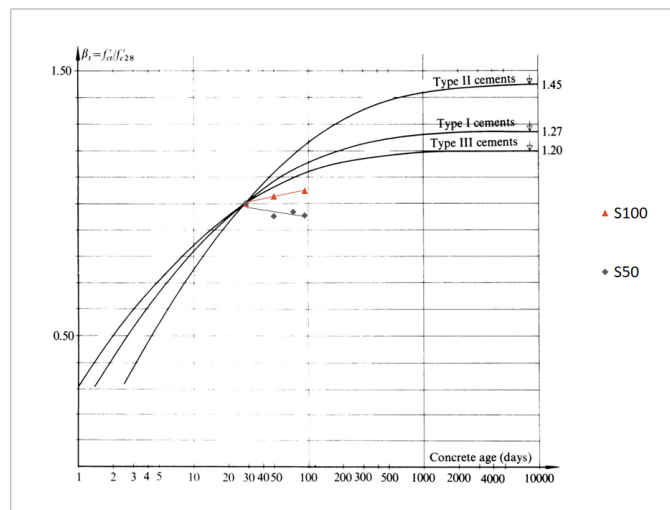


Fig. 6.13: Development of compressive strength over time, a comparison between regular OPC concrete (wet-cured for 7 days and then exposed to drying) for American CEM type I, II, III according to ASTM C150¹ (Rüsch et al., 1983, p. 21) and alkali-activated concrete S50 and S100 (orange and grey lines). The coefficient $\beta_t = f_c / f_{c28}$ describes the effect of concrete age on compressive strength, by comparing all values with the 28 day strength.

³ Three different types of Portland cements according to ASTM C150. Type I: For use when the special properties specified for any other cement type are not required. Type II: For general use, especially when moderate sulphate resistance is desired. Type III: For use when high early strength is desired.

However, based on the research by Maruyama et al. (2014), it is clear that drying has influence on the material properties of OPC concrete, like has been observed for AAC in this research. Maruyama et al. observed lower values for compressive strength of OPC concrete that was exposed to 40% RH when compared to 80% RH (Fig. 6.14, left). Fig. 6.14 (right) shows the same trend for E-modulus of OPC concrete, a lower elastic modulus is observed for samples that were exposed to lower relative humidity. According to Maruyama et al. (2014), this is caused by cracks that are formed in the concrete because of differences in the change in volume between the aggregate and mortar.

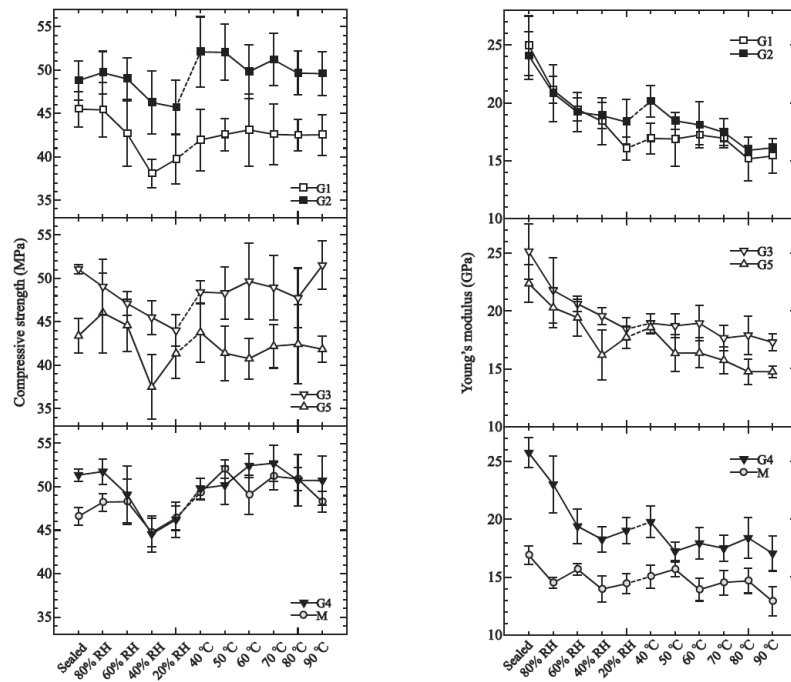


Fig. 6.14: Compressive strength (left) and E-modulus (right) of OPC concretes (G1-5) and mortar (M) under different heating or drying conditions (Maruyama et al., 2014, pp. 60-61). The specimens were cured under sealed conditions for 2 months at 20°C, after this, the specimens were placed in RH-controlled chambers at 80%, 60%, 40%, or 20% RH, or in temperature-controlled chambers at 40, 50, 60, 70, 80, or 90 °C for about 5 months.

It has been observed, therefore, that drying causes changes in strength and stiffness also for OPC concrete. For the samples that were exposed to relative humidity of 40% and 60% after 28 days of sealed curing, the reduction of E-modulus and compressive strength can be up to 30 % and 15 % (see Fig. 6.15, highlighted area), respectively, and depending on the concrete mixture and type of aggregates used. Therefore, the decrease of properties over time that has been observed for alkali-activated concrete in this research might be related to the behaviour that is also happening in regular concrete.

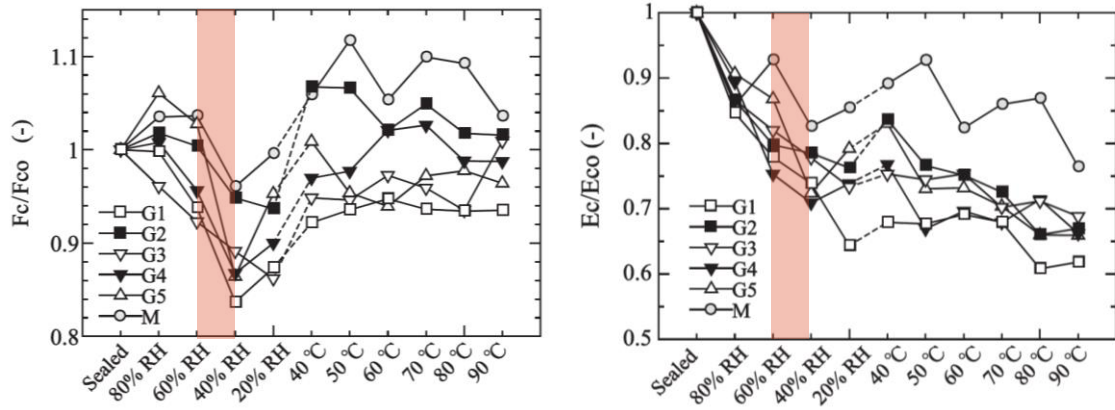


Fig. 6.15: Normalized compressive strength (left) and elastic modulus (right) for OPC concretes (G1-5) and mortar (M) under different heating or drying conditions (Maruyama et al., 2014, pp. 61-62). The specimens were cured under sealed conditions for 2 months at 20°C, after this, the specimens were placed in RH-controlled chambers at 80%, 60%, 40%, or 20% RH, or in temperature-controlled chambers at 40, 50, 60, 70, 80, or 90 °C for about 5 months.

6.6.2. Measured properties for AAC versus Eurocode 2 for OPC concrete

In order to be able to apply alkali-activated concrete for structural applications on a bigger scale, codes and standards should be available. The design codes for OPC concrete are based on a set of implicit assumptions relating its microstructure to macro-behaviour of the material, and because the composition of the binder in AAC is chemically different, these assumptions might not be valid for alkali-activated concrete (J. Provis & van Deventer, 2014). Therefore, research is, and should be applied in order to check if the concrete codes can be applied for alkali-activated concrete, or that modifications should be made. In this paragraph, the acquired results on alkali-activated concrete are compared with Eurocode 2 for OPC concrete.

Table 6.2 shows a comparison between the tested properties for AAC and estimated properties for concrete with similar compressive strength, where the properties are estimated based on Eurocode 2 equations.

Table 6.2: Comparison of the Equations in Eurocode 2 versus the 28d test results from S50 and S100 specimens.

COMPARISON	OPCC codes		S50 test results		%	OPCC codes		S100 test results		%
$f_{cm, cube}$	75.3	MPa	75.3	MPa		93.5	MPa	93.5	MPa	
$f_{cm} = 0.8 * f_{cm, cube}$	60.2	MPa	-	MPa		74.8	MPa	-	MPa	
$f_{ctm} = 2.12 * \ln(1 + \frac{f_{cm}}{10})$	4.1	MPa	-	MPa		4.5	MPa	-	MPa	
$f_{ct, sp} = \frac{f_{ctm}}{0.9}$	4.6	MPa	4.2	MPa	-8.5%	5.0	MPa	5.4	MPa	6.9%
$E_{cm} = 22000 \left[\frac{f_{cm}}{10} \right]^{0.3}$	37.7	GPa	26.4	GPa	-30.0%	40.2	GPa	33.0	GPa	-18.0%

From Table 6.2, it can be concluded that the splitting tensile strength ($f_{ct,sp}$) can be estimated quite well using Eurocode 2. But, the value for S50 concrete is overestimated by about 8% using the EC2 equations,

this would not give a safe estimation for design calculations. However, the order of magnitude of this equation seems to be correct. For the elastic modulus, this is not the case. For S50 concrete, the results based upon experiments are 30% lower than the values common for regular OPC concrete. It can be concluded that EC2 for regular OPC concrete gives unsafe predictions for alkali-activated concrete, with respect to estimation of E-modulus. Revisions, or a completely different approach (maybe not based on mainly compressive strength), are needed.

Although a lot of researchers state that the flexural and tensile strength of AAC is significantly higher than would be expected from the codes on OPC concrete, this is not the case for the experimental results that were obtained in this research. Fig. 6.16 shows the relationship between flexural and compressive strength for different types of alkali-activated concrete, as indicated. The results from this research have also been added. It is clear that the ratio between flexural strength and compressive strength is comparable to OPC concrete. However, the wide variety in reported results proves that this is not necessarily the case for all alkali-activated concrete mixtures.

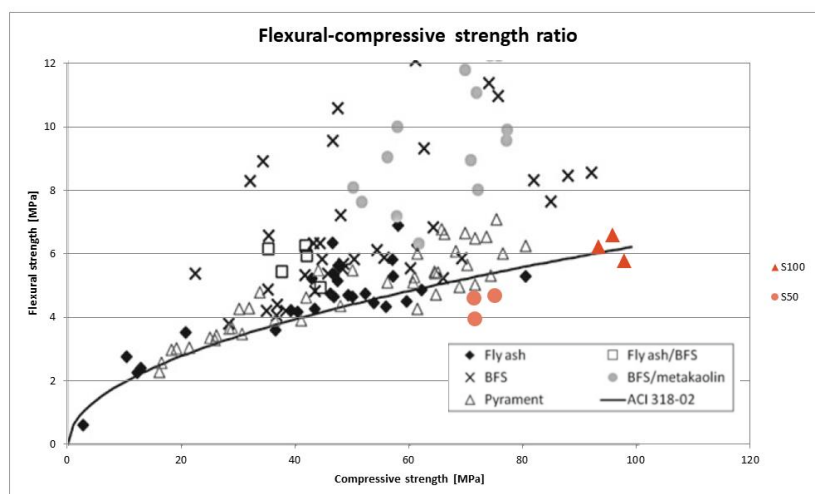


Fig. 6.16: Relationship between flexural and compressive strength of alkali-activated concretes, synthesized from various precursors as marked, at ages between 4 h and 1 year, with the relationship for OPC concretes as specified in ACI 318-02 shown for comparison (J. L. Provis, Bílek, et al., 2014, p. 283). The results from this research have been added in orange, for both S50 and S100 concrete.

To conclude, although the appearance of OPC concrete and alkali-activated concrete might look comparable, this paragraph showed that not all properties are similar. It might even be 'wrong' to compare AAC to OPC concrete, because the hardening process and type of reaction can differ a lot, it can also be categorized as a completely different material. The reported results on alkali-activated concrete vary a lot, properties depend on the used raw materials, chosen activator and curing conditions. For OPC concrete, most of the properties can be influenced by adjusting the water-cement ratio. This approach does not seem to be valid for AAC, which seems to be much more complex and has much more parameters, besides water/solid ratio, which largely influence the mixture properties.

The fact that AAC seems to be a different type of material, or at least with a wider range of possible properties, could also imply that 'habits' for OPC concrete might not be the optimal solution for the whole

range of AAC. An example of this is the type of curing used. Maybe, wet-curing is not the ideal type of curing for the mixtures applied in this research, although it proved itself in OPC concrete. For OPC it is favorable (as water is beneficial for hydration), however for the AAC reaction, less water is needed. It could be that sealed curing is a better choice, resulting in strength and stiffness increase over time, for instance. Instead of comparing the material to OPC concrete, the industry should perhaps consider AAC as a different type of material, and try to develop a design procedure for the alkali activated mixtures and to investigate how mixture compositions and different curing conditions can influence the properties.

7

Conclusions and recommendations

This chapter summarizes the results presented in this thesis. An answer to the main research question will be formulated, based upon the acquired results. Also, practical recommendations and directions for further research will be suggested.

7.1. Conclusions

The main goal of this research was to give insight in the development of strength and stiffness over time for Alkali-Activated Concrete (AAC) containing blast furnace slag, as a few researchers reported a decrease of strength and stiffness over time for slag-based mixtures. Based upon results in literature (Fig. 7.1, left), it was hypothesized that the amount of blast furnace slag in the binder of alkali-activated concrete influences strength and stiffness development over time. Therefore, the development of strength and stiffness was investigated for two alkali-activated concrete mixtures, S50 and S100, characterized by a 50:50 and 0:100 fly ash/slag binder ratio respectively. The results from the experimental research on prism specimens show a decrease of strength and stiffness over time, for both S50 and S100 concrete (Fig. 7.1, right). However, it should be noted that this is the case for the chosen curing conditions and mixtures and does not imply that every AAC mixture shows the same behaviour. The acquired results from the experiments show that S50 concrete is characterized by a higher degree of decrease over time than S100 for all four tested properties (compressive strength, splitting tensile strength, flexural strength and E-modulus). Based on these results, it is obvious that the decrease is not directly related to the amount of BFS. If the amount of slag would be the only reason for the decrease over time, it would be logical to assume that S100 shows a higher degree of decrease than S50 concrete, which has not been observed.

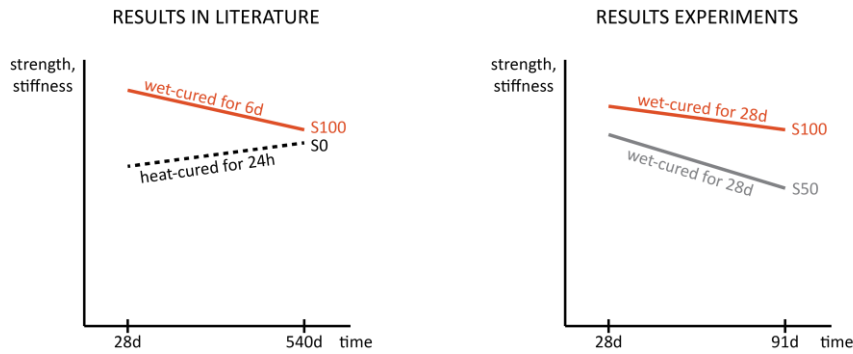


Fig. 7.1: Left: Schematic representation of results in literature (Wardhono et al., 2017). Right: Results from conducted experiments. The three different mixtures with the following BFS/FA binder ratios 0:100, 50:50, 100:0 are named respectively S0, S50 and S100.

The degree of decrease is consistent for both S50 and S100 concrete. Compressive strength shows almost no decrease (or even an increase for S100), flexural strength shows a higher decrease over time, followed by splitting tensile strength and elastic modulus, that shows the highest decrease over time. This is consistent with the few results that have been reported in literature, that also show the biggest decrease for E-modulus and (almost) no decrease for compressive strength (Wardhono et al., 2017).

The results of four-point bending tests on reinforced AAC beams might confirm that the elastic modulus is decreasing over time, as a decrease of the overall stiffness was observed in time. The same trend was observed both for S50 and S100 reinforced beams. However, because only one beam is tested for each mixture and moment over time, these observations might not be representative. Furthermore, a contradictory phenomenon for S50 concrete beams tested at the age of 33 and 69 days was observed. When performing the four-point bending test on the reinforced specimen at the age of 33 days, the failure mode was reinforcement failure, no concrete crushing in the compressive zone was observed. The beam tested at 69 days showed compressive failure, while the compressive strength tested on cubes was comparable to cubes tested at 33 days. It is therefore assumed that the compressive strength of the top zone in the beam might have been different than the tests on cubes showed. Right before failure, the height of the compressive zone is about 15mm and different properties in the top layer can influence the failure mode of reinforced beams. Two possible reasons were named, one is the fact that due to vibrating during casting, aggregates are not evenly distributed across the concrete cross section. This results in a different compressive strength for this small top layer than expected based on the cube tests. Another reason could be that the strength and/or stiffness properties are decreasing due to a phenomenon that has to do with drying (for example, due to microcracking or eigenstresses), causing a decrease of strength over time, especially in the outer layers initially. It is advised to saw the specimens in order to be able to examine the cross-sections at midspan.

In general, the structural behavior and development of cracks (spacing and width), seem to be comparable for reinforced AAC and conventional concrete. But, due to the relatively lower E-modulus, reinforced AAC shows higher deflections and exhibits more ductile behavior (higher rotational capacity). This should be taken into account with considering possible structural applications for AAC.

With the acquired results from the conducted experiments, the main research question has been answered partially. The development of strength and stiffness for AAC over time is known, for the chosen mixture compositions and curing conditions. For most mechanical properties, a decrease over time is observed. Steps towards understanding the cause for this phenomenon were made, by conducting additional research.

All the samples were wet-cured for 28 days and then exposed to laboratory conditions, while tests were performed at different ages (28, 56 and 91 days). It might be that exposing the samples to dry after the wet-curing period has influence on the strength development. A few extra samples that were wet-cured for 92 days were also tested. Samples that are exposed after 28 days of wet-curing show a decrease in properties, while extra samples that are tested after 92 days of wet-curing show an increase when compared to the 28 day properties (Fig. 7.2). Therefore, the acquired results indicate that the decrease of strength and stiffness that has been observed might be related to drying.

Furthermore, an approximately linear relationship between moisture loss and decrease of elastic modulus was observed, giving another indication that drying (moisture loss) might be causing a decrease of properties. For OPC concrete, this is also the case. OPC concrete specimens that are tested in wet conditions show an E-modulus that is approximately 15% higher than corresponding specimens tested in a dry condition, disregarding any difference in mix proportions or curing age. Depending on the microstructure, alkali-activated concrete loses more moisture because, compared to OPC concrete, less water is required to form reaction products in the alkali-activation process. This might be the reason for the fact that the observed drop in E-modulus is significantly higher than 15%.

However, for regular OPC concrete the compressive strength is about 15% higher when specimens are tested in a dry condition, compared to testing under wet conditions, the results on AAC show contradictory behaviour. Therefore, it is not yet clear if the decrease in elastic modulus can be explained by only moisture loss. To investigate if any difference in microstructure was visible, an ESEM (Environmental Scanning Electron Microscope) analysis was performed on samples that were wet-cured for 28 days and then exposed to drying at laboratory conditions and samples that were wet-cured for 92 days. The ESEM analysis did not show explicit differences in microstructure between the samples that were cured for 28 days or 92 days.

To conclude, this research has confirmed that alkali-activated concrete containing BFS can show a decrease of strength and stiffness properties over time, at least for the investigated mixtures and chosen curing conditions. Especially for E-modulus, quite a significant decrease has been observed. The acquired results indicate that the observed decrease of properties is related to drying (moisture loss). However, more research is needed to get a grip on the observed phenomenon, especially related to the aimed practical application of alkali-activated concrete.

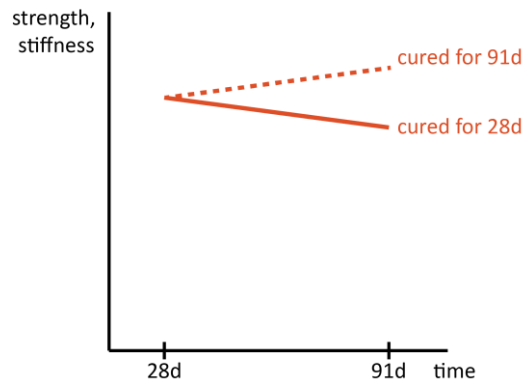


Fig. 7.2: Schematic representation of results and the effect of wet-curing on strength and stiffness development over time.

7.2. Recommendations for further research

In order to use the material for practical applications, it is important that the observed phenomenon of a decrease of properties over time is understood. Subsequently, it can be judged what this phenomenon means for structural application of the material, or how it can be dealt with. So, further research should focus on a deeper understanding of the strength and stiffness reduction over time.

A first aim could be to study the influence of drying on strength and stiffness development of AAC, because the results from this thesis research suggest that the observed decrease over time might be related to moisture loss. If moisture loss is the main reason for the drop in investigated material properties, maybe sealed conditions might be more appropriate for curing alkali-activated concrete and moist curing should be absolutely avoided, for instance.

A suggestion is to experiment with a quantitative approach to analyze the microstructure of the material for different curing conditions and concrete mixtures. Possibly, comparing the size and amount of microcracks in the microstructure while varying curing conditions might help to identify if, and how, drying affects the material. Investigating the behaviour of only paste is another possible research direction to check if, and under which conditions, strength or stiffness reduction occurs.

However, apart from zooming in, it is also wise to upscale. It could be that the observed decrease only plays a role for small-sizes samples, or at least, that the effect is (almost) negligible in large reinforced elements. In addition to this, it is advised to investigate the behaviour of AAC over a longer period of time. In this research, the age of the material was only 91 days during the last tests. In literature (Wardhono et al., 2017) the samples have been tested until 540 days. As long as it does not cause cracking, it might be that the observed decrease is only temporary (due to eigenstresses caused by shrinkage gradient), so examining the material behaviour over a longer period of time could lead to other conclusions. The applications that were discussed in paragraph 2.6 showed a significant strength gain for alkali-activated slag concrete over almost 30 years. This indicates that the observed decrease of properties in this research does not necessarily mean that AAC shows this phenomenon for every mixture composition, curing regime or over every period of time.

It should be emphasized that the physical and chemical properties of alkali-activated concrete vary a lot. For traditional OPC concrete, a lot of properties can be adjusted by modifying the water-cement ratio, this is not exactly the same in AAC. Instead of using Portland cement and water, a lot of different raw materials and alkali activator solutions can be combined to form a binder. The properties of alkali-activated concrete depend largely on the used raw materials, chosen activator and the curing conditions. Therefore, this does not mean that the observed phenomenon of a drop of properties over time would occur for every alkali-activated concrete mixture or for every curing regime. It is necessary to investigate how the composition of AAC mixtures and different types of curing can affect the properties of alkali-activated concrete.

References

- Aldin, Z., Nedeljković, M., Luković, M., Liu, J., Blom, K., & Ye, G. (2017). *Optimization of a geopolymer mixture design for a reinforced cantilever concrete bench*. Paper presented at the The 9th International Symposium on Cement and Concrete (ISCC 2017).
- Aldred, J., & Day, J. (2012). *Is geopolymer concrete a suitable alternative to traditional concrete*. Paper presented at the 37th Conference on our world in concrete & structures, Singapore.
- Arbi, K., Nedeljković, M., Zuo, Y., & Ye, G. (2016). A Review on the Durability of Alkali-Activated Fly Ash/Slag Systems: Advances, Issues, and Perspectives. *Industrial & Engineering Chemistry Research*, 55(19), 5439-5453.
- Bakharev, T., Sanjayan, J. G., & Cheng, Y. B. (1999). Effect of elevated temperature curing on properties of alkali-activated slag concrete. *Cement and Concrete Research*, 29(10), 1619-1625.
- Bernal, S. A., Mejía de Gutiérrez, R., & Provis, J. L. (2012). Engineering and durability properties of concretes based on alkali-activated granulated blast furnace slag/metakaolin blends. *Construction and Building Materials*, 33, 99-108.
- Bernal, S. A., Provis, J. L., Fernández-Jiménez, A., Krivenko, P. V., Kavalerova, E., Palacios, M., & Shi, C. (2014). Binder Chemistry – High-Calcium Alkali-Activated Materials. In J. L. Provis & J. S. J. van Deventer (Eds.), *Alkali Activated Materials: State-of-the-Art Report, RILEM TC 224-AAM* (pp. 59-91). Dordrecht: Springer Netherlands.
- Cement&BetonCentrum. (2015). Cementmarkt. Retrieved May 2 2017 from <http://www.cementenbeton.nl/marktinformatie/cementmarkt>
- Chang, J. J., Yeih, W., & Hung, C. C. (2005). Effects of gypsum and phosphoric acid on the properties of sodium silicate-based alkali-activated slag pastes. *Cement and Concrete Composites*, 27(1), 85-91.
- Chi, M. (2012). Effects of dosage of alkali-activated solution and curing conditions on the properties and durability of alkali-activated slag concrete. *Construction and Building Materials*, 35, 240-245.
- Collins, F. G., & Sanjayan, J. G. (1999). Workability and mechanical properties of alkali activated slag concrete. *Cement and Concrete Research*, 29(3), 455-458.
- Collins, F. G., & Sanjayan, J. G. (2001). Microcracking and strength development of alkali activated slag concrete. *Cement and Concrete Composites*, 23(4-5), 345-352.
- de Rooij, M., Valcke, S., & Visser, J. (2010). Mythe of mogelijkheden? *Cement*, 7-2010, 74-79.
- Diaz-Loya, E. I., Allouche, E. N., & Saiprasad, V. (2013). Mechanical Properties of Fly-Ash-Based Geopolymer Concrete. *Materials Journal*, 108(3).
- Ding, Y., Dai, J.-G., & Shi, C.-J. (2016). Mechanical properties of alkali-activated concrete: A state-of-the-art review. *Construction and Building Materials*, 127, 68-79.
- Douglas, E., Bilodeau, A., Brandstetr, J., & Malhotra, V. M. (1991). Alkali activated ground granulated blast-furnace slag concrete: Preliminary investigation. *Cement and Concrete Research*, 21(1), 101-108.
- Duxson, P. (2009). 3 - Geopolymer precursor design *Geopolymers* (pp. 37-49): Woodhead Publishing.
- Duxson, P., Fernández-Jiménez, A., Provis, J. L., Lukey, G. C., Palomo, A., & van Deventer, J. S. J. (2007). Geopolymer technology: the current state of the art. *Journal of Materials Science*, 42(9), 2917-2933.
- Duxson, P., Provis, J. L., Lukey, G. C., Mallicoat, S. W., Kriven, W. M., & van Deventer, J. S. J. (2005). Understanding the relationship between geopolymer composition, microstructure and mechanical properties. *Colloids and Surfaces A: Physicochemical and Engineering Aspects*, 269(1-3), 47-58.
- E. Douglas, Bilodeau, A., & Malhotra, V. M. (1992). Properties and Durability of Alkali-Activated Slag Concrete. *Materials Journal*, 89(5).
- Fernández-Jiménez, A., López Hombrados, C., & Palomo, Á. (2006). Engineering Properties of Alkali-Activated Fly Ash Concrete. *Materials Journal*, 103, 106-112.
- Garcia-Lodeiro, I., Palomo, A., & Fernández-Jiménez, A. (2015a). 2 - An overview of the chemistry of alkali-activated cement-based binders *Handbook of Alkali-Activated Cements, Mortars and Concretes* (pp. 19-47). Oxford: Woodhead Publishing.

- Garcia-Lodeiro, I., Palomo, A., & Fernández-Jiménez, A. (2015b). 3 - Crucial insights on the mix design of alkali-activated cement-based binders *Handbook of Alkali-Activated Cements, Mortars and Concretes* (pp. 49-73). Oxford: Woodhead Publishing.
- Geopolymer Institute. (2013). World's first public building with structural Geopolymer Concrete. Retrieved 21 April 2017 from <https://www.geopolymer.org/news/worlds-first-public-building-with-structural-geopolymer-concrete/>
- Geopolymer Institute. (2015). Why Alkali-Activated Materials are NOT Geopolymers ? Retrieved May 20 2017 from <https://www.geopolymer.org/faq/alkali-activated-materials-geopolymers/>
- Greenpeace. (2010). The True Cost of Coal - An Investigation Into Coal Ash in China. Retrieved June 5 2017 from <http://www.greenpeace.org/usa/research/dow-inspection-report/>
- Gunasekara, C., Setunge, S., & Law, D. W. (2017). Long-Term Mechanical Properties of Different Fly Ash Geopolymers. *Structural Journal*, 114(03).
- Häkkinen, T. (1993). The influence of slag content on the microstructure, permeability and mechanical properties of concrete. *Cement and Concrete Research*, 23(3), 518-530.
- Husbands, T. B., Malone, P. G., & Wakeley, L. D. (1994). Performance of Concretes Proportioned with Pyrament Blended Cement. *U.S. Army Corps of Engineers Construction Productivity; Advancement Research Program, Report CPAR-SL-94-2*.
- ISO. (2010). Testing of concrete - Part 10: Determination of static modulus of elasticity in compression *ISO 1920-10:2010(E)*.
- Joseph, B., & Mathew, G. (2012). Influence of aggregate content on the behavior of fly ash based geopolymer concrete. *Scientia Iranica*, 19(5), 1188-1194.
- Juenger, M. C. G., Winnefeld, F., Provis, J. L., & Ideker, J. H. (2011). Advances in alternative cementitious binders. *Cement and Concrete Research*, 41(12), 1232-1243.
- Kameswara Rao, C. V. S., Swamy, R. N., & Mangat, P. S. (1974). Mechanical behaviour of concrete as a composite material. *Matériaux et Construction*, 7(4), 265-271.
- Komljenović, M. (2015). Mechanical strength and Young's modulus of alkali-activated cement-based binders *Handbook of Alkali-Activated Cements, Mortars and Concretes* (pp. 171-215). Oxford: Woodhead Publishing.
- Kumar, S., Kumar, R., & Mehrotra, S. P. (2010). Influence of granulated blast furnace slag on the reaction, structure and properties of fly ash based geopolymer. *Journal of Materials Science*, 45(3), 607-615.
- Kumaravel, S., & Thirugnanasambandam, S. (2013). *Flexural behaviour of geopolymer concrete beams*. Annamalai University: India
- Lee, N. K., & Lee, H. K. (2013). Setting and mechanical properties of alkali-activated fly ash/slag concrete manufactured at room temperature. *Construction and Building Materials*, 47, 1201-1209.
- Li, C., Sun, H., & Li, L. (2010). A review: The comparison between alkali-activated slag (Si + Ca) and metakaolin (Si + Al) cements. *Cement and Concrete Research*, 40(9), 1341-1349.
- Manz, O. E. (1997). Worldwide production of coal ash and utilization in concrete and other products. *Fuel*, 76(8), 691-696.
- Maruyama, I., Sasano, H., Nishioka, Y., & Igarashi, G. (2014). Strength and Young's modulus change in concrete due to long-term drying and heating up to 90°C. *Cement and Concrete Research*, 66, 48-63.
- Monteiro, P., & Kuhmar Mehta, P. (2006). *Concrete: Microstructure, Properties, and Materials, Fourth Edition*: McGraw-Hill Publishing.
- Mors, R. M. (2011). *Autogenous Shrinkage of Cementitious materials containing BFS*. (Master), Delft University of Technology, Delft.
- National Development and Reform Commission of the People's Republic of China. (2012). Annual Report on Comprehensive Utilization of Resources of China. Retrieved August 31 2017 from http://www.gov.cn/gzdt/2013-04/08/content_2372577.htm
- Nedeljković, M., Zuo, Y., Arbi, K., & Ye, G. (2017). Natural Carbonation of Alkali-Activated Fly Ash and Slag Pastes. In D. A. Hordijk & M. Luković (Eds.), *High Tech Concrete: Where Technology and*

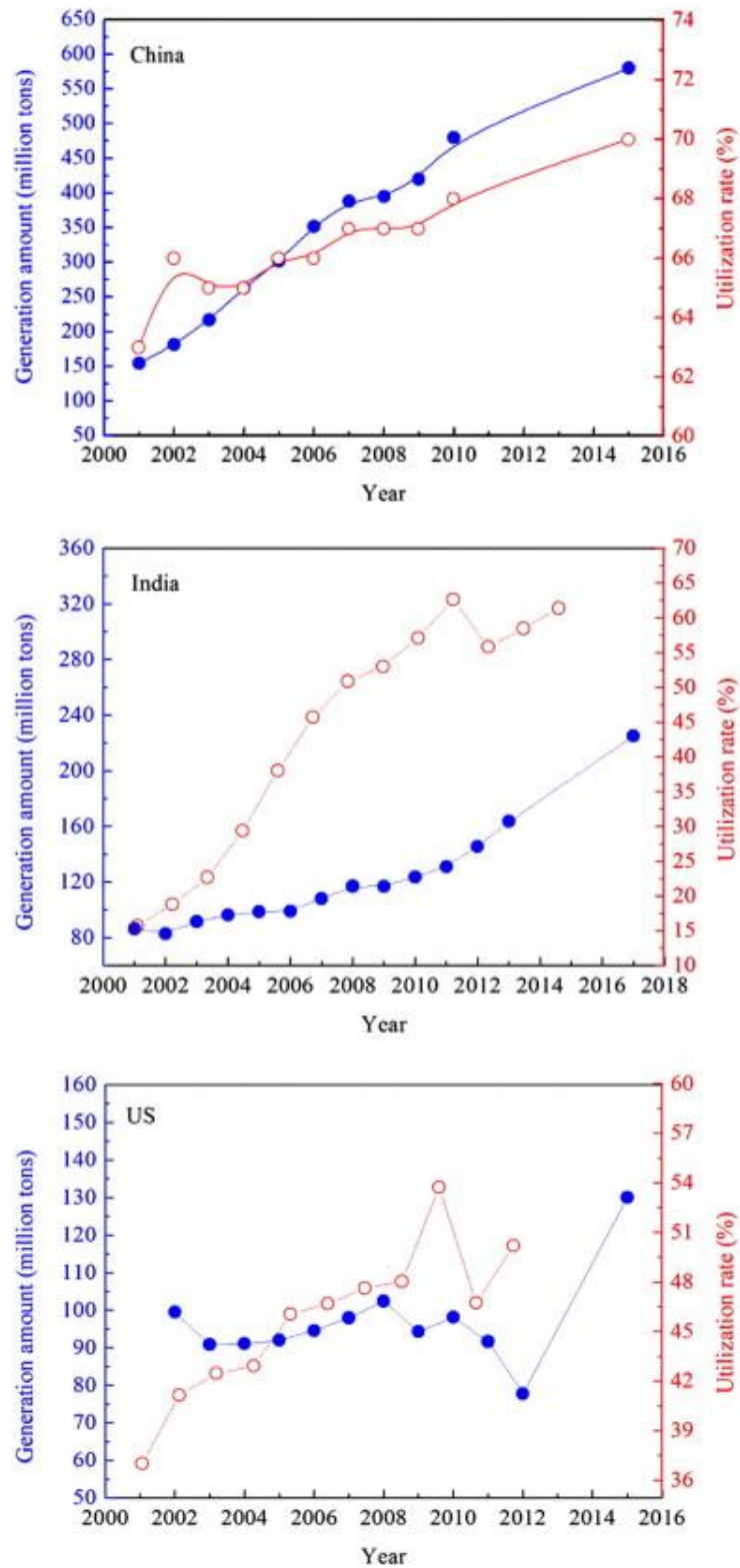
- Engineering Meet: Proceedings of the 2017 fib Symposium, held in Maastricht, The Netherlands, June 12-14, 2017* (pp. 2213-2223): Springer International Publishing.
- NEN. (2013). NEN-EN 197-1. Delft: Nederlands Normalisatie-instituut
- Neville, A. M. (1995). *Properties of concrete*: Pearson: Prentice Hall.
- Pacheco-Torgal, F. (2014). 1 - Introduction to the environmental impact of construction and building materials *Eco-efficient Construction and Building Materials* (pp. 1-10): Woodhead Publishing.
- Pacheco-Torgal, F. (2015). 1 - Introduction to Handbook of Alkali-activated Cements, Mortars and Concretes *Handbook of Alkali-Activated Cements, Mortars and Concretes* (pp. 1-16). Oxford: Woodhead Publishing.
- Palomo, A., Grutzeck, M. W., & Blanco, M. T. (1999). Alkali-activated fly ashes: A cement for the future. *Cement and Concrete Research*, 29(8), 1323-1329.
- Pan, Z., Sanjayan, J. G., & Rangan, B. V. (2011). Fracture properties of geopolymer paste and concrete. *Magazine of Concrete Research*, 63(10), 763-771.
- Provis, J., & van Deventer, J. (2014). *Alkali Activated Materials; State-of-the-Art Report, RILEM TC 224-AAM*. Dordrecht: Springer Netherlands.
- Provis, J. L. (2014). Geopolymers and other alkali activated materials: why, how, and what? *Materials and Structures*, 47(1), 11-25.
- Provis, J. L., & Bernal, S. A. (2014). Binder Chemistry – Blended Systems and Intermediate Ca Content. In J. L. Provis & J. S. J. van Deventer (Eds.), *Alkali Activated Materials: State-of-the-Art Report, RILEM TC 224-AAM* (pp. 125-144). Dordrecht: Springer Netherlands.
- Provis, J. L., Bílek, V., Buchwald, A., Dombrowski-Daube, K., & Varela, B. (2014). Durability and Testing – Physical Processes. In J. L. Provis & J. S. J. van Deventer (Eds.), *Alkali Activated Materials: State-of-the-Art Report, RILEM TC 224-AAM* (pp. 277-307). Dordrecht: Springer Netherlands.
- Provis, J. L., Brice, D. G., Buchwald, A., Duxson, P., Kavalerova, E., Krivenko, P. V., . . . Wiercx, J. A. L. M. (2014). Demonstration Projects and Applications in Building and Civil Infrastructure. In J. L. Provis & J. S. J. van Deventer (Eds.), *Alkali Activated Materials: State-of-the-Art Report, RILEM TC 224-AAM* (pp. 309-338). Dordrecht: Springer Netherlands.
- Provis, J. L., Duxson, P., Kavalerova, E., Krivenko, P. V., Pan, Z., Puertas, F., & van Deventer, J. S. J. (2014). Historical Aspects and Overview. In J. L. Provis & J. S. J. van Deventer (Eds.), *Alkali Activated Materials: State-of-the-Art Report, RILEM TC 224-AAM* (pp. 11-57). Dordrecht: Springer Netherlands.
- Puertas, F., Martínez-Ramírez, S., Alonso, S., & Vázquez, T. (2000). Alkali-activated fly ash/slag cements: Strength behaviour and hydration products. *Cement and Concrete Research*, 30(10), 1625-1632.
- Rüsch, H., Jungwirth, D., & Hilsdorf, H. K. (1983). *Creep and shrinkage: their effect on the behavior of concrete structures*: Springer-Verlag.
- Ryu, G. S., Lee, Y. B., Koh, K. T., & Chung, Y. S. (2013). The mechanical properties of fly ash-based geopolymer concrete with alkaline activators. *Construction and Building Materials*, 47, 409-418.
- Sarker, P. K. (2011). Bond strength of reinforcing steel embedded in fly ash-based geopolymer concrete. *Materials and Structures*, 44(5), 1021-1030.
- Sarker, P. K., Haque, R., & Ramgolam, K. V. (2013). Fracture behaviour of heat cured fly ash based geopolymer concrete. *Mater. Des.*, 44, 580-586.
- SBRCURnet. (2016). *Kennispaper: geopolymeerbeton*. Delft: SBRCURnet
- Shah, A., & Shah, C. B. (2017). *Comparison of Load-displacement Relationship and Crack Development Mechanism in Reinforced Geopolymer Concrete Beams with that of Regular Reinforced Concrete Beams*. Paper presented at the RILEM 2017, Chennai, India.
- Singh, B., Ishwarya, G., Gupta, M., & Bhattacharyya, S. K. (2015). Geopolymer concrete: A review of some recent developments. *Construction and Building Materials*, 85, 78-90.
- Sofi, M., van Deventer, J. S. J., Mendis, P. A., & Lukey, G. C. (2007). Engineering properties of inorganic polymer concretes (IPCs). *Cement and Concrete Research*, 37(2), 251-257.

- Sumajouw, D., Hardjito, D., Wallah, S., & Rangan, B. (2005). *Behaviour and strength of reinforced fly ash-based geopolymer concrete beams*. Paper presented at the Australian Structural Engineering Conference 2005.
- Thomas, R. J., & Peethamparan, S. (2015). Alkali-activated concrete: Engineering properties and stress-strain behavior. *Construction and Building Materials*, 93, 49-56.
- U.S. Bureau of Reclamation. (1981). *Concrete Manual* (8th ed.).
- Van Deventer, J. S. J., Provis, J. L., & Duxson, P. (2012). Technical and commercial progress in the adoption of geopolymer cement. *Minerals Engineering*, 29, 89-104.
- Vermeulen, E., & de Vries, P. (2015). De uitdagingen van geopolymeerbeton. *Betoniek Vakblad*, 2015-2, 20-27.
- vom Berg, W., & Feuerborn, H. J. (2015). *Present Situation and Perspectives of CCP Management in Europe*. Paper presented at the 2005 World of Coal Ash (WOCA), Lexington, Kentucky, USA. <http://infohouse.p2ric.org/ref/45/44753.pdf>
- Wallah, S. E., & Rangan, B. V. (2006). *Low-Calcium Fly Ash-Based Geopolymer Concrete: Long-Term Properties*. Research Report GC2, Faculty of Engineering, Curtin University of Technology: Perth
- Wan, H., Shui, Z., & Lin, Z. (2004). Analysis of geometric characteristics of GGBS particles and their influences on cement properties. *Cement and Concrete Research*, 34(1), 133-137.
- Wang, S.-D., Pu, X.-C., Scrivener, K. L., & Pratt, P. L. (1995). Alkali-activated slag cement and concrete: a review of properties and problems. *Advances in Cement Research*, 7(27), 93-102.
- Wardhono, A., Gunasekara, C., Law, D. W., & Setunge, S. (2017). Comparison of long term performance between alkali activated slag and fly ash geopolymer concretes. *Construction and Building Materials*, 143, 272-279.
- Wongpa, J., Kiattikomol, K., Jaturapitakkul, C., & Chindaprasirt, P. (2010). Compressive strength, modulus of elasticity, and water permeability of inorganic polymer concrete. *Materials & Design*, 31(10), 4748-4754.
- Wu, Y., Cai, L., & Fu, Y. (2011). Durability of green high performance alkali-activated slag pavement concrete. *Appl. Mech. Mater.*, 99-100, 158-161.
- Yang, K.-H., Cho, A.-R., & Song, J.-K. (2012). Effect of water-binder ratio on the mechanical properties of calcium hydroxide-based alkali-activated slag concrete. *Construction and Building Materials*, 29, 504-511.
- Yang, K.-H., Song, J.-K., & Song, K.-I. (2013). Assessment of CO₂ reduction of alkali-activated concrete. *Journal of Cleaner Production*, 39(Supplement C), 265-272.
- Yao, Z. T., Ji, X. S., Sarker, P. K., Tang, J. H., Ge, L. Q., Xia, M. S., & Xi, Y. Q. (2015). A comprehensive review on the applications of coal fly ash. *Earth-Science Reviews*, 141(Supplement C), 105-121.
- Zhang, Z., Provis, J. L., Reid, A., & Wang, H. (2014). Geopolymer foam concrete: An emerging material for sustainable construction. *Construction and Building Materials*, 56, 113-127.

TU Delft alkali-activated concrete mixtures:

- Arbi, K., Nedeljković, M., Zuo, Y., Grünewald, S., Keulen, A. & Ye, G. (2015). *Experimental study on workability of alkali activated fly ash and slag-based geopolymer concretes*. Paper presented at Geopolymers 2015 –An ECI Conference, Austria.
- Arbi, K., M. Nedeljković, Y. Zuo & G. Ye (2016). *Durability of alkali-activated fly ash and slag concrete*. Paper presented at the 9th International Concrete Conference 2016-Environment, Efficiency and Economic Challenges for Concrete (Dundee, Scotland).
- M. Nedeljković (2014) *Long-term performance of geopolymer concrete systems for production of environment friendly building materials*. On-going Ph.D. thesis (Delft University of Technology, The Netherlands, 2014-2018). This research is carried out under the project S81.1.13498 in the framework of the Partnership Program of the Materials innovation institute M2i (www.m2i.nl) and the Technology Foundation STW (www.stw.nl), which is part of the Netherlands Organisation for Scientific Research (www.nwo.nl).

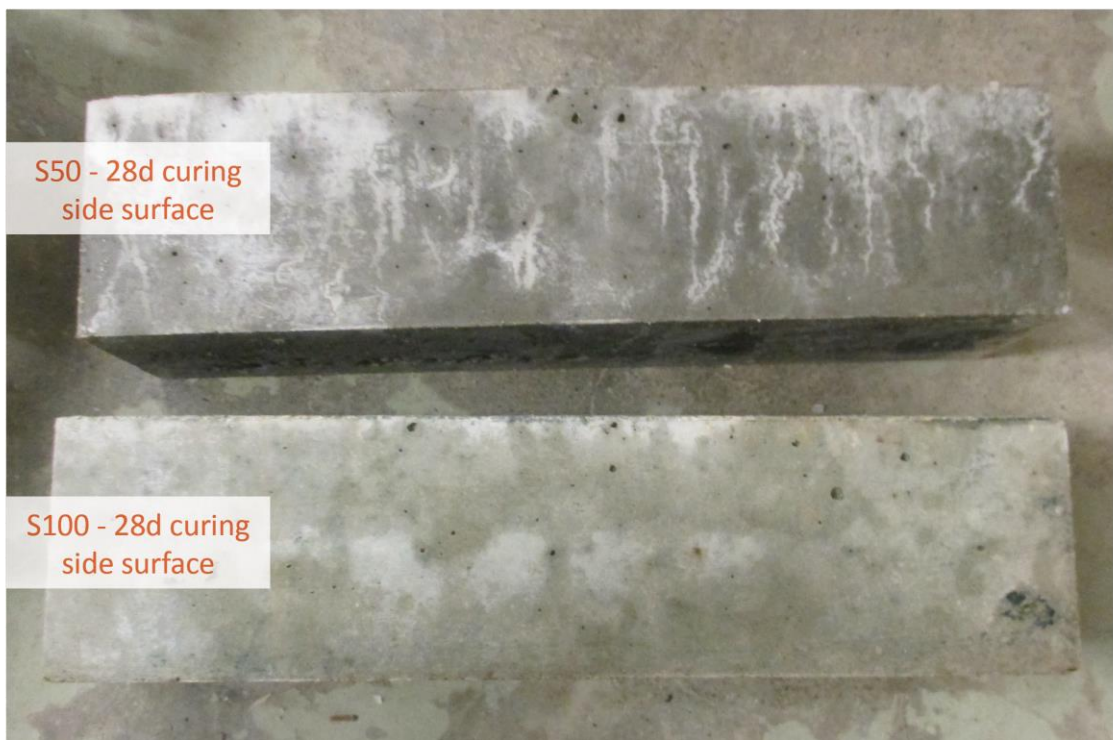
Appendix A. – Generation and utilization of coal fly ash

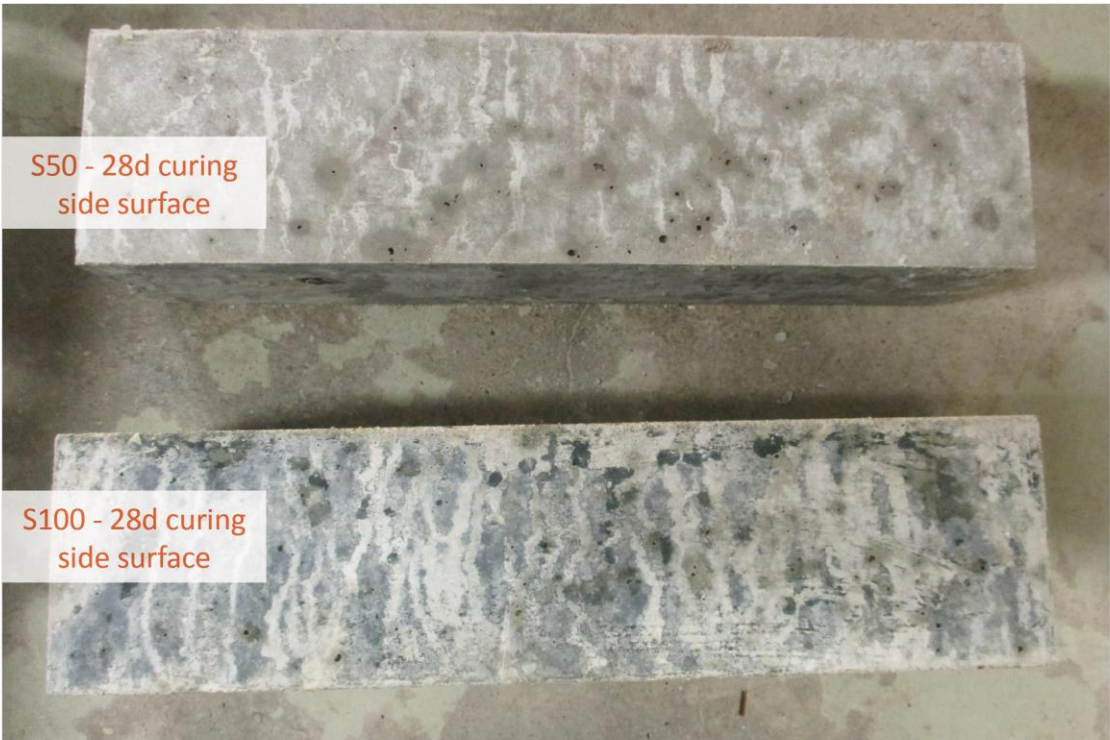


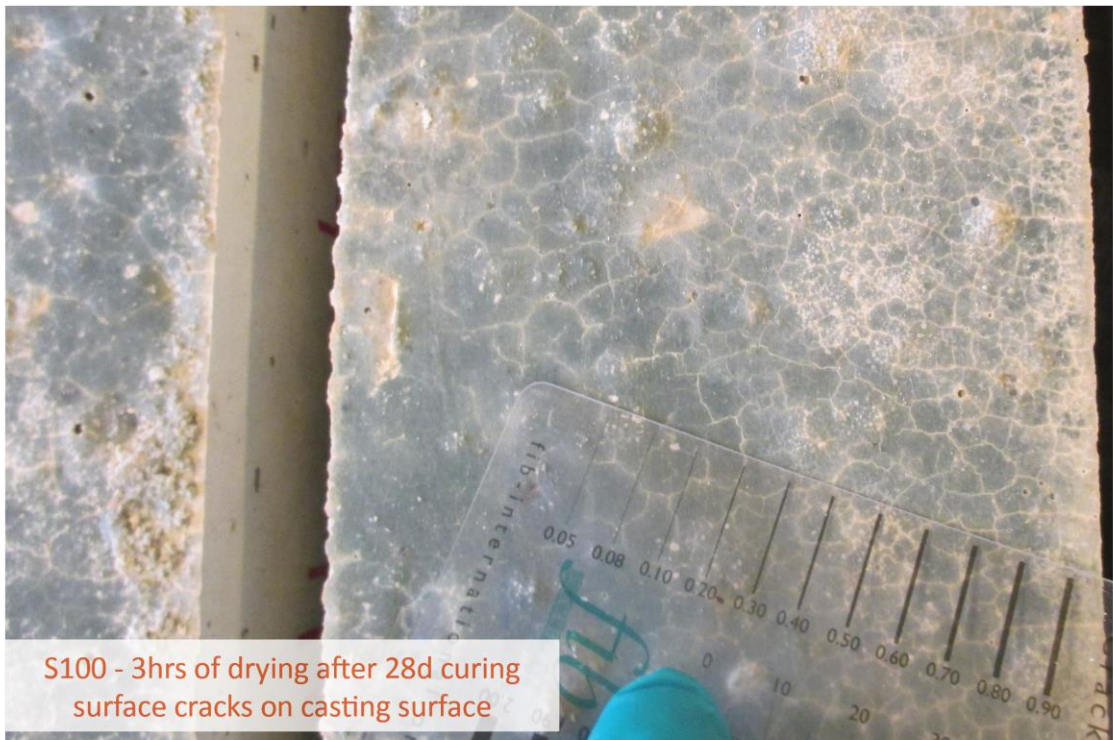
The graphs were published in a paper by Yao et al. (2015). Data taken from National Development and Reform Commission of the People's Republic of China (2012)

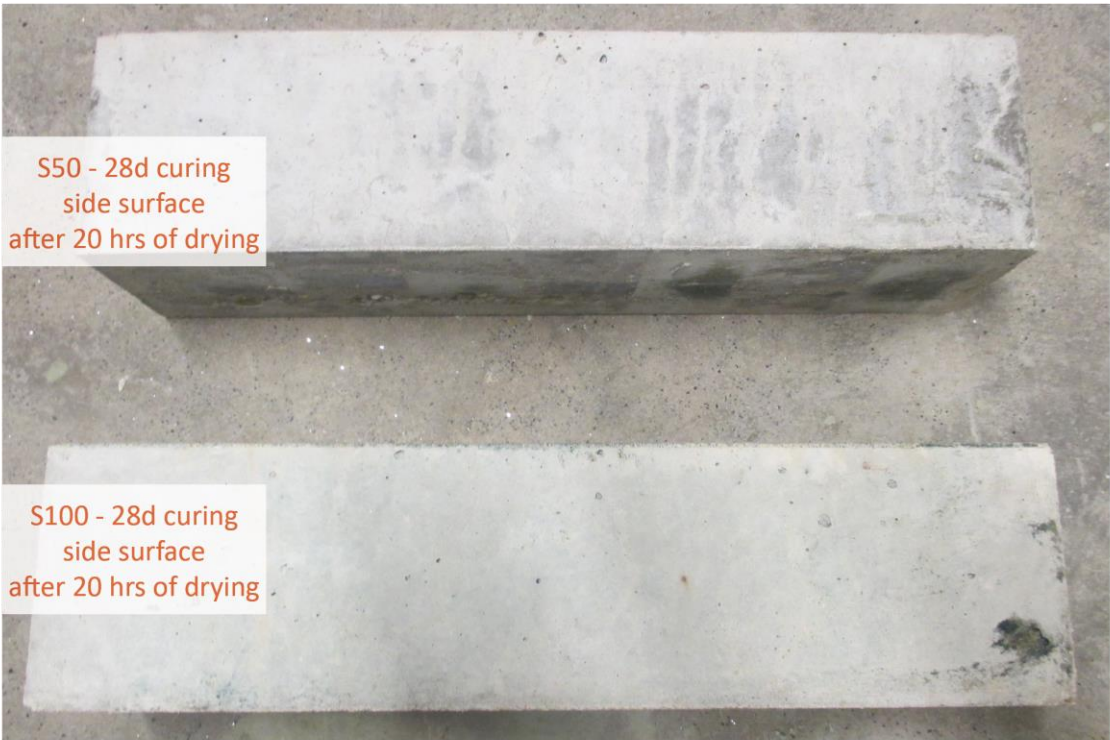
Appendix B. – Surfaces after curing

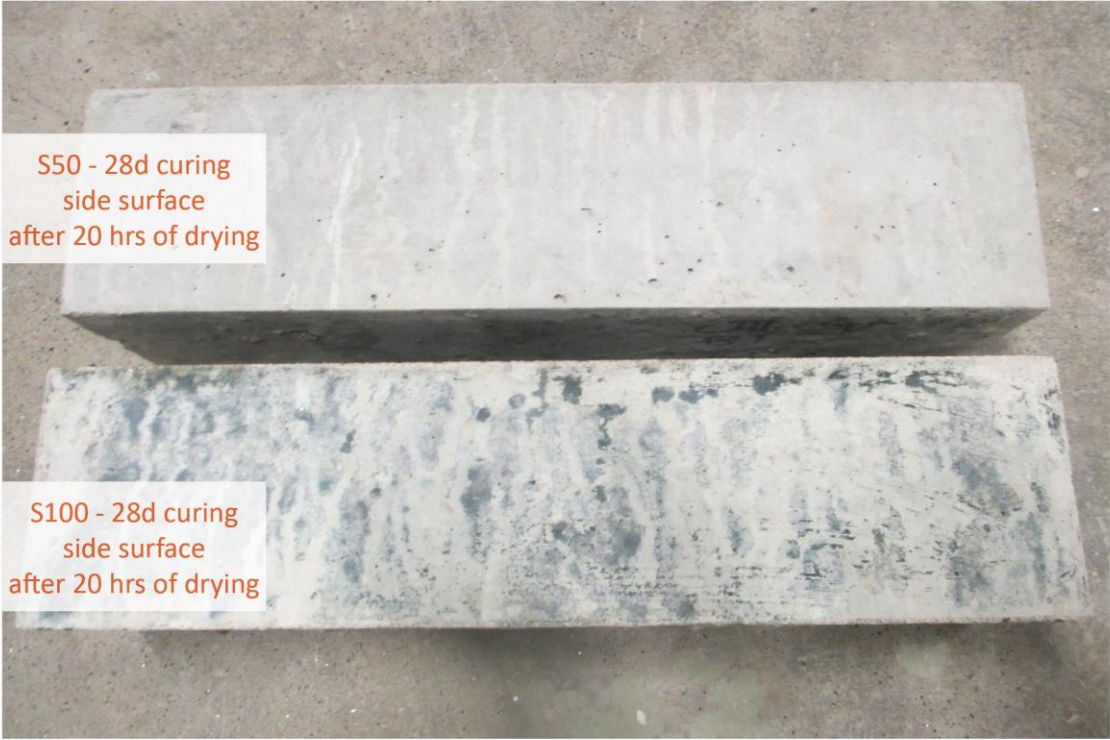
The following photos show the surfaces of alkali-activated concrete a few moments after it was taken out of the curing room. Both S50 (50% slag and 50% fly ash) and S100 (100% slag) are shown in the pictures. For S100, small surface cracks have been observed, mainly on the casting surface.





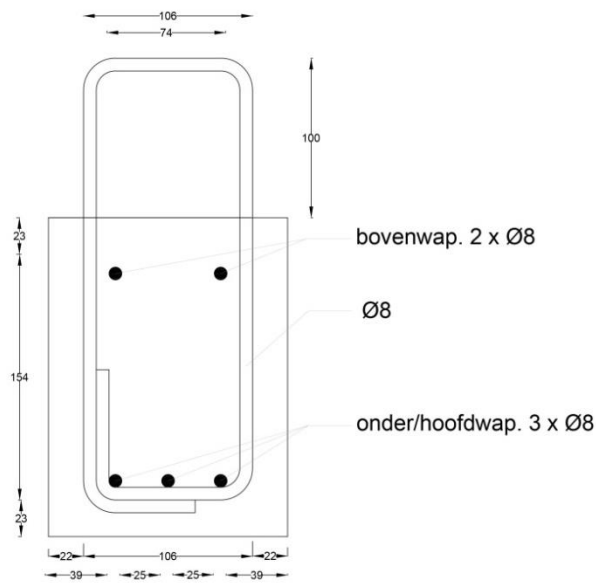






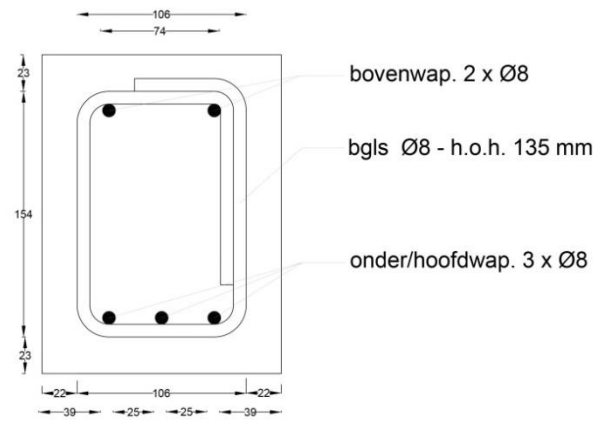
Appendix C. – Reinforcement drawings

This appendix contains the reinforcement drawings that have been sent to the manufacturer.



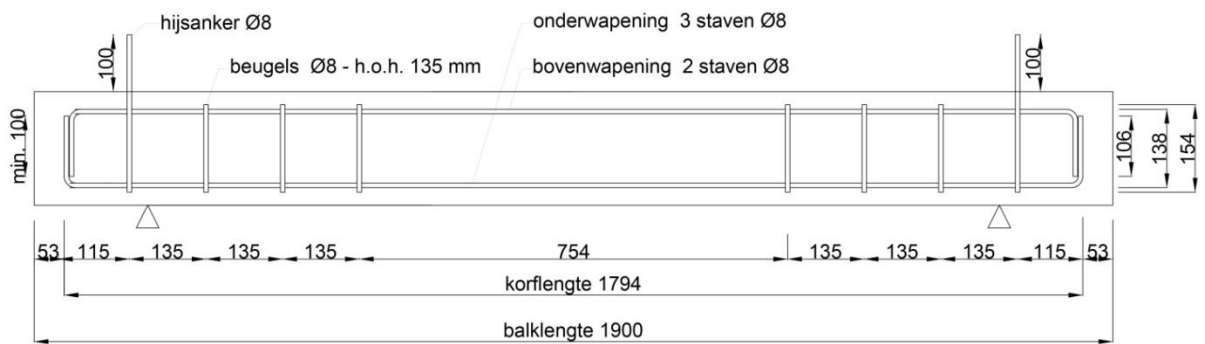
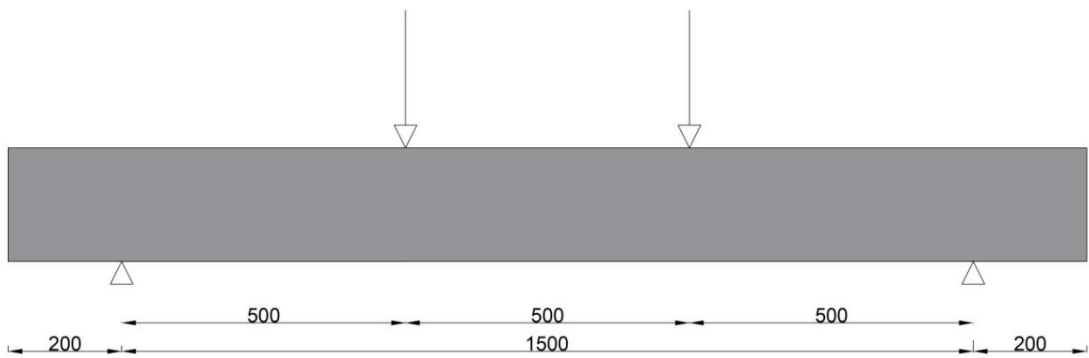
hijssanker Ø8

betonstaalsoort: B500-B



beugel Ø8

betonstaalsoort: B500-B



Betonstaalsoort: B500-B

Appendix D. – Calculation of reinforced beams

Introduction

This appendix contains the calculations that were made before testing the reinforced beams, and recalculations after testing. The calculations have been made using Excel, to make it easy to adjust. The step-by-step procedure with all formulas, using Eurocode 2, can be read from the Excel-sheet, but a few things are explained in a bit more detail in the following paragraphs.

Because alkali-activated concrete has different material properties than OPC concrete, the stress-strain curve probably also looks different. Therefore, area factor α and distance factor β are calculated based on the implemented stress-strain curve.

In order to compare the theoretical estimation with the test results, two approaches have been followed to make the step from a moment/kappa diagram to expected deformation. The first approach (named w_1 in the sheet) is shown in Fig. 1. From the calculated κ , the radius R can be calculated. Using geometry, an estimation of the deflection at midspan (measured between the two supports) can be calculated.

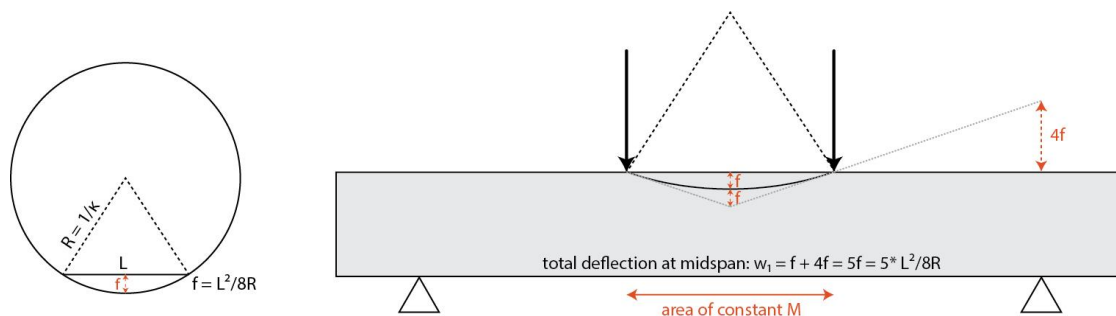


Fig. 1: Theoretical approach 1 for estimated deflection.

Another approach, named w_2 , is presented in Fig. 2. Here, a standard ‘forget-me-not’ from structural mechanics is used. Using the calculated maximum Moment- κ diagram, the corresponding EI can be calculated for every part of the diagram, and then the formula can be filled in. However, this is the average EI , assumed to be constant over the whole beam. In reality, this is not the case, close to the supports, the stiffness will be higher because less cracks initiate in these parts. So, this approach might overestimate the deflections.

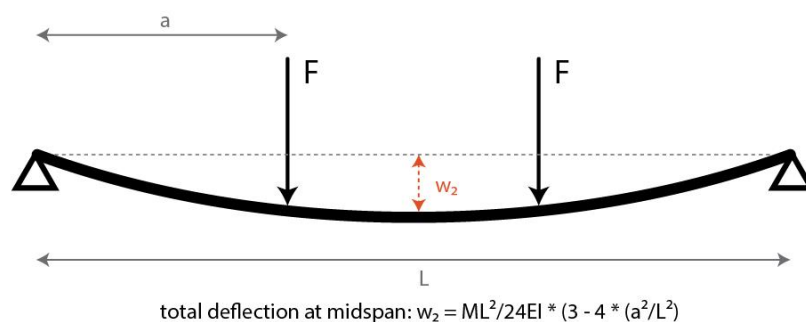


Fig. 2: Theoretical approach 2 for estimated deflection, based upon the structural mechanics ‘forget-me-nots’.

S50 – 33d

The concrete strain ϵ_{cu3} was set as 2.9‰, because the compressive strength of the mixture can be compared to high-strength concrete, and is therefore assumed to be more brittle. Furthermore, the calculation is based on measured properties (E-modulus, splitting tensile strength and compr. strength). These values have been highlighted in the Excel sheet. Based on this calculation, a concrete compressive failure mode was expected at a load of around 48 kN.

Calculation S50 reinforced concrete beam - 33 days

Concrete			
$f_{cm,cube}$	75.25 MPa	$f_{cm} = f_{c2,apl} \cdot 0.9$	4.203 MPa
$f_{ct,apl}$	4.67 MPa	$f_{cm} = 0.8 \cdot f_{cm,cube}$	60.2 MPa
E_{cm}	26420 MPa	$f_{ck} \approx f_{cm} - 8$	52.2 MPa
		$f_{ctm,fl} = (1.6 - h) \cdot f_{ctm}$	5.8842 MPa

Steel	
E_s	200000 MPa

Reinforcement			
$A_{s,min} = 0.26 \frac{f_{ctm}}{f_{yk}} b d$	62.18 mm ²	$\alpha_s = \frac{E_s}{E_c}$	7.57
A_s	150.80 mm ²	ϕ	8 mm
$\rho = \frac{A_s}{A_c} = \frac{A_s}{b \cdot d}$	0.006	n	3 bars
	0.609 %	enough reinforcement?	enough reinforcement?

M-k diagram

1. Concrete bottom fibre crack $\epsilon_{cr} = f_{ctm}$	
$M_{cr} = W_c \cdot f_{ctm} + f_{ctm} \cdot I$	5.8842 kNm
$\epsilon_{ct} = \frac{f_{ctm}}{E_{cm}}$	2.23E-04
ϵ_s	1.45E-04
$\kappa_{cr} = \frac{2 \cdot \epsilon_{ct}}{h}$	2.22718E-06 1/mm

2. Force redistribution	
$M_{cr} = N_s \cdot z = A_s \cdot E_s \cdot \epsilon_s + (d - \frac{1}{3}x)$	$\frac{\epsilon_s}{\epsilon_c} = \frac{x}{d-x}$
$\frac{1}{2} b \cdot x \cdot \epsilon_s + E_{cm} = A_s \cdot E_s + \epsilon_s$	
SO, $x = d \cdot (-\alpha_s \cdot \rho + \sqrt{(\alpha_s \cdot \rho)^2 + 2\alpha_s \cdot \rho})$	
x	43.08 mm
$\epsilon_s = \frac{M_{cr}}{A_s \cdot E_s + (d - \frac{1}{3}x)}$	1.30E-03
	1: enough steel
	0: not enough steel
$\epsilon_c = \frac{x \cdot \epsilon_s}{d-x}$	4.58E-04
$\sigma_s = E_s \cdot \epsilon_s$	259.03 MPa
$\sigma_c = E_c \cdot \epsilon_c$	12.09 MPa
$\kappa_p = \frac{\epsilon_s + \epsilon_c}{d}$	1.06E-05 1/mm

3. Steel yielding or plastic zone concr? Yielding of reinforcement	
$N_s = A_s \cdot f_{yk}$	65596.455 N
$M_{pl} = N_s \cdot z = N_s \cdot (d - \frac{1}{3}x)$	9881495.5 Nmm
ϵ_{cs}	2.28 ‰ vs $\epsilon_{sy} = 2.175 ‰$
ϵ_s	6.4489847 ‰
$\kappa_{sy} = \frac{\epsilon_s}{d-x}$	1.78E-05 1/mm
	1: steel yielding
	0: concrete plastic zone

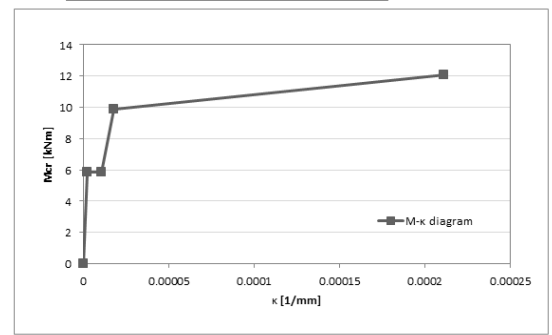
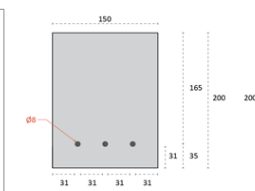
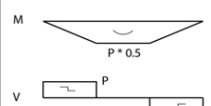
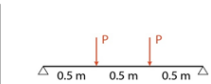
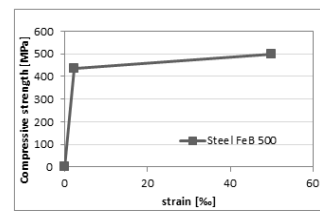
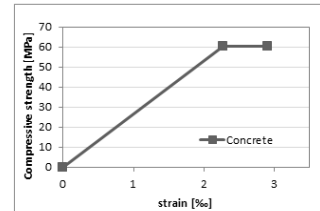
4. Moment of failure: concrete/steel? Concrete failure	
$N_s = A_s \cdot f_{yk}$	75398.224 N
$x_u = \frac{N_s}{\alpha_s \cdot f_{cm} + b}$	13.753 mm
$z = d - \beta \cdot x_u$	160.242 mm
$M_{rd} = N_s \cdot z$	12081998 Nmm
ϵ_s	31.9 ‰
$\epsilon_{cu} = \frac{M_{rd}}{F = 2P \cdot 2 \cdot M_{rd}/0.5}$	2.11E-04
	48.3 kN
	Concrete failure

stage	Mcr [kNm]	ϵ_c [‰]	ϵ_s [‰]	κ [1/mm]	R = 1/k	$w_1 = S^3 L^2 / 8R$	E [Mpa]	VGM	F [kN]
0	0	0	0	0	0	0	0	0.00	0.00
1	5.8842	0.22272	0.14477	2.23E-06	448999	0.348	26420	0.53	23.54
2	5.8842	0.45761	1.29516	1.06E-05	94137	1.660	5539	2.55	23.54
3	9.881	0.76848	2.17500	1.78E-05	56056	2.787	5539	4.27	39.53
4	12.081998	2.90000	31.89355	2.11E-04	4742	32.971	573	50.52	48.33

measured property		adjustable properties	
Concrete			
strain [%]	stress [MPa]	area1	11.62362
0	0	area2	94.7126
ϵ_{cs}	2.28	α	0.607142
ϵ_{cu3}	2.90	β	0.345938

Steel FeB 500	
strain [%]	stress [MPa]
0	0
f_{yk}	2.175
f_{tu}	500

Dimensions	
h	200 mm
b	150 mm
c	31 mm
d_s	8 mm
d	165 mm
I	1E+08 mm ⁴



However, the test showed a different result (see Fig. 3, left), the estimation was not so close. No concrete compressive failure was observed, but reinforcement failure and a much higher failure load.

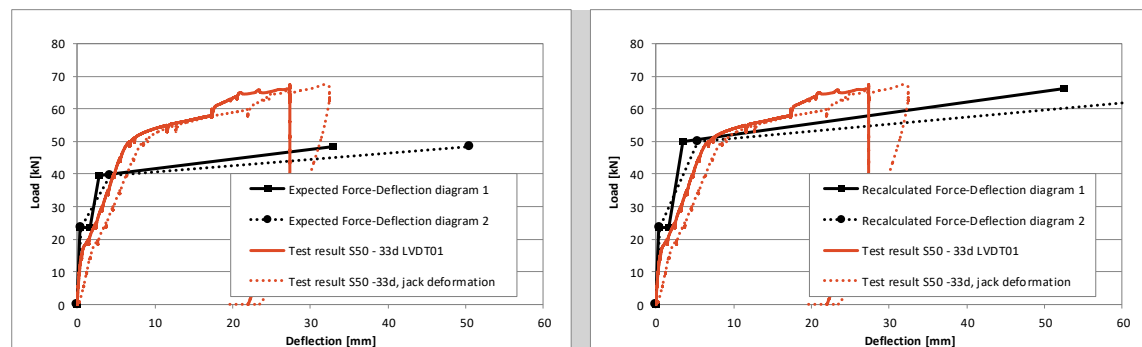


Fig. 3: Left: Expected Force-Deflection diagram vs. test results, both approach 1 and 2 (see previous paragraph) are plotted. Right: Recalculated Force-Deflection diagram based on the experiment, compared with the test results.

After the test, a recalculation has been done. The values that were changed compared to the original calculation, have been highlighted yellow in the Excel sheet below. It seems that the maximum concrete strain (ϵ_{cu3}) is higher than the assumed 2.9%, and the steel strength is higher than the characteristic value of 500 MPa. The balance between these two values determines the failure mode, if ϵ_{cu3} is very high, the maximum steel strain will be reached earlier, and reinforcement failure will occur before concrete crushing, like observed. Fig. 3 (right) shows the adjusted Force-Deflection diagram. It is clear that the theoretical estimation is better than initially, but the calculated deflections are too big.

Recalculation S50 reinforced concrete beam - 33 days			
Failure load was	67.4 kN	reinforcement failure observed!	
Concrete			
$f_{cm,cube}$	75.25 MPa	$f_{ctm} = f_{ct,sp1} * 0.9$	4.203 MPa
$f_{ct,sp1}$	4.67 MPa	$f_{cm} = 0.8 * f_{cm,cube}$	60.2 MPa
E_{cm}	26420 MPa	$f_{ck} \approx f_{cm} - 8$	52.2 MPa
		$f_{ctm,fl} = (1.6 - h) * f_{ctm}$	5.8842 MPa

Steel	
E_s	200000 MPa

Reinforcement			
$A_{s,min} = 0.26 \frac{f_{ctm}}{f_{yk}} bd$	49.18 mm ²	$a_s = \frac{e_s}{\epsilon_c}$	7.57
A_s	150.80 mm ²	ϕ	8 mm
$\rho = \frac{A_s}{A_c} = \frac{A_s}{b * d}$	0.006	n	3 bars
	0.609 %	enough reinforcement?	
enough reinforcement? Green = YES, Red = NO			

M-κ diagram		
1. Concrete bottom fibre crack $\sigma_n = f_{ctm}$		
$M_{cr} = W_y * f_{ctm,fl}$	5.8842 kNm	$\sigma_n = f_{ctm}$
$\epsilon_{ct} = \frac{f_{ctm,fl}}{E_{cm}}$	2.23E-04	
ϵ_s	1.45E-04	
$\kappa_r = \frac{2 * \epsilon_{ct}}{h}$	2.22718E-06 1/mm	

2. Force redistribution		
$M_{cr} = N_s * z = A_s * E_s * \epsilon_s * (d - \frac{1}{3}x)$		$\epsilon_s = \frac{x}{d-x}$
$\frac{1}{2} b * x * \epsilon_c + E_{cm} = A_s * E_s * \epsilon_s$		
so, $x = d * (-a_s * \rho + \sqrt{(a_s * \rho)^2 + 2a_s * \rho})$		
x	43.08 mm	
$\epsilon_s = \frac{M_{cr}}{A_s * E_s * (d - \frac{1}{3}x)}$	1.30E-03	1: enough steel
$\epsilon_c = \frac{x * \epsilon_s}{d-x}$	4.58E-04	0: not enough steel
$\sigma_c = E_s * \epsilon_s$	259.03 MPa	
$\sigma_c = E_c * \epsilon_c$	12.09 MPa	
$\kappa_r = \frac{\epsilon_s + \epsilon_c}{d}$	1.06E-05 1/mm	

measured property	adjustable properties		
Concrete			
strain [%]	stress [MPa]	area1	222.9249
0	0	area2	238.7414
ϵ_{cu3}	2.28	α	0.772142
	5.00	β	0.397278

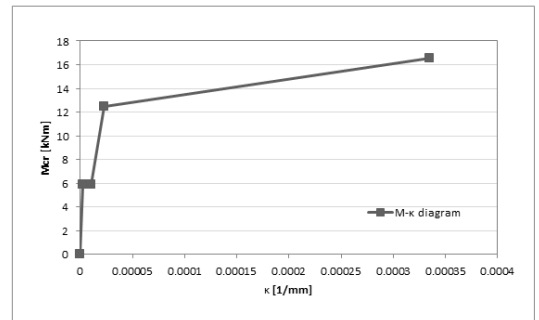
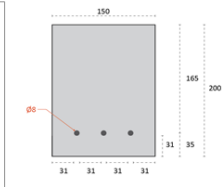
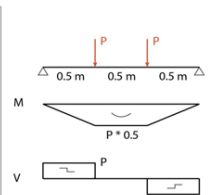
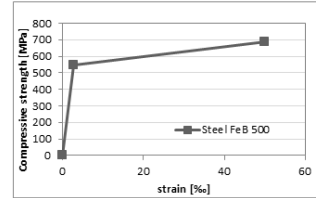
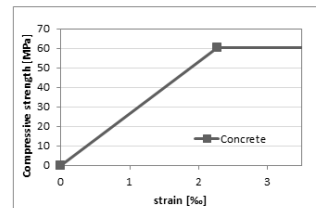
Steel FeB 500	
strain [%]	stress [MPa]
0	0
f_{yk}	550
f_{yu}	690

Dimensions	
h	200 mm
b	150 mm
c	31 mm
ϵ_s	8 mm
$d = h - c - 0.5 * d_s$	165 mm
	1E+08 mm ⁴

3. Steel yielding or plastic zone concr? Yielding of reinforcement		
$N_s = A_s * f_{yk}$	82938.046 N	
$M_{pl} = N_s * z = N_s * (d - \frac{1}{3}x)$	12493845 Nmm	or 12.494 kNm
ϵ_{cu3}	2.28 ‰	vs $\epsilon_{sy} = 2.75 ‰$
ϵ_s	6.4489847 ‰	1: steel yielding
$\kappa_{sy} = \frac{\epsilon_s}{d-x}$	2.26E-05 1/mm	0: concrete plastic zone

4. Moment of failure: concrete/steel? Reinforcement fails		
$N_s = A_s * f_{yu}$	104049.55 N	or 104.0495 kN
$x_u = \frac{N_s}{\alpha * f_{cm} * b}$	14.923 mm	
$z = d - \beta * x_u$	159.071 mm	
$M_{rd} = N_s * z$	16551311 Nmm	or 16.55131 kNm
ϵ_s	50.3 ‰	Reinforcement fails
$\kappa_u = \frac{\epsilon_{cu3}}{d}$	3.35E-04	
$F = 2P \approx 2 * M_{rd} / 0.5$	66.2 kN	

stage	Mcr [kNm]	εc [%]	εs [%]	κ [1/mm]	R = 1/κ	w ₂ = 5*L ² /8R	E [Mpa]	w ₂	F [kN]
0	0	0	0	0	0	0	0	0.00	0.00
1	5.8842	0.22272	0.14477	2.23E-06	448999	0.348	26420	0.53	23.54
2	5.8842	0.45761	1.29516	1.06E-05	94137	1.660	5539	2.55	23.54
3	12.494	0.97164	2.75000	2.26E-05	44335	3.524	5539	5.40	49.98
4	16.551311	5.00000	50.28392	3.35E-04	2985	52.444	494	80.27	66.21



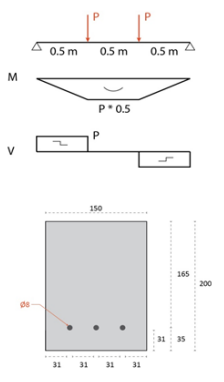
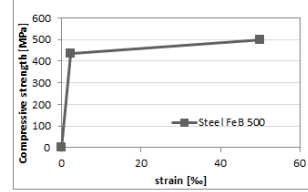
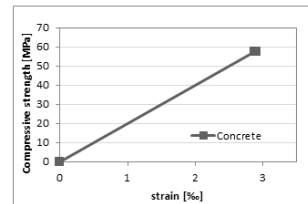
S50 – 69d

The same procedure was followed as for S50-33d. Again, the concrete strain ϵ_{cu3} was set as 2.9‰, because the compressive strength of the mixture can be compared to high-strength concrete, and is therefore assumed to be more brittle. The calculation is based on approximate measured properties, because the properties have not been tested exactly at 69d. Therefore, a rough estimation based on the results from 49 days (Table 5.2) has been applied. Based on the initial calculation, concrete compressive failure was expected. However, as explained in the previous paragraph, the four-point bending test for S50 at 33d showed reinforcement failure instead of concrete compressive failure. Therefore, not based on this calculation, but on the gained experience, it was expected that the maximum concrete strain would be higher than 2.9‰. And that, again, reinforcement would fail before concrete crushing occurs.

Calculation S50 reinforced concrete beam - 69 days

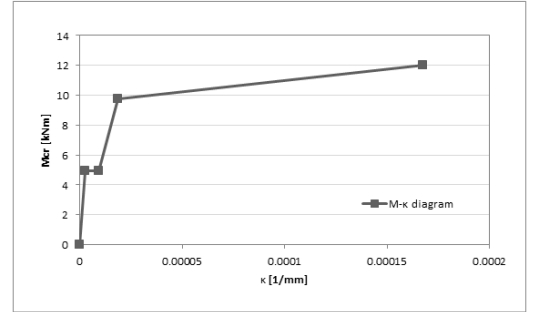
Concrete			
$f_{cm.cube}$	72 MPa	$f_{ctm} = f_{ct,api} = 0.9$	3.51 MPa
$f_{ct,api}$	3.9 MPa	$f_{cm} = 0.8 + f_{cm.cube}$	57.6 MPa
E_{cm}	20000 MPa	$f_{ck} \approx f_{cm} - 8$	49.6 MPa
		$f_{ctm,fi} = (1.6 - h) + f_{ctm}$	4.914 MPa
Steel			
E_s	200000 MPa		
Reinforcement			
$A_{s,min} = 0.26 \frac{f_{ctm}}{f_{yk}} b d$	51.92 mm ²	$\alpha_s = \frac{E_s}{E_c}$	10.00
A_s	150.80 mm ²	ϕ	8 mm
$\rho = \frac{A_s}{A_c} = \frac{A_s}{b \cdot d}$	0.006	n	3 bars
	0.609 %	enough reinforcement?	
enough reinforcement? Green = YES, Red = NO			

measured property		adjustable properties	
Concrete			
strain [%]	stress [MPa]	area1	0.01152
0	0	area2	81.28512
ϵ_{cs}	2.88	α	0.503448
ϵ_{cu3}	2.90	β	0.333349
Steel FeB 500			
strain [%]	stress [MPa]		
0	0		
f_{yk}	2.175	435	
f_{tu}	50	500	
Dimensions			
h	200 mm		
b	150 mm		
c	31 mm		
\bar{d}	8 mm		
d	165 mm		
I	1E+08 mm ⁴		



1. Concrete bottom fibre crack		$\epsilon_{ct} = f_{ctm}$
$M_{cr} = W_k + f_{ctm,fi}$	4.914 kNm	
$\epsilon_{ct} = \frac{f_{ctm,fi}}{E_{cm}}$	2.46E-04	
$\epsilon_s = \frac{2 + \epsilon_{ct}}{h}$	1.60E-04	
$\kappa_r = \frac{\epsilon_s}{d}$	0.00002457 1/mm	
2. Force redistribution		
$M_{rr} = N_s + z = A_s + E_s + \epsilon_s + (d - \frac{1}{3}x)$		$\frac{\epsilon_c}{\epsilon_s} = \frac{x}{d-x}$
$b \cdot x + \epsilon_c + E_{cm} = A_s + E_s + \epsilon_s$		
so, $x = d + (-\alpha_s + \rho + \sqrt{(\alpha_s + \rho)^2 + 2\alpha_s + \rho})$		
$x = 48.42$ mm		
$\epsilon_s = \frac{M_{rr}}{A_s + E_s + (d - \frac{1}{3}x)}$	1.09E-03	1: enough steel
		0: not enough steel
$\epsilon_c = \frac{x + \epsilon_s}{d - x}$	4.55E-04	
$\sigma_s = E_s + \epsilon_s$	218.91 MPa	
$\sigma_c = E_c + \epsilon_c$	9.09 MPa	
$\kappa_r = \frac{\epsilon_s + \epsilon_c}{d}$	9.39E-06 1/mm	

3. Steel yielding or plastic zone concr? Yielding of reinforcement	
$N_s = A_s + f_{yk}$	65596.455 N
$M_{sp} = N_s + z = N_s + (d - \frac{1}{3}x)$	9764784.8 Nmm or 9.765 kNm
ϵ_{cs}	2.88 ‰ vs $\epsilon_{sy} = 2.175$ ‰
ϵ_s	6.9350216 ‰
$\kappa_{sp} = \frac{\epsilon_s}{d - x}$	1.87E-05 1/mm
1: steel yielding 0: concrete plastic zone	
4. Moment of failure: concrete/steel? Concrete failure	
$N_s = A_s + f_{tu}$	75398.224 N or 75.39822 kN
$x_u = \frac{N_s}{\alpha + f_{cm} + b}$	17.334 mm
$z = d - \beta + x_u$	159.222 mm
$M_{Rd} = N_c + z$	12005042 Nmm or 12.00504 kNm
ϵ_s	24.7 ‰
$\kappa_u = \frac{\epsilon_{cu3}}{d}$	1.67E-04
$F = 2P \approx 2 \cdot M_{rd}/0.5$	48.0 kN



stage	Mcr [kNm]	εc [%]	εs [%]	κ [1/mm]	R = 1/k	w ₁ = 5*L ² /8R	E [Mpa]	w ₂	F [kN]
0	0	0	0	0	0	0	0	0.00	0.00
1	4.914	0.24570	0.15971	2.46E-06	407000	0.384	20000	0.59	19.66
2	4.914	0.45454	1.09454	9.39E-06	106515	1.467	5234	2.25	19.66
3	9.765	0.90324	2.17500	1.87E-05	53602	2.915	5234	4.47	39.06
4	12.005042	2.90000	24.70511	1.67E-04	5977	26.153	718	40.08	48.02

Surprisingly, the test results showed concrete compressive failure. Although it was the hypothesized failure mode from the calculations, it was unexpected because both S50 – 33d and S100 – 33d days (next paragraph) showed reinforcement failure. Still, the maximum load was higher than expected (Fig. 4, left).

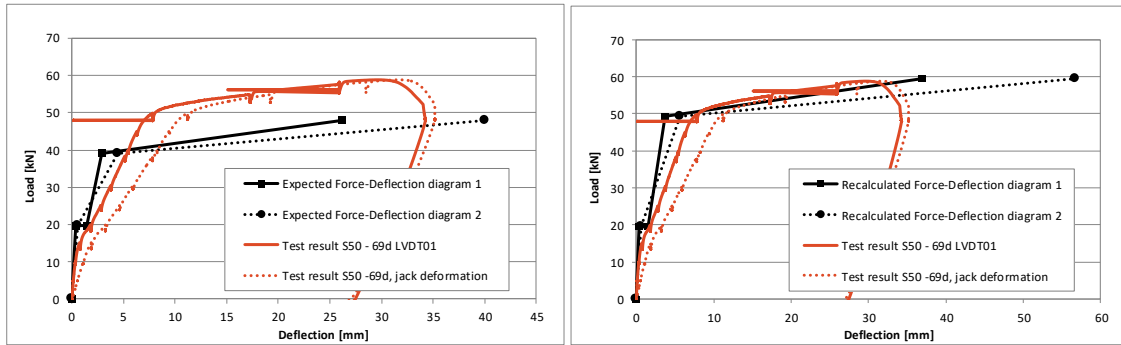


Fig. 4: Left: Expected Force-Deflection diagram vs. test results, both approach 1 and 2 (see previous paragraph) are plotted. Right: Recalculated Force-Deflection diagram based on the experiment, compared with the test results.

It seems that the steel had a higher strength, in the recalculation this was adjusted (see yellow-highlighted cells in the recalculation sheet). Furthermore, it is estimated that the maximum concrete strain (ϵ_{cu3}) is higher than the assumed 2.9%, although it will be lower than for beam S50-33d. Beam S50-33d showed no concrete compressive failure, so the maximum concrete strain ϵ_{cu3} should be higher for S50-33d when compared to S50-69d (if the reinforcement is assumed to be completely similar). Fig. 3 (right) shows the adjusted Force-Deflection diagram, the estimated deflection is now almost correct for theoretical model 1 (shown in the graph as *Recalculated Force-Deflection diagram 1*).

Recalculation S50 reinforced concrete beam - 69 days

Failure load was **58.8 kN** concrete compressive failure

Concrete	measured property	adjustable properties
$f_{cm, cube}$	72 MPa	$f_{ctm} = f_{ct,api} \cdot 0.9$ 3.51 MPa
$f_{ct,api}$	3.9 MPa	$f_{cm} = 0.8 \cdot f_{cm, cube}$ 57.6 MPa
f_{cm}	20000 MPa	$f_{ck} \approx f_{cm} - 8$ 49.6 MPa
		$f_{ctm, fl} = (1.6 - h) \cdot f_{ctm}$ 4.914 MPa

Steel	measured property	adjustable properties
E_s	200000 MPa	

Reinforcement	measured property	adjustable properties
$A_{s, min} = 0.26 \frac{f_{ctm}}{f_{yk}} b d$	41.07 mm ²	$\alpha_e = \frac{E_s}{E_c}$ 10.00
A_s	150.80 mm ²	ϕ 8 mm
$\rho = \frac{A_s}{A_c} = \frac{A_s}{b \cdot d}$	0.006	n 3 bars
	0.609 %	enough reinforcement?

M-k diagram

1. Concrete bottom fibre crack $\sigma_{ct} = f_{ctm}$

$M_{cr} = W_c \cdot f_{ctm, fl}$ 4.914 kNm

$\epsilon_{ct} = \frac{f_{ctm, fl}}{E_{cm}}$ 2.46E-04

ϵ_s 1.60E-04

$\kappa_r = \frac{2 + \epsilon_{ct}}{h}$ 0.00002457 1/mm

3. Steel yielding or plastic zone conctr? Yielding of reinforcement

$N_z = A_s \cdot f_{yk}$ 82938.046 N

$M_{yp} = N_z \cdot z = N_z \cdot (d - \frac{1}{2}x)$ 12346280 Nmm or 12.346 kNm

ϵ_{cr} 2.88 ‰ vs $\epsilon_{sy} = 2.75$ ‰

ϵ_s 6.9350216 ‰ **1: steel yielding**

$\kappa_{sy} = \frac{\epsilon_s}{d - x}$ 2.36E-05 1/mm **0: concrete plastic zone**

2. Force redistribution

$M_{cr} = N_z + z = A_s \cdot E_s + \epsilon_s \cdot (d - \frac{1}{2}x)$ $\frac{\epsilon_s}{\epsilon_c} = \frac{x}{d - x}$

$\frac{1}{2} b \cdot x \cdot \epsilon_c + E_{cm} = A_s \cdot E_s + \epsilon_s$

so, $x = d + (-\alpha_e + \rho + \sqrt{(\alpha_e + \rho)^2 + 2\alpha_e \cdot \rho})$

x 48.42 mm

$\epsilon_s = \frac{M_{cr}}{A_s \cdot E_s + (d - \frac{1}{2}x)}$ 1.09E-03 **1: enough steel**

ϵ_c 4.55E-04 **0: not enough steel**

$\sigma_s = \frac{x}{d - x} \cdot \epsilon_c$ 218.91 MPa

$\sigma_c = E_c \cdot \epsilon_c$ 9.09 MPa

$\kappa_r = \frac{\epsilon_s + \epsilon_c}{d}$ 9.39E-06 1/mm

4. Moment of failure: concrete/steel? Concrete failure

$N_z = A_s \cdot f_{yk}$ 93493.797 N or 93.4938 kN

$x_u = \frac{N_z}{\alpha \cdot f_{cm} + b}$ 16.908 mm

$z = d - \beta \cdot x_u$ 159.019 mm

$M_{Rd} = N_c + z$ 14867275 Nmm or 14.86728 kNm

ϵ_s 35.0 ‰ **Concrete failure**

$\kappa_{cu} = \frac{\epsilon_{cu3}}{d}$ 2.37E-04

$F = 2P \geq 2^* M_{rd}/0.5$ 59.5 kN

Concrete	measured property	adjustable properties
strain [%]	stress [MPa]	area1 36.12672
0	0	area2 172.5235
ϵ_{cr} 2.88	57.6	α 0.64
4.00	57.6	β 0.35375

Steel FeB 500	measured property	adjustable properties
strain [%]	stress [MPa]	
0	0	
f_{yk} 2.75	550	
f_{yk} 50	620	

Dimensions	measured property	adjustable properties
h	200 mm	
b	150 mm	
c	31 mm	
a_s	8 mm	
$d = h - c - 0.5 \cdot a_s$	165 mm	
I	1E+08 mm ⁴	

stage	Mcr [kNm]	εc [%]	εs [%]	κ [1/mm]	R = 1/κ	w ₁ = 5*L ² /8R	E [Mpa]	w ₂	F [kN]
0	0	0	0	0	0	0	0	0.00	0.00
1	4.914	0.24570	0.15971	2.46E-06	407000	0.384	20000	0.59	19.66
2	4.914	0.45454	1.09454	9.39E-06	106515	1.467	5234	2.25	19.66
3	12.346	1.14203	2.75000	2.36E-05	42394	3.686	5234	5.65	49.39
4	14.867275	4.00000	35.03506	2.37E-04	4227	36.997	628	56.68	59.47

S100 – 33d

The initial calculation was conducted in the same way as for S50 - 33d. Again, the concrete strain ϵ_{cu3} was set as 2.9‰, because the compressive strength of the mixture can be compared to high-strength concrete, and is therefore assumed to be more brittle. Furthermore, the calculation was based on measured properties (E-modulus, splitting tensile strength and compr. strength). These values have been highlighted in the Excel sheet below. Based on this calculation, concrete compressive failure was expected, but the numbers are closer to reinforcement failure than in case of S50 (because the compressive strength of S100 is higher when compared to the values for S50).

Calculation S100 reinforced concrete beam - 34 days

Concrete			
$f_{cm, cube}$	93.45 MPa	$f_{ctm} = f_{ct, spl} * 0.9$	4.842 MPa
$f_{ct, spl}$	5.38 MPa	$f_{cm} = 0.8 * f_{cm, cube}$	74.76 MPa
E_{cm}	32960 MPa	$f_{yk} \approx f_{cm} - 8$	66.76 MPa
		$f_{ctm, fl} = (1.6 - h) * f_{ctm}$	6.7788 MPa

Steel	
E_s	200000 MPa

Reinforcement			
$A_{s, min} = 0.26 \frac{f_{ctm}}{f_{yk}} b d$	71.63 mm ²	$\alpha_s = \frac{M_{cr}}{E_s}$	6.07
A_s	150.80 mm ²	ϕ	8 mm
$\rho = \frac{A_s}{A_c} = \frac{A_s}{b * d}$	0.006	n	3 bars
	0.609 %	enough reinforcement?	
enough reinforcement? Green = YES, Red = NO			

M-k diagram

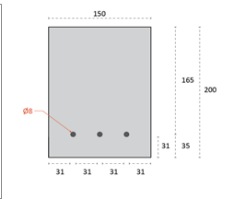
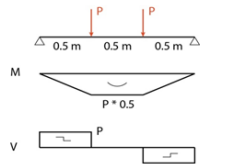
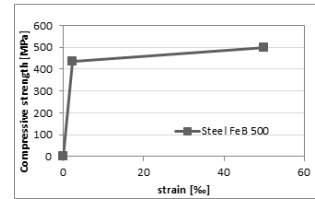
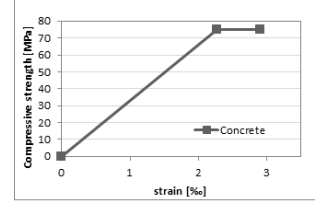
1. Concrete bottom fibre crack $\epsilon_{ct} = f_{ctm}$		
$M_{cr} = W_c * f_{ctm, fl}$	6.7788 kNm	
$\epsilon_{ct} = \frac{f_{ctm, fl}}{E_{cm}}$	2.06E-04	
ϵ_s	1.34E-04	
$\kappa_r = \frac{2 * \epsilon_{ct}}{h}$	2.05667E-06 1/mm	

2. Force redistribution		
$M_{cr} = N_s * z = A_s * E_s * \epsilon_s + \epsilon_s * (d - \frac{1}{3} * x)$		$\frac{\epsilon_s}{\epsilon_c} = \frac{x}{d - x}$
$\frac{1}{2} b * x * \epsilon_c * E_{cm} = A_s * E_s * \epsilon_s$		
so, $x = d * (-\alpha_s * \rho + \sqrt{(\alpha_s * \rho)^2 + 2 * \alpha_s * \rho})$	39.18 mm	
$\epsilon_s = \frac{M_{cr}}{A_s * E_s * (d - \frac{1}{3} * x)}$	1.48E-03	1: enough steel
$\epsilon_c = \frac{x * \epsilon_s}{d - x}$	4.61E-04	0: not enough steel
$\sigma_s = E_s * \epsilon_s$	295.86 MPa	
$\sigma_c = E_c * \epsilon_c$	15.18 MPa	
$\kappa_r = \frac{\epsilon_s + \epsilon_c}{d}$	1.18E-05 1/mm	

measured property		adjustable properties	
Concrete			
strain [%]	stress [MPa]	area1	14.92084
0	0	area2	117.6707
ϵ_{ca}	2.27	α	0.60893
ϵ_{cu3}	2.90	β	0.346324

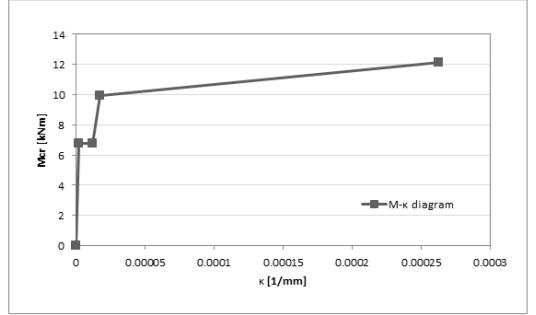
Steel FeB 500			
strain [%]	stress [MPa]		
0	0		
f_{yk}	2.175	435	
f_{yk}	50	500	

Dimensions	
h	200 mm
b	150 mm
c	31 mm
e_s	8 mm
$d = h - c - 0.5 * d_s$	165 mm
	1E+08 mm ⁴



3. Steel yielding or plastic zone concr? Yielding of reinforcement			
$N_s = A_s * f_{yk}$	65596.455 N		
$M_{pl} = N_s * z = N_s * (d - \frac{1}{3} * x)$	9966730.9 Nmm	or	9.967 kNm
ϵ_{ca}	2.27 %	vs	$\epsilon_{sy} = 2.175 \%$
ϵ_s	7.2840187 %		1: steel yielding
$\kappa_{sy} = \frac{\epsilon_s}{d - x}$	1.73E-05 1/mm		0: concrete plastic zone

4. Moment of failure: concrete/steel? Concrete failure			
$N_s = A_s * f_{yk}$	75398.224 N	or	75.39822 kN
$x_u = \frac{N_s}{\alpha * f_{cm} * b}$	11.042 mm		
$z = d - \beta * x_u$	161.176 mm		
$M_{rd} = N_s * z$	12152385 Nmm	or	12.15239 kNm
ϵ_s	40.4 %		Concrete failure
$\epsilon_c = \frac{\epsilon_{cu3}}{2}$	2.63E-04		
$F = 2P = 2 * M_{rd} / 0.5$	48.6 kN		



stage	from M/k diag				VGM				
	Mcr [kNm]	εc [%]	εs [%]	x [1/mm]	R = 1/k	w ₁ = 5*L ² /8R	E [Mpa]	w ₂	F [kN]
0	0	0	0	0	0	0	32960	0.49	0.00
1	6.7788	0.20567	0.13368	2.06E-06	486222	0.321	32960	0.49	27.12
2	6.7788	0.46065	1.47931	1.18E-05	85053	1.837	5766	2.82	27.12
3	9.967	0.67728	2.17500	1.73E-05	57848	2.701	5766	4.14	39.87
4	12.152385	2.90000	40.43602	2.63E-04	3807	41.082	463	62.92	48.61

The test showed reinforcement failure, unlike the calculation predicted. And, the maximum force was higher than calculated (see Fig. 5, left).

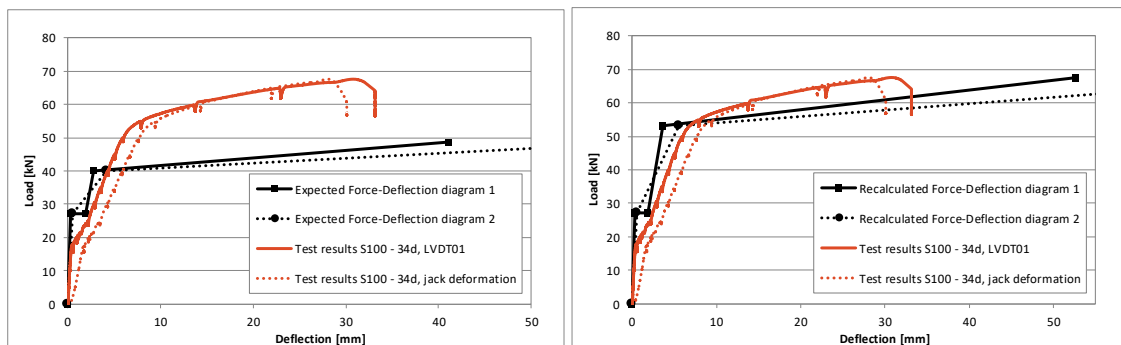


Fig. 5: Left: Expected Force-Deflection diagram vs. test results, both approach 1 and 2 (see previous paragraph) are plotted. Right: Recalculated Force-Deflection diagram based on the experiment, compared with the test results.

The maximum concrete strain (ϵ_{cu3}) is higher than the assumed 2.9‰, and the steel strength is higher than the characteristic value of 500 MPa, as was also the case for the other beams. The adjusted values are highlighted yellow in the recalculation sheet below. Fig. 5 (right) shows the recalculated Force-Deflection diagram. It is clear that the recalculated theoretical estimation is better than initially, but the calculated deflections are too big, as was also the case for beam S50-33d.

Recalculation S100 reinforced concrete beam - 34 days -			
Failure load was	67.6 kN	reinforcement failure	
Concrete			
$f_{cm,cube}$	93.45 MPa	$f_{ctm} = f_{ct,sp1} * 0.9$	4.842 MPa
$f_{ct,sp1}$	5.38 MPa	$f_{ctm} = 0.8 * f_{cm,cube}$	74.76 MPa
E_{cm}	32960 MPa	$f_{ck} \approx f_{cm} - 8$	66.76 MPa
		$f_{ctm,fl} = (1.6 - h) * f_{ctm}$	6.7788 MPa

Steel	
E_s	200000 MPa

Reinforcement			
$A_{s,min} = 0.26 \frac{f_{ctm}}{f_{yk}} b d$	53.72 mm ²	$\alpha_e = \frac{E_s}{E_c}$	6.07
A_s	150.80 mm ²	ϕ	8 mm
$\rho = \frac{A_s}{A_c} = \frac{A_s}{b * d}$	0.006	n	3 bars
	0.609 %	enough reinforcement?	
enough reinforcement? Green = YES, Red = NO			

1. Concrete bottom fibre crack		
$M_{cr} = W_c * f_{ctm,fl}$	6.7788 kNm	$\sigma_{ct} = f_{ctm}$
$e_{ct} = \frac{f_{ctm,fl}}{E_{cm}}$	2.06E-04	
ϵ_s	1.34E-04	
$\kappa_r = \frac{2 * e_{ct}}{h}$	2.05667E-06 1/mm	

2. Force redistribution		
$M_{cr} = N_s * z = A_s * E_s * \epsilon_s * (d - \frac{1}{3} x)$	$\frac{\epsilon_s}{\epsilon_c} = \frac{x}{d - x}$	
$\frac{1}{2} b * x * \epsilon_c * E_{cm} = A_s * E_s * \epsilon_s$		
SO, $x = d * (-\alpha_e * \rho + \sqrt{(\alpha_e * \rho)^2 + 2 * \alpha_e * \rho})$		
x	39.18 mm	
$\epsilon_s = \frac{M_{cr}}{A_s * E_s * (d - \frac{1}{3} x)}$	1.48E-03	1: enough steel
$\frac{x * \epsilon_s}{d - x}$	4.61E-04	0: not enough steel
$\sigma_s = E_s * \epsilon_s$	295.86 MPa	
$\sigma_c = E_c * \epsilon_c$	15.18 MPa	
$\kappa_r = \frac{\epsilon_s + \epsilon_c}{d}$	1.18E-05 1/mm	

3. Steel yielding or plastic zone concr? Yielding of reinforcement		
$N_s = A_s * f_{yk}$	87461.939 N	
$M_{sp1} = N_s * z = N_s * (d - \frac{1}{3} x)$	13288975 Nmm	or 13.289 kNm
ϵ_{cs}	2.27 ‰ vs $\epsilon_{sp} =$	2.9 ‰
ϵ_s	7.2840187 ‰	1: steel yielding
$\kappa_{xy} = \frac{\epsilon_s}{d - x}$	2.30E-05 1/mm	0: concrete plastic zone

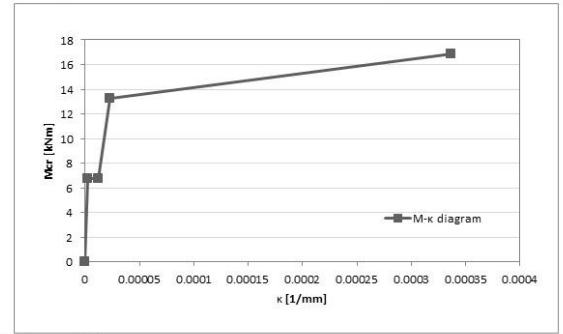
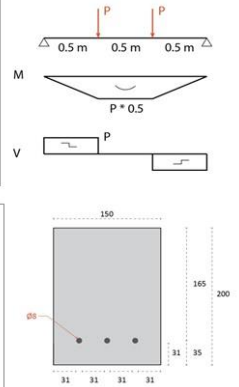
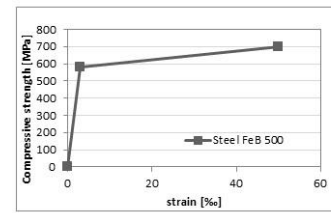
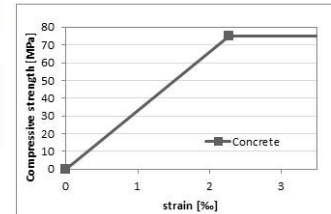
4. Moment of failure: concrete/steel? Reinforcement failure		
$N_s = A_s * f_{tu}$	105557.51 N	or 105.5575 kN
$x_u = \frac{N_s}{\alpha * f_{cm} * b}$	12.785 mm	
$z = d - \beta * x_u$	160.092 mm	
$M_{sd} = N_c * z$	16898932 Nmm	or 16.89893 kNm
ϵ_s	51.2 ‰	Reinforcement failure
$\kappa_u = \frac{\epsilon_{cu3}}{d}$	3.36E-04	
$F = 2P \stackrel{x}{=} 2 * M_{rd}/0.5$	67.6 kN	

stage	Mcr [kNm]	εc [‰]	εs [‰]	κ [1/mm]	R = 1/κ	w ₁ = 5*L ² /8R	E [Mpa]	w ₂	F [kN]
0	0	0	0	0	0	0	0.00	0.00	0.00
1	6.7788	0.20567	0.13368	2.06E-06	486222	0.321	32960	0.49	27.12
2	6.7788	0.46065	1.47931	1.18E-05	85053	1.837	5766	2.82	27.12
3	13.289	0.90304	2.90000	2.30E-05	43386	3.601	5766	5.52	53.16
4	16.898932	4.30000	51.19480	3.36E-04	2973	52.645	502	80.58	67.60

measured property		adjustable properties	
Concrete			
strain [‰]	stress [MPa]	area1	154.3119
0	0	area2	236.3703
ϵ_{cs}	2.27	α	0.736255
ϵ_{cu3}	4.30	β	0.383874

Steel FeB 500	
strain [‰]	stress [MPa]
0	0
f_{yk}	580
f_{ym}	700

Dimensions	
h	200 mm
b	150 mm
c	31 mm
β_s	8 mm
$d = h - c - 0.5 * d_s$	165 mm
l	1E+08 mm ⁴



S100-70d

The same procedure was followed as for all the other beams. The calculation is based on approximate measured properties, because the properties have not been tested exactly at 69d. Therefore, a rough estimation based on the results from 47 days (Table 5.1) has been applied. Based on the initial calculation (shown below), concrete compressive failure was expected. However, as explained in the previous paragraphs, the four-point bending test for the S100 beam tested at 28 days showed reinforcement failure instead of concrete compressive failure. Therefore, not based on this calculation, but on the gained experience, it was expected that the maximum strain in the concrete would be higher than 2.9‰. And that, again, reinforcement would fail before concrete crushing occurs.

The test showed reinforcement failure, unlike the calculation predicted, but as expected. And, the maximum force was higher than calculated (see Fig. 6, left), as was the case for all the other beams.

Calculation S100 reinforced concrete beam - 70 days

Concrete			
$f_{cm,cube}$	96 MPa	$f_{ctm} = f_{ct,api} * 0.9$	4.86 MPa
$f_{ct,api}$	5.4 MPa	$f_{cm} = 0.8 * f_{cm,cube}$	76.8 MPa
E_{cm}	31000 MPa	$f_{ck} \approx f_{cm} - 8$	68.8 MPa
		$f_{ctm,fi} = (1.6 - h) * f_{ctm}$	6.804 MPa

Steel	
E_s	200000 MPa

Reinforcement			
$A_{s,min} = 0.26 \frac{f_{ctm}}{f_{yk}} b d$	71.89 mm ²	$a_s = \frac{e_s}{\epsilon_c}$	6.45
A_s	150.80 mm ²	ϕ	8 mm
$\rho = \frac{A_s}{A_c} = \frac{A_s}{b * d}$	0.006	n	3 bars
	0.609 %	enough reinforcement?	

M-k diagram

1. Concrete bottom fibre crack $\epsilon_{ct} = f_{ctm}$	
$M_{cr} = W_z * f_{ctm,fi}$	6.804 kNm
$\epsilon_{ct} = \frac{f_{ctm,fi}}{E_{cm}}$	2.19E-04
ϵ_s	1.43E-04
$\kappa_r = \frac{2 * \epsilon_{ct}}{h}$	2.19484E-06 1/mm

2. Force redistribution	
$M_{cr} = N_s * z = A_s * E_s * \epsilon_s * (d - \frac{1}{3} * x)$	$\epsilon_c = \frac{x}{d - x}$
$\frac{1}{2} * b * x * \epsilon_c * E_{cm} = A_s * E_s * \epsilon_s$	$\epsilon_s = \frac{x}{d - x}$
$x = d * (-\alpha_s * \rho + \sqrt{(\alpha_s * \rho)^2 + 2 * \alpha_s * \rho})$	
x	40.23 mm
$\epsilon_s = \frac{M_{cr}}{A_s * E_s * (d - \frac{1}{3} * x)}$	1.49E-03
$\epsilon_c = \frac{x * \epsilon_s}{d - x}$	4.80E-04
$\sigma_s = E_s * \epsilon_s$	297.65 MPa
$\sigma_c = E_c * \epsilon_c$	14.88 MPa
$\kappa_r = \frac{\epsilon_s + \epsilon_c}{d}$	1.19E-05 1/mm

3. Steel yielding or plastic zone concr? Yielding of reinforcement	
$N_s = A_s * f_{yk}$	65596.455 N
$M_{pl} = N_s * z = N_s * (d - \frac{1}{3} * x)$	9943759.4 Nmm or 9.944 kNm
$\epsilon_{c2} = \frac{N_s}{A_c}$	2.48 ‰ vs $\epsilon_{sy} = 2.175 ‰$
ϵ_s	7.6834269 ‰
$\kappa_{sy} = \frac{\epsilon_s}{d - x}$	1.74E-05 1/mm

4. Moment of failure: concrete/steel? Concrete failure	
$N_s = A_s * f_{yk}$	75398.224 N or 75.39822 kN
$x_u = \frac{N_s}{\alpha * f_{cm} * b}$	11.425 mm
$z = d - \beta * x_u$	161.121 mm
$M_{fd} = N_c * z$	12148240 Nmm or 12.14824 kNm
ϵ_s	39.0 ‰
$\kappa_u = \frac{\epsilon_{cu2}}{d}$	2.54E-04
$F = 2P = 2 * M_{fd} / 0.5$	48.6 kN

stage	Mcr [kNm]	εc [%]	εs [%]	κ [1/mm]	from M/k diagram			VGM	
					R = 1/κ	w _s = 5 * L ² / 8R	E [Mpa]	w _s	F [kN]
0	0	0	0	0	0	0	0.00	0.00	
1	6.804	0.21948	0.14266	2.19E-06	455614	0.343	31000	0.53	27.22
2	6.804	0.47986	1.48824	1.19E-05	83837	1.864	5704	2.86	27.22
3	9.944	0.70130	2.17500	1.74E-05	57365	2.724	5704	4.18	39.78
4	12.14824	2.90000	38.98137	2.54E-04	3940	39.700	479	60.81	48.59

measured property		adjustable properties	
Concrete			
strain [%]	stress [MPa]	area1	6.857257
0	0	area2	118.7627
ϵ_{c2}	2.48	α	0.572859
ϵ_{cu2}	2.90	β	0.339511

Steel FeB 500	
strain [%]	stress [MPa]
0	0
f_{yk}	2.175
f_{vu}	50

Dimensions	
h	200 mm
b	150 mm
c	31 mm
d	8 mm
$d_s = h - c - 0.5 * d_s$	165 mm
I	1E+08 mm ⁴

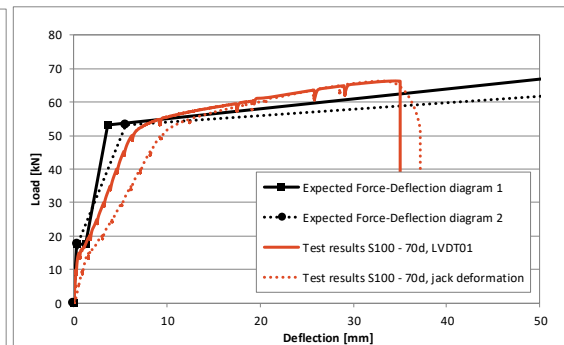
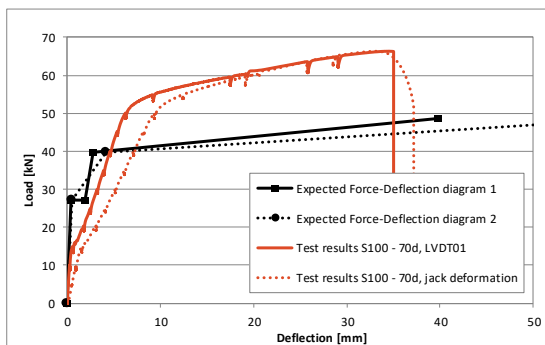
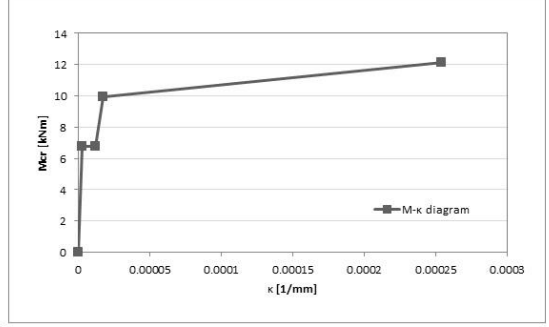
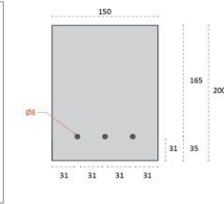
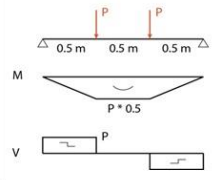
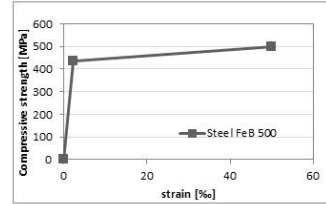
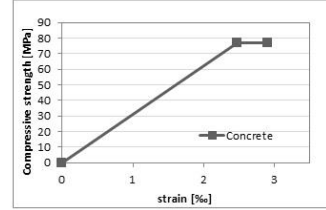


Fig. 6: Left: Expected Force-Deflection diagram vs. test results, both load approach 1 and 2 (see previous paragraph) are plotted. Right: Recalculated Force-Deflection diagram based on the experiment, compared with the test results.

The maximum concrete strain (ϵ_{cu3}) is higher than the assumed 2.9‰, and the steel strength is higher than the characteristic value of 500 MPa, as was also the case for the other beams. The adjusted values are highlighted yellow in the recalculation sheet below. Fig. 5 (right) shows the recalculated Force-Deflection diagram. It is clear that the recalculated theoretical estimation is better than initially, but the calculated deflections are too big, as was also the case for beam S50-33d.

Recalculation S100 reinforced concrete beam - 70 days

Failure load was **66.3 kN** reinforcement failure

Concrete	96 MPa	$f_{ctm} = f_{ct,sp1} * 0.9$	3.15 MPa
$f_{ct,cube}$	96 MPa	$f_{ctm} = 0.8 * f_{ct,cube}$	76.8 MPa
$f_{ct,sp1}$	3.5 MPa	$f_{ck} \approx f_{ctm} - 8$	68.8 MPa
E_{cm}	31000 MPa	$f_{ctm,fl} = (1.6 - h) * f_{ctm}$	4.41 MPa

Steel	200000 MPa
E_s	200000 MPa

Reinforcement			
$A_{s,min} = 0.26 \frac{f_{ctm}}{f_{yk}} b d$	34.95 mm ²	$\alpha_e = \frac{E_s}{E_c}$	6.45
A_s	150.80 mm ²	ϕ	8 mm
$\rho = \frac{A_s}{A_c} = \frac{A_s}{b * d}$	0.006	n	3 bars
	0.609 %	enough reinforcement?	
enough reinforcement? Green = YES, Red = NO			

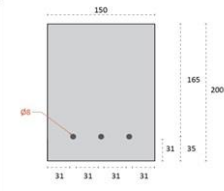
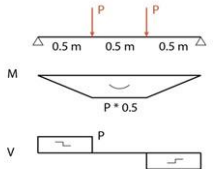
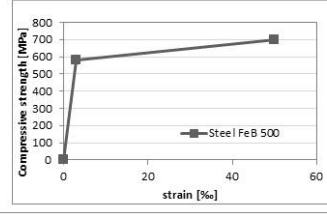
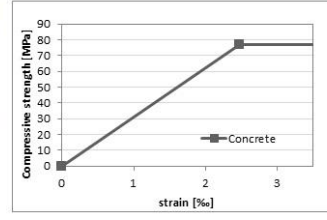
M-k diagram		
1. Concrete bottom fibre crack	$\sigma_n = f_{ctm}$	
$M_{cr} = W_c * f_{ctm,fl}$	4.41 kNm	
$\epsilon_{ct} = \frac{f_{ctm,fl}}{E_{cm}}$	1.42E-04	
ϵ_s	9.25E-05	
$\kappa_f = \frac{2 * \epsilon_{ct}}{h}$	1.42258E-06 1/mm	

Force redistribution		
$M_{cr} = N_s * z = A_s * E_s * \epsilon_s * (d - \frac{1}{3} x)$		$\frac{t_s}{t_c} = \frac{x}{d - x}$
$\frac{1}{2} b * x * x * \epsilon_c + E_{cm} = A_s * E_s * \epsilon_s$		
so, $x = d * (-\alpha_e * \rho + \sqrt{(\alpha_e * \rho)^2 + 2\alpha_e * \rho})$		
x	40.23 mm	
$\epsilon_s = \frac{M_{cr}}{A_s * E_s * (d - \frac{1}{3} x)}$	9.65E-04	1: enough steel
$\epsilon_c = \frac{x * \epsilon_s}{d - x}$	3.11E-04	0: not enough steel
$\sigma_s = E_s * \epsilon_s$	192.92 MPa	
$\sigma_c = E_c * \epsilon_c$	9.64 MPa	
$\kappa_f = \frac{\epsilon_s + \epsilon_c}{d}$	7.73E-06 1/mm	

measured property	adjustable properties	
Concrete	strain [%]	stress [MPa]
ϵ_{cu}	0	0
ϵ_{cu3}	2.48	76.8
	4.30	76.8
	area1	127.5571
	area2	251.9488
	α	0.711928
	β	0.375391

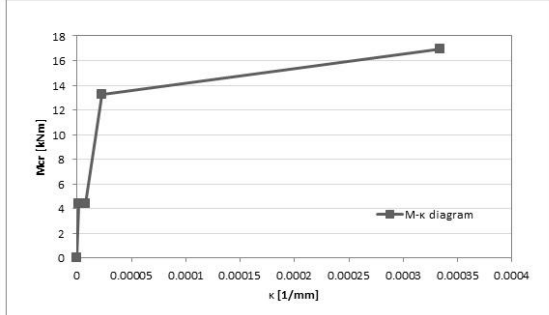
Steel FeB 500	strain [%]	stress [MPa]
	0	0
f_{yk}	2.9	580
f_{tu}	50	700

Dimensions	
h	200 mm
b	150 mm
c	31 mm
d_s	8 mm
$d = h - c - 0.5 * d_s$	165 mm
I	1E+08 mm ⁴



3. Steel yielding or plastic zone concr?	Yielding of reinforcement
$N_s = A_s * f_{yk}$	87461.939 N
$M_{spt} = N_s * z = N_s * (d - \frac{1}{3} x)$	13258346 Nmm or 13.258 kNm
ϵ_{cu}	2.48 % vs $\epsilon_{sy} = 2.9$ %
ϵ_s	7.6834269 %
$\kappa_{sy} = \frac{\epsilon_s}{d - x}$	2.32E-05 1/mm
	1: steel yielding
	0: concrete plastic zone

4. Moment of failure: concrete/steel?	Reinforcement failure
$N_s = A_s * f_{tu}$	105557.51 N or 105.5575 kN
$x_u = \frac{N_s}{\alpha * f_{cm} * b}$	12.871 mm
$z = d - \beta * x_u$	160.168 mm
$M_{sd} = N_c * z$	16906985 Nmm or 16.90699 kNm
ϵ_s	50.8 %
$\kappa_u = \frac{\epsilon_{cu3}}{d}$	3.34E-04
$F = 2P = 2 * M_{rd}/0.5$	67.6 kN
	Reinforcement failure



stage	Mcr [kNm]	εc [%]	εs [%]	κ [1/mm]	R = 1/κ	w1 = 5*L ² /8R	E [Mpa]	w2	F [kN]
0	0	0	0	0	0	0	0	0.00	0.00
1	4.41	0.14226	0.09247	1.42E-06	702948	0.222	31000	0.34	17.64
2	4.41	0.31102	0.96460	7.73E-06	129349	1.208	5704	1.85	17.64
3	13.258	0.93507	2.90000	2.32E-05	43024	3.632	5704	5.57	53.03
4	16.906985	4.30000	50.82540	3.34E-04	2993	52.293	506	80.04	67.63

Conclusion

It should be emphasized that the conducted calculations are only a simplified version of the realistic behaviour, so therefore it will never perfectly fit the test results. Then, a finite element model should be made. To conclude, the steel strength was significantly higher than the characteristic value of 500 MPa, which is imaginable, as the characteristic value is on the "safe side". Based on the experimental results, it is also clear that the maximum concrete strain (ϵ_{cu3}) is higher than for regular OPC concrete with similar compressive strengths. This means that AAC exhibits more ductile behaviour and therefore a higher rotational capacity than OPC concrete. The maximum concrete strain (ϵ_{cu3}) seems to be around 4-5 %, according to the recalculations.

Appendix E. – Development of cracks

This appendix contains the graphs that show a comparison between crack development for beams tested at the same moment over time.

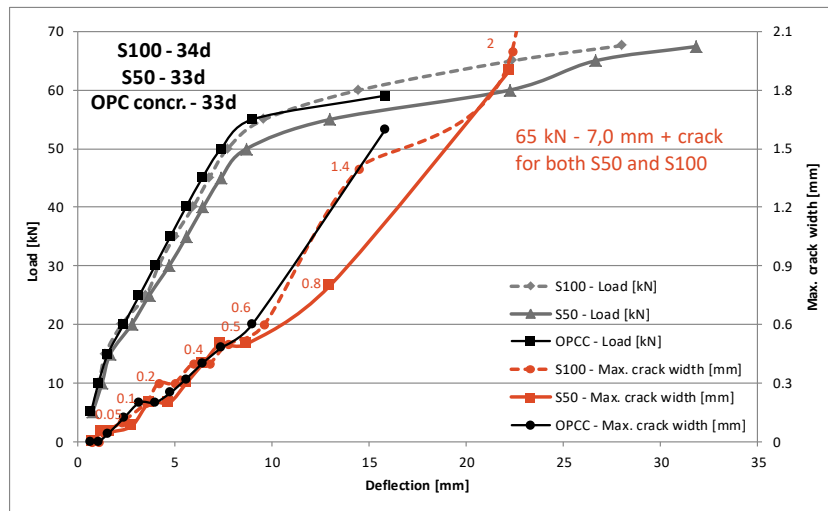


Fig. 1: Development of cracks during four-point bending tests on S50 and S100 beams at 33/34 days and comparison with regular OPCC beam, results by Zhekang Huang. S50 and S100 specimens have been cured (20°C and 95% RH) for 28 days. After this, the samples were exposed to laboratory conditions (20°C and 55% RH) until testing. OPC concrete was kept in the mould for 33 days (covered with plastic) in lab conditions and then unmoulded.

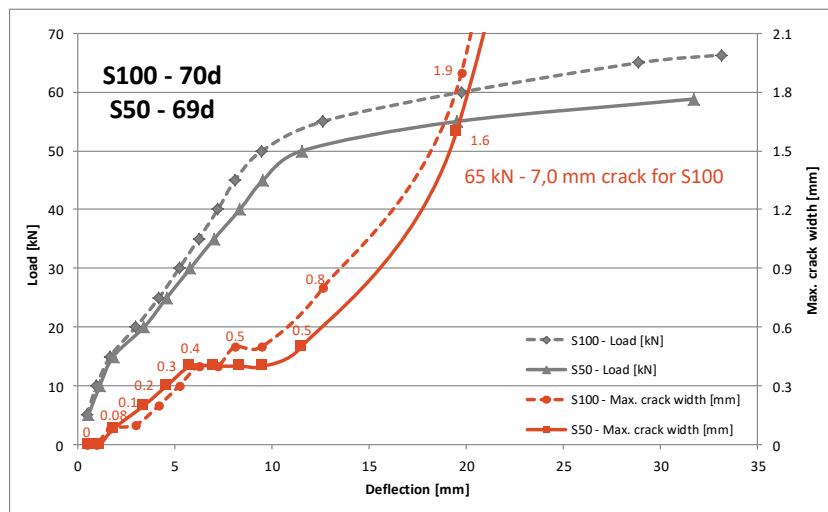


Fig. 2: Development of cracks during four-point bending tests on S50 and S100 beams at 69/70 days. Specimens have been cured (20°C and 95% RH) for 28 days. After this, the samples were exposed to laboratory conditions (20°C and 55% RH) until testing.

Appendix F. – Location of ESEM images

The ESEM images that are shown in paragraph 6.3 *ESEM analysis of microstructure* were taken at the following locations in the sample:

